Development of a Semi-active Intelligent Suspension System for Heavy Vehicles

by

Nima Eslaminasab

A thesis
presented to the University of Waterloo
in fulfillment of the
thesis requirement for the degree of
Doctor of Philosophy
in
Mechanical Engineering

Waterloo, Ontario, Canada, 2008

AUTHOR'S DECLARATION

I hereby declare that I am the sole author of this thesis. This is a true copy of the thesis, including any required final revisions, as accepted by my examiners.

I understand that my thesis may be made electronically available to the public.

Abstract

With the new advancements in the vibration control strategies and controllable actuator manufacturing, the semi-active actuators (dampers) are finding their way as an essential part of vibration isolators, particularly in vehicle suspension systems. This is attributed to the fact that in a semi-active system, the damping coefficients can be adjusted to improve ride comfort and road handling performances. The currently available semi-active damper technologies can be divided into two main groups. The first uses controllable electromagnetic valves. The second uses magnetorheological (MR) fluid to control the damping characteristics of the system. Leading automotive companies such as General Motors and Volvo have started to use semi-active actuators in the suspension systems of high-end automobiles, such as the Cadillac Seville and Corvette, to improve the handling and ride performance in the vehicle. But much more research and development is needed in design, fabrication, and control of semi-active suspension systems and many challenges must be overcome in this area. Particularly in the area of heavy vehicle systems, such as light armored vehicles, little related research has been done, and there exists no commercially available controllable damper suitable for the relatively high force and large displacement requirements of such application.

As the first response to these requirements, this thesis describes the design and modeling of an in-house semi-active twin-tube shock absorber with an internal variable solenoid-actuated valve. A full-scale semi-active damper prototype is developed and the shock absorber is tested to produce the required forcing range. The test results are compared with results of the developed mathematical model.

To gain a better understanding of the semi-active suspension controlled systems and evaluate the performance of those systems, using perturbation techniques this thesis provides a detailed nonlinear analysis of the semi-active systems and establishes the issue of nonlinearity in on-off semi-active controlled systems.

Despite different semi-active control methods and the type of actuators used in a semi-active controlled system, one important practical aspect of all hydro-mechanical computer controlled systems is the response-time. The longest response-time is usually introduced by the actuator –in this case, controllable actuator – in the system. This study investigates the effect of response-time in a semi-active controlled suspension system using semi-active dampers. Numerical simulations and

analytical techniques are deployed to investigate the issue. The performance of the system due to the response-time is then analyzed and discussed.

Since the introduction of the semi-active control strategy, the challenge was to develop methods to effectively use the capabilities of semi-active devices. In this thesis, two semi-active control strategies are proposed. The first controller to be proposed is a new hybrid semi-active control strategy based on the conventional Rakheja-Sankar (R-S) semi-active control to provide better ride-handling quality for vehicle suspension systems as well as industrial vibration isolators. To demonstrate the effectiveness of this new strategy, the analytical method of averaging and the numerical analysis method are deployed. In addition, a one-degree-of-freedom test bed equipped with a semi-active magnetorheological (MR) damper is developed. The tests are performed using the MATLAB XPC-target to guarantee the real-time implementation of the control algorithm. The second controller is an intelligent fuzzy logic controller system to optimize the suspension performance. The results from this intelligent system are compared with those of several renowned suspension control methods such as Skyhook. It is shown that the proposed controller can enhance concurrently the vehicle handling and ride comfort, while consuming less energy than existing control methodologies.

The key goal of this thesis is to employ the existing knowledge of the semi-active systems together with the new ideas to develop a semi-active suspension system. At the same time, development of an experimental simulation system for real-time control of an experimental test bed is considered. To achieve its goals and objectives, this research study combines and utilizes the numerical simulations and analytical methods, as well as lab-based experimental works. The challenge in this research study is to identify practical and industrial problems and develop proper solutions to those problems using viable scientific approaches.

Acknowledgements

I wish to express my gratitude to my supervisor, Professor F. Golnaraghi, for his constant support, guidance and encouragement. I feel especially blessed since he is not only my supervisor but also my friend.

I would also like to thank my entire comprehensive exam and thesis defense committee members for their time, support, and constructive comments. Of equal importance are my thanks to Prof. Glenn R. Heppler, Prof. Eihab M. Abdel-Rahman, Prof. William W. Melek, and Dr. Xiong Zhang.

This research was supported in part by General Kinetics Engineering Inc., Natural Sciences and Research Council of Canada, and Ontario Centres of Excellence (OCE). While everyone at OCE was supportive of my work, I am particularly pleased to thank Mr. Ross Bradsen and Ms. Leanne Gelsthorpe for their generous support.

Many thanks to my colleagues at General Kinetics Engineering Inc, special thanks go to Mr. Mike Ward, the advanced engineering manager of General Kinetics Engineering Inc., for sharing his knowledge and expertise with me. He was a constant support throughout and beyond this research work.

I am particularly in debt to Dr. Arash Narimani for his true friendship and support. He saved me a one-way ticket to Waterloo; he showed me the gate, putting me in debt to OSAP for a long time.

Throughout the past years as a graduate student, there have been many joyful moments in life, the moments which have been made more enjoyable by our friends; also sad times, which have been made bearable by the support of friends both in and out of the school. Of equal importance are my happy memories of Godrat and Lila Esmaeili, Ali and Parisa Naserri moghaddam, Orang and Maryam Vahid, Ashkan and Shiva Bagheri, Kiarash Narimani, Sara Behjat, Roshanak Moradi, Arshia Rafat, Majid Bahrami, Saleh Tabandeh, Babak Ebrahimi, Siamak Arzanpour, Shahab and Bahar Gaffari, Brad Schubert, Tom Gillespie, Brian Koiter, Peter Won, Peter liu, Antony kim, Sina Valadkhan, Sami Chackman, Shen Yu, Alex Weilhelm, Geoff Stacy, Javad and Mahkame Goolipoor, Hamid and Behnoosh Sabetfar, Amin Kamalzadeh, Amir Rouzrokh, Neda Parnian, and Golzar Taravati.

I get disappointed when reading the acknowledgement part of my many friends' thesis whenever I fail to see my name mentioned; this thank-you is extended to all my friends whose names I have forgotten to mention. You are all a big part of my life.

As a graduate student, I have had the honor of attending many lectures and courses at University of Waterloo; in particular, I enjoyed and learned much from attending lectures by Prof. Wei-Chau Xie of civil engineering and Prof. Dwight Aplevich of electrical engineering. Special thanks also go to Prof. Fathy Ismail and Prof. Chris Clark for their supports and encouragements.

Many thanks to Robert Wagner and Andy Barber, the technical staff, Jennifer Nickerson and Celia McGill, the administrative staff, all of MME department of University of Waterloo; Many thanks to Elaine Garner of GSO and Susan Spaetzel of Dean of Engineering Office both of University of Waterloo.

Throughout the last few years, while I was enjoying the pleasant and peaceful academic environment at Waterloo, many people around the world were suffering from various unpleasant, unjustified, and unfair events including war, terrorism, dictatorship, poverty, hunger, and even the consequences of global warming. Although I am happy that I have not consciously supported or generated any of those events, I am truly in debt to all the people who have suffered in any such disastrous events that I could possibly have prevented, stopped, or even protested against. I hope to use my knowledge and training to help make the world for all of us a more pleasant place to live.

I wish to express thanks to all my family members for their constant support, encouragement, and understanding. To my brother Ramin, whose honesty and unpretentious behavior has inspired me throughout life. To my father in-law, Mr. Ahmad Mansouri, one of the few people I have ever found to express anything but goodness of others; he has always been a shelter in the worst moments. Special thanks to my mother-in-law, Ms. Farideh Kashef, for her understanding and support, and to my brothers-in-law Pouya and Azad for their kindness and encouragement.

I will be short on words to express my gratitude to my Mother, Ms. Mahvash Allamehzade, for what she has done for me over the years. She has never stopped loving, even in the hardest moments. She has always been my biggest inspiration. This work would not be possible without her love and support.

Last but not least, I value the memory of my father, a physics teacher, who was my first source of encouragement and appreciation for science, math, and physics. I believe you have been watching me up-close in all moments of my life.

Dedication

This thesis is dedicated to the one who gave me The Love, who stood by me all the moments of her life during the last few years, who chose to share the ride of life with me, and who is always a blessing for me

To my Wife, Afarin

Table of Contents

List of Figures

xiv

List of Tables

Nomenclature

c, C	linear damping
k	linear stiffness
k_3	nonlinear stiffness
f	force
I	current
m	mass
m_b	unsprung mass
m_w	sprung mass
$r = \omega/\omega_n = \nu/\omega_n$	frequency ratio
t	Time
ω	base excitation frequency of oscillation
x	mass displacement
x_1	unsprung mass displacement
z_1	state variable
z_2	state variable
z_3	state variable
z_4	state variable
x_2	sprung mass displacement
$x_r = x - y$	mass-base relative displacement
X	displacement amplitude
y	base displacement
Y	base harmonic displacement excitation amplitude
η	acceleration transmissibility
λ	relative displacement transmissibility
$\zeta = c/2\sqrt{km}$	damping ratio
$\omega_n = \sqrt{k/m}$	natural frequency

r_{max}, r_{min}	frequency analysis range boundary
V_{abs}	absolute velocity of unsprung mass
V_{rel}	relative velocity between sprung mass and unsprung mass
V_{abs-w}	absolute velocity of sprung mass
a_{abs}	absolute acceleration of unsprung mass
Z_{rel}	relative displacement between sprung mass and unsprung mass
$()'$	$d()/d\tau$
$\tau = \nu t$	time scaling parameter
I	moment of inertia
$\ddot{\varphi}, \ddot{\theta}$	angular acceleration
$\varphi, \beta, \theta, \phi$	angle and phase
h_b, R, L, h_R	element length

Chapter 1

Introduction

Traditionally, suspension systems perform multiple tasks such as maintaining contact between vehicle tires and the road, addressing the stability of the vehicle, and isolating the frame of the vehicle from road-induced vibration and shocks. The latter deals with both ride comfort and road handling characteristics of vehicles. Road-induced vibrations are typically below 30 Hz, and have amplitude greater than 0.3 mm (Brach and Haddow, 1993).

In general, ride comfort, road handling, and stability are the most important factors in evaluating suspension performance. Ride comfort is proportional to the absolute acceleration of the vehicle body, while road handling is linked to the relative displacement between vehicle body and the tires. On the other hand, stability of vehicles is related to the tire-ground contact. The main concern in suspension design and control is the fact that currently, achieving improvement in these three objectives poses a challenge because these objectives will likely conflict with each other in the vehicle operating domain (Eslaminasab *et al.,* 2007b).

In the case of large off-road vehicles, the extremes in operating conditions to which the vehicle suspension system is exposed make this conflict even greater. Vehicles must be able to traverse rough terrain including steep hills, ditches, and boulder, as well as relatively smooth surfaces such as paved roads and highways. The challenges faced in developing an optimized suspension system for the off-road vehicles include the higher damping forces encountered with heavy vehicles moving over rough terrain, the costs of producing large shock absorbers, and the unique requirements of control systems that must operate under widely varying conditions and vehicle configurations.

In the following sections, a review of the prior-art and the concept at hand is presented, followed by the thesis objectives and outline.

1.1 Vehicle Suspension Systems and Suspension Controllability[1]

Based on the mechanical design and configuration, suspension systems are generally categorized in two main groups: solid axle suspension and independent suspension. Each group can be functionally

---

[1] The controllability in this section is used as a general term not the classical definition of controllability in the linear systems theory.

1

quite different (Gillespie, 1992), and they are studied and discussed accordingly. In a solid axle suspension, the movement and vibration of one wheel are transmitted to the opposite wheel directly. In an independent suspension on the other hand, the movement of each wheel is independent of the other wheel. Figure 1 shows a schematic front view of two suspension groups.
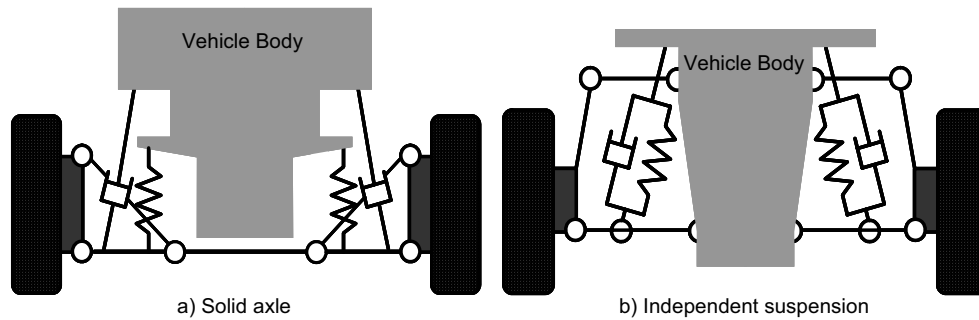
Figure 1: Schematic of two main groups of suspension systems

Going in chronological order, the first mass-produced front suspension design was the solid axle type. New developments in springs, roll bars, and dampers have kept the solid axle practical for some applications. However, given the performance of the solid axle suspension, it is far from being used in the high-performance vehicles and passenger cars. Independent suspension systems such as MacPherson and Double-wishbone have a better resistance in the steering vibration and offer higher performance in passengers comfort than the solid axle system. As a result, they are the most commonly-used suspension systems in the automotive industry.

When controllability, not the mechanical design, is the main concern in categorizing the suspension systems, they are classified as passive, active, and semi-active systems. In addition to the inherent advantages and disadvantages of each of these suspension classes, they are composed of conventional components, including springs and dampers (shock absorbers).

Passive suspensions are the most common systems currently used in most vehicles. These systems are composed of springs and dampers with fixed properties. The designer, according to the design goals and the intended application, determines and pre-sets these fixed characteristics. By setting the spring stiffness and the damping, an optimum performance is achieved. However, since the optimal values are not tune-able, the suspension performance is different for different operating conditions.

Active suspension systems in most cases use hydraulic actuators to generate the desired force. These systems are operated by using external power. Although active components alter the vertical force

2

reactions of the suspension, they do not alter the kinematics. Despite the higher performance of these systems, high power consumption, size, heavy weight, and cost of active suspension systems are serious setback.

Semi-active suspension systems may also contain springs and dampers. However, the properties of these elements (stiffness and damping) may be controlled and adjusted, in real time, externally. These properties can be controlled by supplying an electrical signal or other type of external power to the system. Semi-active systems are a compromise between the active and passive systems (Alanoly and Sankar, 1986), offering some essential advantages over the active systems. Active control systems rely entirely on external power to operate the actuators and supply the control forces. In many applications, they require a large power source. Semi-active devices require a lot less energy. Another critical issue with active control is the stability robustness with respect to sensor failure; this problem is a big concern when centralized controllers are used. On the contrary, semi-active control devices are essentially passive devices in which properties (stiffness, damping. . .) can be adjusted, but they cannot input energy directly into the system being controlled (Preumont, 2002); thus, they are robustly stable.

1.2 Simplified Vehicle Models and Suspension Performance Indexes

"All models are wrong but some are useful"

(Box, 1979)

Although vehicles are made of numerous components, for many of the analyses all components move together (Gillespie, 1992); for instance, in the turning maneuver the entire vehicle acts as a unit. As a result, it is possible to analyze the fundamental concepts of vehicle dynamics based on the simplified vehicle models. For instance, the dynamic behavior of vehicle vertical isolation properties can be represented and analyzed by one or two degree-of-freedom (DOF) quarter-car models, as shown in Figure 2.

a) 1DOF quarter-car model   b) 2DOF quarter-car model
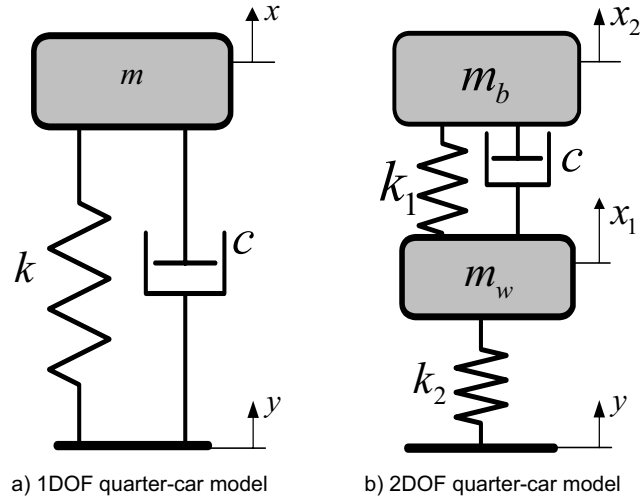
Figure 2: 1 and 2 DOF Quarter-car models

Because the two models are frequently used in this thesis, the governing equation of motion and the parameters used are defined in the following sections.

1.2.1 1DOF Quarter-Car Model

The Governing equation of motion for the 1DOF system shown in Figure 2-a is

$$m\ddot{x} + c(\dot{x} - \dot{y}) + k(x - y) = 0 \tag{1-1}$$

In this equation, m represents a quarter of the whole vehicle mass, k is the total suspension stiffness, and c is the damping coefficient. In addition, x is the mass movement, and y represents the road disturbances. This equation is rewritten in the state space form as

$$\begin{bmatrix} \dot{z}_1 \\ \dot{z}_2 \end{bmatrix} = \begin{bmatrix} 0 & 1 \\ -\dfrac{k}{m} & -\dfrac{c}{m} \end{bmatrix} \begin{bmatrix} z_1 \\ z_2 \end{bmatrix} + \begin{bmatrix} 0 & 0 \\ \dfrac{k}{m} & \dfrac{c}{m} \end{bmatrix} \begin{bmatrix} y \\ \dot{y} \end{bmatrix} \tag{1-2}$$

where $z_1 = x, z_2 = \dot{x}$ are the state variables. If the road disturbance input is a sinusoidal function ($y = Y\sin(\omega t)$), the equation of motion is expressed as

$$\ddot{x}_r + 2\zeta\omega_n\dot{x}_r + \omega_n^2 x_r = Y\omega^2 \sin(\omega t) \tag{1-3}$$

where the parameters are

4

$$\zeta = \frac{c}{2\sqrt{km}}, \ \omega_n = \sqrt{\frac{k}{m}} = 2\pi f_n, \ x_r = x - y \qquad \text{(1-4)}$$

1.2.2 2DOF Quarter-Car Model

The Governing equation of motion for the 2DOF system shown in Figure 2-b is

$$m_b \ddot{x}_2 = -k_1(x_2 - x_1) - c(\dot{x}_2 - \dot{x}_1) \qquad \text{(1-5)}$$

$$m_w \ddot{x}_1 = k_1(x_2 - x_1) + c(\dot{x}_2 - \dot{x}_1) - k_2(x_1 - y) \qquad \text{(1-6)}$$

In this equation, m_b represents a quarter of the whole vehicle mass; m_w is the unsprung mass of the vehicle; K_1 is the suspension stiffness, K_2 is the tire stiffness, and c is the damping coefficient. In addition, $x_{1,2}$ are the mass movements and y represents the road disturbances. This equation is rewritten in the state space form as

$$\begin{bmatrix} \dot{z}_1 \\ \dot{z}_2 \\ \dot{z}_3 \\ \dot{z}_4 \end{bmatrix} = \begin{bmatrix} 0 & 1 & 0 & 0 \\ -(\dfrac{k_1}{m_w} + \dfrac{k_2}{m_w}) & -\dfrac{c}{m_w} & \dfrac{k_1}{m_w} & \dfrac{c}{m_w} \\ 0 & 0 & 0 & 1 \\ \dfrac{k_1}{m_b} & \dfrac{c}{m_b} & -\dfrac{k_1}{m_b} & -\dfrac{c}{m_b} \end{bmatrix} \begin{bmatrix} z_1 \\ z_2 \\ z_3 \\ z_4 \end{bmatrix} + \begin{bmatrix} 0 \\ \dfrac{k_2}{m_w} \\ 0 \\ 0 \end{bmatrix} [y] \qquad \text{(1-7)}$$

where $z_1 = x_1, z_2 = \dot{x}_1, z_3 = x_2, z_4 = \dot{x}_2$ are the state variables.

1.2.3 Vehicle Roll-Plane Models

Although the models introduced above are frequently used in research work as well as in this thesis to understand the vehicle vertical motion, they are unable to generate any information on the vehicle roll characteristics. The simplest model to address the roll-plane of vehicle is shown in Figure 3; the model presented here is adopted from (Bernard *et al.* 1991) but with some modifications including elimination of tires and addition to the system of the second degree of freedom, which compensates for the tire deflections .
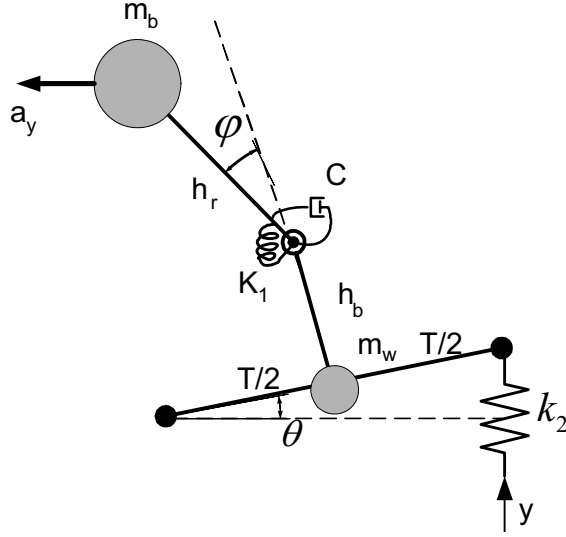
Figure 3: 2DOF roll-plane vehicle lumped-mass model

The governing equation of motion for this model is developed using the Newton's law. The final equations of motion, assuming $\theta, \varphi, \dot{\theta},$ and $\dot{\varphi}$ are small, are

$$\ddot{\varphi} = (-\frac{h_b}{h_r} - 1)\ddot{\theta} + \frac{g}{h_r}\theta + (\frac{g}{h_r} - \frac{k_1}{m_b h_r^2})\varphi - \frac{c}{m_b h_r^2}\dot{\varphi} + \frac{1}{h_r}a_y \tag{1-8}$$

$$\ddot{\theta} = b\left((-m_b h_b h_r)\ddot{\varphi} + (m_b g h_b - k_2 T^2 + \frac{m_b T}{2}a_y)\theta + k_2 Ty + m_b h_b a_y \right)$$

$$, b = \left(\frac{1}{\dfrac{m_w T^2}{4} + h_b^2 m_b + m_b h_b h_r + \dfrac{m_b T^2}{4}} \right) \tag{1-9}$$

In these equations, m_b represents half of the whole vehicle mass, m_w is the unsprung mass of the vehicle, K_1 is the equivalent suspension stiffness, K_2 is the tire stiffness, and c is the damping coefficient. θ and φ are the mass movements, y represents the road disturbances, and a_y is the axial acceleration of vehicle due to the certain maneuver. In addition, T is the vehicle track size, h_b is the vehicle roll-center height, and h_r is the height of vehicle's centre of gravity from vehicle roll-center.

6

This model is capable of demonstrating the roll behavior of vehicles; however, its application is limited because the model cannot predict the vertical motion of the vehicle. To investigate vehicles roll behavior under road disturbances (tripping roll over), a 4DOF system model, as shown in Figure 4, has been developed and has already been used in the numerous research works (Hrovat, 1997), (Kyongsu *et al.*, 2007).
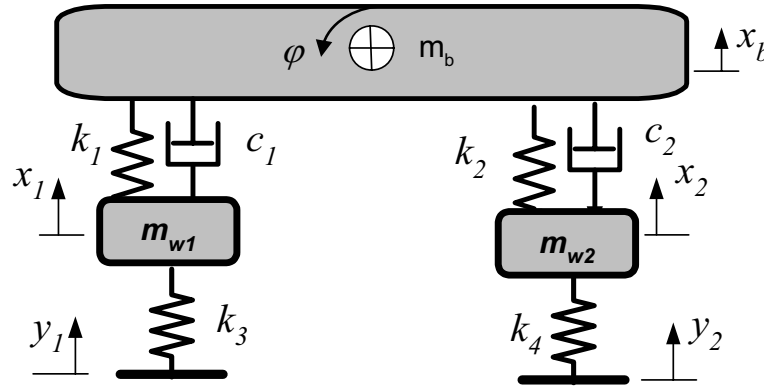
Figure 4: 3DOF roll-plane vehicle lumped-mass model

In these equations, m_b represents half of the whole vehicle mass; m_w is the unsprung mass of the vehicle, K_1 and K_2 are the equivalent suspension stiffness, K_3 and K_4 are the tire stiffness, and $c_{1,2}$ are the damping coefficients, φ is the roll angle, and y represents the road disturbances. The governing equation of motion for this system, assuming φ is small, is

$$
m_b\ddot{x}_b + c_1(\dot{x}_b - \dot{x}_1 - t_m\dot{\varphi}) + c_2(\dot{x}_b - \dot{x}_2 + t_m\dot{\varphi})
$$
$$
+ k_1(x_b - x_1 - t_m\varphi) + k_2(x_b - x_2 + t_m\varphi) = 0 \tag{a}
$$

$$
m_{w1}\ddot{x}_1 - c_1(\dot{x}_b - \dot{x}_1 - t_m\dot{\varphi}) - k_1(x_b - x_1 - t_m\varphi) + k_3 x_1 = k_3 y_1 \tag{b}
$$

$$
m_{w2}\ddot{x}_2 - c_2(\dot{x}_b - \dot{x}_2 - t_m\dot{\varphi}) - k_2(x_b - x_2 - t_m\varphi) + k_4 x_2 = k_4 y_2 \tag{c}
$$

(1-10)

$$
I_{xx}\ddot{\varphi} + c_1 t_m(\dot{x}_b - \dot{x}_1 - t_m\dot{\varphi}) + c_2 t_m(\dot{x}_b - \dot{x}_2 - t_m\dot{\varphi})
$$
$$
- k_1 t_m(x_b - x_1 - t_m\varphi) + k_2 t_m(x_b - x_2 - t_m\varphi) = T_b \tag{d}
$$

where t_m is half track size and T_b is the input moment resulting from different vehicle maneuvers.

7

The above models are used in this thesis to illuminate the concept of vehicle rollover and the application of the semi-active suspension system to reduce the rollover propensity of vehicles as discussed in further chapters. In addition, a professional software package, CarSim[2], is also used to validate the outcomes.

1.2.4 Suspension Performance Indexes

In the field of vibration control theory and particularly in the suspension control analysis, researchers and industries, use various common indexes to compare the performance of different systems. Differences in performance might be due to damper type, suspension category, or even the suspension control method. Some of the most commonly used benchmarking indexes for ride comfort, road handling, and rollover propensity performances are introduced in this section and detailed later in the thesis.

1.2.4.1 Ride comfort Index – Acceleration Transmissibility

The first index is the acceleration transmissibility, η. It is identified as the principal source of discomfort for the driver (Anon, 1997), (Griffin, 1998), and (BS6841, 1987). As a result, η is a valid and recommended parameter to measure the performance of a suspension system.

By definition, acceleration transmissibility is the ratio of the maximum acceleration, sensed by the driver, to the road-induced vibration as a result of road-tire interaction. For a 1DOF system as shown in Figure 2-a, η is calculated as

$$\eta = \left| \frac{\max(\ddot{x})}{\omega_n^2 Y} \right| \tag{1-11}$$

In a 1DOF system with a sinusoidal base excitation, the acceleration transmissibility is defined as (Shen, 2005)

$$\eta = \frac{\omega^2 \sqrt{\omega_n^4 + (2\zeta\omega_n\omega)^2}}{\omega_n^2 \sqrt{(\omega_n^2 - \omega^2)^2 + 4\zeta^2\omega_n^2\omega^2}} \tag{1-12}$$

---

[2] CarSim is registered trademarks of Mechanical Simulation Corporation in the USA and other countries.

Consequently, in a 2DOF system, as shown in Figure 2-b, with the sinusoidal base excitation, the transferred acceleration is defined as (Shen, 2005):

$$\eta = \left| \frac{\max(\ddot{x}_2)}{\omega_b^2 Y} \right| = \frac{\omega^2 \sqrt{A^2 + B^2}}{\omega_b^2 \Delta} \tag{1-13}$$

where the equation parameters are $\Delta = \sqrt{C^2 + D^2}$, $A = -\omega_b^2 \omega_w^2$, $B = 2\omega_b \omega_w^2 \omega \zeta$,

$$\omega_b = \sqrt{\frac{k_1}{m_b}}, \ \omega_w = \sqrt{\frac{k_2}{m_w}}, \ \zeta = \frac{c}{2m_b \omega_b}, r_m = \frac{m_b}{m_w}, C = \omega^4 - (r_m \omega_b^2 + \omega_w^2 + \omega_b^2)\omega^2 + \omega_w^2 \omega_b^2,$$

and $D = 2\omega \omega_b \omega_w (\zeta \omega_w) - 2\omega^3 (\zeta \omega_b + r_m \zeta \omega_b)$.

In some recent experiments, as Cole (Cole, 2001) notes, the phase angle between the acceleration transferred to the driver's feet from the vehicle body and the acceleration transferred to the driver's body through the vehicle seat has shown a significant effect in the discomfort level as well. However, this effect is not considered in the current version of British standards (BS) or ISO standards, and, hence, not in this thesis.

1.2.4.2 Road Handling Index – Relative Displacement Transmissibility

The relative displacement transmissibility, λ, represents the ratio of the maximum magnitude of the relative displacement to the input displacement as

$$\lambda = \left| \frac{\max(x_r)}{Y} \right| \tag{1-14}$$

For a quarter-car system, this value also reflects the damper (shock absorber) play. In most cases, this is translated to the vehicle's centre of gravity height and is considered as a proper parameter for measuring the road handling performance. In a 1DOF system with a sinusoidal base excitation ($y = Y \sin(\omega t)$), the displacement transmissibility is defined as (Shen, 2005)

$$\lambda = \frac{\omega^2}{\sqrt{(\omega_n^2 - \omega^2)^2 + 4\zeta^2 \omega_n^2 \omega^2}} \tag{1-15}$$

Note that the maximum lateral acceleration, tire-ground interaction, and other parameters interpreted as the handling performance are not the main concern in this thesis.

9

Consequently, as shown in Figure 2-b, in a 2DOF, a system with the harmonic base excitation, the transferred displacement will be defined as (Shen, 2005)

$$\lambda = \frac{\omega^2 \omega_b \sqrt{\omega_b^2 + (2\zeta\omega)^2}}{\Delta} \tag{1-16}$$

where the equation parameters are $\Delta = \sqrt{C^2 + D^2}$, $A = -\omega_b^2 \omega_w^2$, $B = 2\omega_b \omega_w^2 \omega\zeta$,

$\omega_b = \sqrt{\dfrac{k_1}{m_b}}$, $\omega_w = \sqrt{\dfrac{k_2}{m_w}}$, $\zeta = \dfrac{c}{2m_b\omega_b}$, $r_m = \dfrac{m_b}{m_w}$, $C = \omega^4 - (r_m\omega_b^2 + \omega_w^2 + \omega_b^2)\omega^2 + \omega_w^2\omega_b^2$,

and $D = 2\omega\omega_b\omega_w(\zeta\omega_w) - 2\omega^3(\zeta\omega_b + r_m\zeta\omega_b)$

As stated earlier in this section, λ also states the damper stroke. So, $\lambda = \lambda_{\max}$ serves as a constraint in the design of a suspension system.

As discussed already, an interesting aspect of suspension design is the conflict among the different performance indexes in the operating region. For instance, consider equation (1-15) and assume our goal is to reduce the displacement transmissibility of the system. To do so, a theoretical and practical solution might be to increase the damping ratio. It is obvious from equation (1-15) that λ will decrease consequently, as shown in Figure 5-a. As illustrated in this figure, as the damping ratio increases, the acceleration transmissibility, η, decreases (Figure 5-b) up to a certain excitation frequency which depends on the system's characteristics – for instance in case of a 1DOF system, this certain frequency is $\omega = \sqrt{2}\,\omega_n$. Beyond this critical point, for larger damping ratios, as the excitation frequency increases, the acceleration transmissibility approaches infinity.
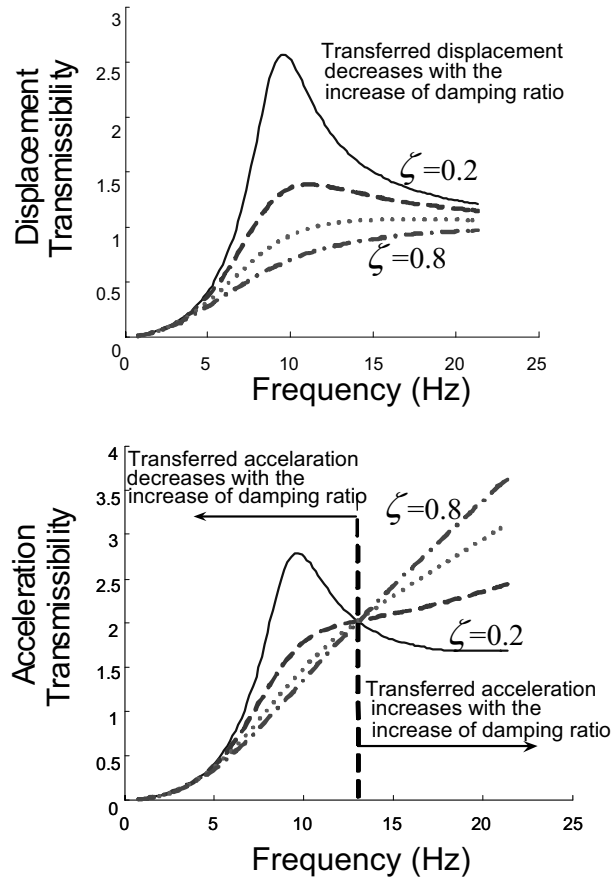
Figure 5: The conflict between two suspension performance indexes: a) Top - displacement transmissibility, b) Bottom - acceleration transmissibility

1.2.4.3 Rollover Stability Index

Rollover propensity is an obvious indication of vehicle instability, and many efforts have been made to develop a practical and comprehensive method to measure it. For instance, Uys (Uys *et al.*, 2006) have investigated through a literature survey different criteria to measure vehicle handling, and in particular rollover. Different criteria such as yaw-rate, lateral-acceleration, roll-angle, and effective-dynamic-wheel-load have been discussed. They performed various tests on three different instrumented vehicles, and, based on the resulting empirical data, the authors strongly suggest that the roll angle is a suitable metric to measure handling. The national highway safety administration (NHTSA) recommends two vehicle stability measures. The first is the static stability factor (SSF), which represents static rollover propensity; it equals half of a vehicle's track width divided by its height at its centre of gravity

$(SSF = \dfrac{T}{h_b + h_r}$, see Figure 3). The second measure is based on the vehicle's dynamic performance on the J-turn and the fishhook maneuver (Uys *et al*., 2006). However, because of the high cost of such tests, analytical and numerical simulation methods are used as much as possible in the design and development process. The challenge is in providing reasonable parameters for this type of analysis and in understanding the range of validity of the computed results (Bernard *et al*., 1991).

Unlike the other two indexes mentioned before, the transient effects are important in rollover propensity, because the rollover may happen over a short period. On the other hand, since rollover is a phenomenon that is happening or not happening, normally a threshold instead of an index is used for the rollover stability. The dynamic threshold for the rollover (DRT) of a vehicle is defined as the moment when the vehicle loses its contact with the ground. A detailed discussion on this subject is presented in Chapter 6.

1.3 Damper and its Roles in Vibration Control and Suspension System

A damper, commonly referred to as shock absorber, is a mechanical device that dissipates energy in the motion direction. The mathematical theory of vibration largely uses the concept of linear damping – with force being proportional to the velocity – mainly because it gives equations for which the solutions are well understood (Dixon, 1999). There is no requirement that a damper must exhibit such characteristics; nevertheless, the typical modern hydraulic damper does so approximately (Dixon, 1999). The most commonly used damper in the industry is the hydraulic damper, which works based on the fluid friction concept. Figure 6 depicts a simple hydraulic damper. The main aspect of the damper as shown in this figure is the energy loss due to the fluid flow through the opening in the piston. Assuming laminar flow, the governing equation of the damper shown in Figure 6 is

$$F = c\frac{dx}{dt}, c = 8\pi\mu L\left[\left(\frac{D}{d}\right)^2 - 1\right]^2 \tag{1-17}$$

where μ is the dynamic viscosity of the fluid.
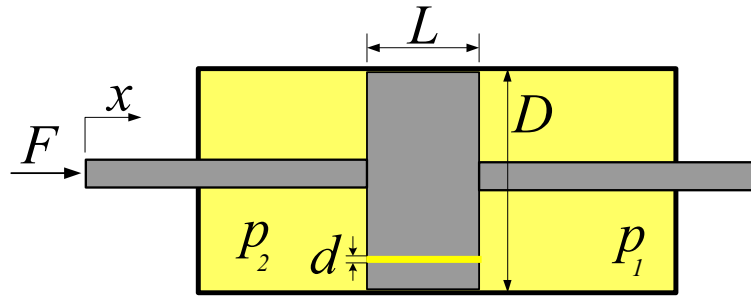
Figure 6: Schematic of a simple hydraulic damper

In an actual industrial damper, the damping effect is created by the fluid passage through a complex series of orifices and adjustable valves, which is normally complicated to model.

Identifying a damper can be immensely complex due to the number of parameters involved in the design process. However, for a normal damper, many of these parameters are standard and may be taken for granted (Dixon, 1999). The primary damper identification parameters are (Dixon, 1999)

- End-fitting
- Stroke range
- Force-velocity curve
- Configuration
- Diameter
- Oil properties
- Corrosion resistance
- Life time and durability
- Cost

Among all these parameters, stroke range, force-velocity curve, configuration, and cost are of extreme importance in the development of new dampers for heavy vehicle application; they are discussed in later chapters.

13

1.3.1 Semi-active Dampers

Semi-active dampers are mechanical (in most cases electro mechanical) control devices with the capability to vary the amount of energy they dissipate using a small source of power. Like hydraulic dampers, they are designed in such a way that controllable force is proportional to the velocity (Preumont, 2002). Such systems extend the possible range of damping characteristics obtainable from a regular (passive) damper. The variable resistance is achievable in a variety of forms, including

- Position controlled valves, such as solenoid valves

- Electrorheological (ER) fluids

- Magnetorheological (MR) fluids

- Piezoelectric actuators

Some of these technologies have already found their way to the commercial vehicles market. Currently available semi-active dampers use the solenoid valves or MR fluids, given their technological advantages and cost efficiency.

The capability to control the damping characteristics in a semi-active damper adds a few important identifying parameters to the list introduced in the previous section, including technology and response time. As a result, in the next sections, a brief overview of the MR fluid technology and solenoid valve technologies is presented; the effect of the response time is the focus of Chapter 5.

1.3.1.1 Magnetorheological Fluid Semi-active Dampers

MR fluid is a non-Newtonian fluid that changes its properties in the presence of a magnetic field. Micron-size iron particles suspended in a carrier fluid (water, petroleum-based oil, or silicon-based oil) align in chain-like structures along the flux lines of a magnetic field, changing the rheological properties of the fluid (Figure 7). Dampers using magnetorheological fluid as the working fluid are disclosed in various U.S. patents, including patent Nos. 5,277,281 (Carlson *et al*., 1992) and 6,131,709 (Jolly *et al.*, 2000). These devices use an electromagnetic coil in close proximity to the magnetorheological fluid flow to create a damping force that is adjustable by the current applied to the coil.
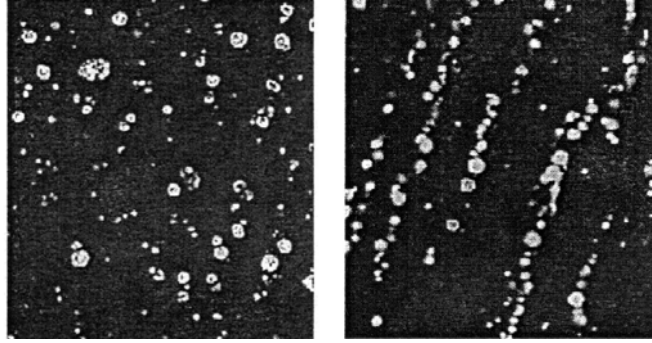
Figure 7: Scanning electron microscope images of iron particles suspended in a non-magnetic matrix in its free state (left), and with a magnetic field applied (right), (Jolly *et al.,* 1998)

Although MR devices are available in different forms and for different applications, their working principle is classified in three categories: flow mode, shear mode, and squeeze mode (Jolly *et al.,* 1999). Figure 8 shows and simplifies all three working modes.
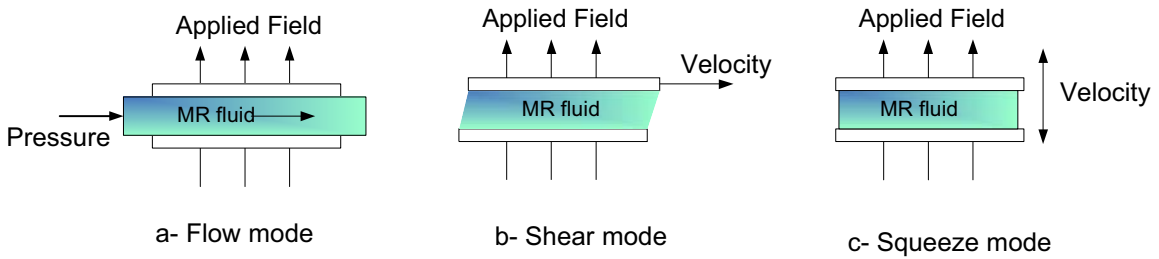
Figure 8: MR fluid working modes (Shen, 2005)

Many research studies have been performed to model the properties of the MR fluids and dampers. A recent and well-received model is that developed by Spencer (1997); this model has used the Bouc-Wen model to analyze the nonlinear hysteresis behavior of an MR damper. The focus of this thesis, in general, is the application of the MR fluids, not the modeling of those systems.

1.3.1.2 Solenoid Valve Semi-active Dampers

In general, the controllable valve requires certain characteristics in order to be useful in semi-active damper applications. The valve must be able to handle at maximum velocity a flow rate corresponding to the volume of displaced fluid in the damper. For heavy-truck and off-road vehicle applications, this

flow rate is much higher than for passenger vehicles. The maximum operating pressure of the valve must also correspond to the maximum pressures found in a passive damper, because of suspension loading. In addition, the controllable valve must have a fast-enough response to cause variations in damping characteristics during operation.

Servo-valves can provide very high speeds, linearity, and accuracy of flow control at high operating pressures. Servo-valves have been used successfully in fully active suspensions which use a hydraulic pump, reservoir, accumulators, etc. and hydraulic cylinders connecting the wheels to the chassis (Milliken, 1988). Unfortunately, servo-valves are very expensive and complicated devices. A typical servo-valve costs US$4200.

Solenoid valves provide an alternative to servo-valves. A solenoid valve does not have as fast or accurate a response as a servo-valve; however, a servo-valve is much more expensive than a solenoid valve. A solenoid valve is much simpler in design than a servo-valve, and it could possibly be manufactured in-house, bringing the added benefit of being able to optimize the valve design for the particular application including force, stroke, and general packaging (Kim *et al.*, 2004). Solenoid valves have also been used in two- or three-state dampers that can change characteristics between hard damping and soft damping by opening or closing a bypass valve. These dampers have resulted in improvements in ride quality when appropriate control schemes are used (Kim *et al*., 2004). Although these dampers do not have the capability of being continuously variable, continuously variable solenoid valve dampers are also available. Solenoid valves of this type have been tested, with promising results (Kitching *et al*., 2000).

One of the disadvantages of solenoid valves is the fact that to provide very accurate proportional damping control, they need to have a precise sense of the valve location at all times. To accomplish this, a linear displacement transducer on the solenoid is required, resulting in an overall more expensive valve.

In the next chapters, the application of this type of damper in the heavy vehicles is discussed, and the proof of concept in presented using the test data obtained from an in-house solenoid valve

1.4 Conventional Semi-active Control Strategies

In general, a controlled system consists of a plant, which is the subject of control; sensors; actuators, discussed briefly in the previous sections; and a control method. Several semi-active control strategies have been proposed and investigated since Crosby and Karnopp (1973) developed the Skyhook control

strategy . The common goal of these initiatives is to achieve a higher level of vibration isolation or to find practical and easy implementation methods, or both. In this section, the most conventional methods are briefly introduced.

1.4.1 Skyhook Control Method

The Skyhook control is an effective vibration control strategy because it dissipates the system's energy at a high rate. A typical Skyhook model is shown Figure 9-a – in some cases, for instance a vehicle, this is not practical. As a result, in many cases the original Skyhook method is modified to the version shown in Figure 9-b. The damping force provided by the damper, c_{sky} , is always opposite to the absolute velocity of m_b . According to the Skyhook working principle, the semi-active on-off control law for a 2DOF system is

$$\zeta_s = \begin{cases} \zeta_{max} & \dot{x}_2(\dot{x}_2 - \dot{x}_1) \geq 0 \\ 0 & \dot{x}_2(\dot{x}_2 - \dot{x}_1) < 0 \end{cases} \qquad\qquad \textbf{(1-18)}$$

For a 1DOF system, the practical control law is

$$\zeta_s = \begin{cases} \zeta_{max} & \dot{x}(\dot{x} - \dot{y}) \geq 0 \\ \zeta_{min} & \dot{x}(\dot{x} - \dot{y}) < 0 \end{cases} \qquad\qquad \textbf{(1-19)}$$

where ζ_s is the controllable damping ratio.

The problem in implementing the Skyhook is that in some applications, especially in the automotive industry, the absolute velocity, $\dot{x}$, is impossible to measure. Many researchers, including Hedrick (Hedrick *et al.,* 1994) and Shen (Shen *et al.,* 2006), have concentrated on this problem.

17

a- Skyhook in theory   b- Skyhook in application
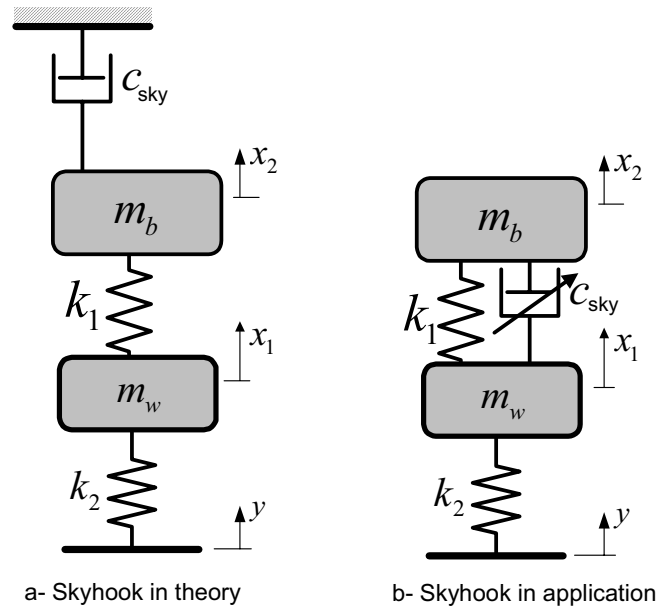
Figure 9: A schematic of the Skyhook control system

1.4.2 Groundhook Control Method

The Groundhook control method is similar to the on-off Skyhook control method, except that control is based on the unsprung mass damping control, as illustrated in Figure 10. The on-off groundhook semi-active policy emulates the ideal-tire-displacement-control-configuration of a passive damper "hooked" between the tire and the "ground." The semi-active on-off control law for a 2DOF system is

$$\zeta_s = \begin{cases} 0 & \dot{x}_1(\dot{x}_2 - \dot{x}_1) \geq 0 \\ \zeta_{max} & \dot{x}_1(\dot{x}_2 - \dot{x}_1) < 0 \end{cases} \qquad \textbf{(1-20)}$$

where ζ_s is the controllable damping ratio.
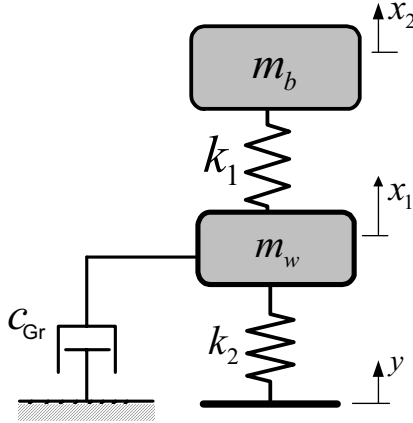
Figure 10: A schematic of the Groundhook control system

1.4.3 Rakheja-Sankar (R-S) Control Method

Rakheja-Sankar (1985) control strategy (which is of the special interest in this thesis) is based on a simple fact, resulting from equation (1-1). The absolute acceleration of the mass based on this equation can be formulated as

$$\ddot{x} = \frac{1}{m}(-F_d - F_k)$$
(1-21)

where F_d and F_k are damping and spring forces, respectively. This equation shows that the damping force in a passive damper tends to increase the mass acceleration when the damping force and the spring force are acting in the same direction. If an ideal semi-active damper is able to produce no damping force, or at least a minimum amount of damping force, when the spring and damping forces are acting in the same direction and produce damping force equal to the spring force when they are acting in different directions, then the mass acceleration and, as a result, the acceleration transmissibility will be minimum. Drawing on this concept, Alanoly and Sankar, (1986) have suggested an on-off control strategy, which for a 1DOF system is expressed mathematically as

$$F_d = \begin{cases} -\alpha k(x-y) & (x-y)(\dot{x}-\dot{y}) \leq 0 \\ 0 & (x-y)(\dot{x}-\dot{y}) > 0 \end{cases}$$
(1-22)

where α is a gain factor.

In practice, it is difficult to have the damping force properly follow the spring force; therefore, the original control strategy developed by Rakheja-Sankar (R-S) (1985) is implemented in the real applications in a modified version. This control strategy is defined as

$$F_d = \begin{cases} F_{\max} & (x-y)(\dot{x}-\dot{y}) \leq 0 \\ F_{\min} & (x-y)(\dot{x}-\dot{y}) > 0 \end{cases}$$
$$F_{\min} = \beta F_{\max}, \quad 0 \leq \beta \leq 1$$
$$F_{\min} \leq F_d \leq F_{\max}$$

$$(1\text{-}23)$$

Assuming the linear damping coefficient, equation (1-23) is re-arranged as

$$\zeta_s = \begin{cases} \zeta_{\max} & (x-y)(\dot{x}-\dot{y}) \leq 0 \\ \zeta_{\min} & (x-y)(\dot{x}-\dot{y}) > 0 \end{cases}$$
$$\zeta_{\min} = \beta \zeta_{\max}, \quad 0 \leq \beta \leq 1$$

$$(1\text{-}24)$$

For a 2DOF system, the above equation will be

$$\zeta_s = \begin{cases} \zeta_{\max} & (x_2 - x_1)(\dot{x}_2 - \dot{x}_1) \leq 0 \\ \zeta_{\min} & (x_2 - x_1)(\dot{x}_2 - \dot{x}_1) > 0 \end{cases}$$
$$\zeta_{\min} = \beta \zeta_{\max}, \quad 0 \leq \beta \leq 1$$

$$(1\text{-}25)$$

where ζ_s is the controllable damping ratio. Equations (1-24) and (1-25) are the R-S control laws.

1.4.4 Limited Relative Displacement (LRD) Control Method

For controlling the relative displacement in this method, a mechanism is required to provide a high damping ratio when the relative displacement is above a specific threshold and a low damping ratio when the relative displacement is below the threshold. This on-off control strategy is expressed as

$$\zeta_s = \begin{cases} \zeta_{\max} & |x_2 - x_1| \geq \delta \\ \zeta_{\min} & |x_2 - x_1| < \delta \end{cases}$$

$$(1\text{-}26)$$

where ζ_s is the controllable damping ratio.

Although this method is capable of controlling the relative displacement and, as a result, lowering the required stroke range of the dampers and springs in a suspension system, it does not offer a better ride

20

quality, which is an improvement of special interest in suspension design in general and this thesis in particular.

1.4.5 Comparison of the Conventional Control Techniques

To gain a better understanding on the effectiveness of the Skyhook and R-S control strategies, the most widely used conventional semi-active strategies, a 1DOF system, has been simulated in MATLAB® / Simulink. Table 1 lists the properties of the simulated system. The indexes introduced in the previous sections – relative displacement transmissibility and acceleration transmissibility – are obtained and compared. Figure 11, the results, shows a significant reduction of transmitted acceleration in higher frequency ranges when the control strategies are in place. At the same time, the amount of displacement transmissibility is slightly changed.

Table 1: The simulated system properties

Item	Value
Mass	5.7 (Kg)
Stiffness	18900 (N/m)
Damping	Variable
Natural Frequency	57.6 (rad/s)

Figure 12 compares the three systems when the controllable damping ratio, ζ_s, for the controlled system is set to be $\zeta_{max} = 0.4, \zeta_{min} = 0$. At the same time, the damping ratio of the passive system is set to $\zeta = 0.4$. As illustrated, in the higher frequency region, R-S and Skyhook have superior performance over the passive system.

® MATLAB is the registered trademark of MathWorks Inc.
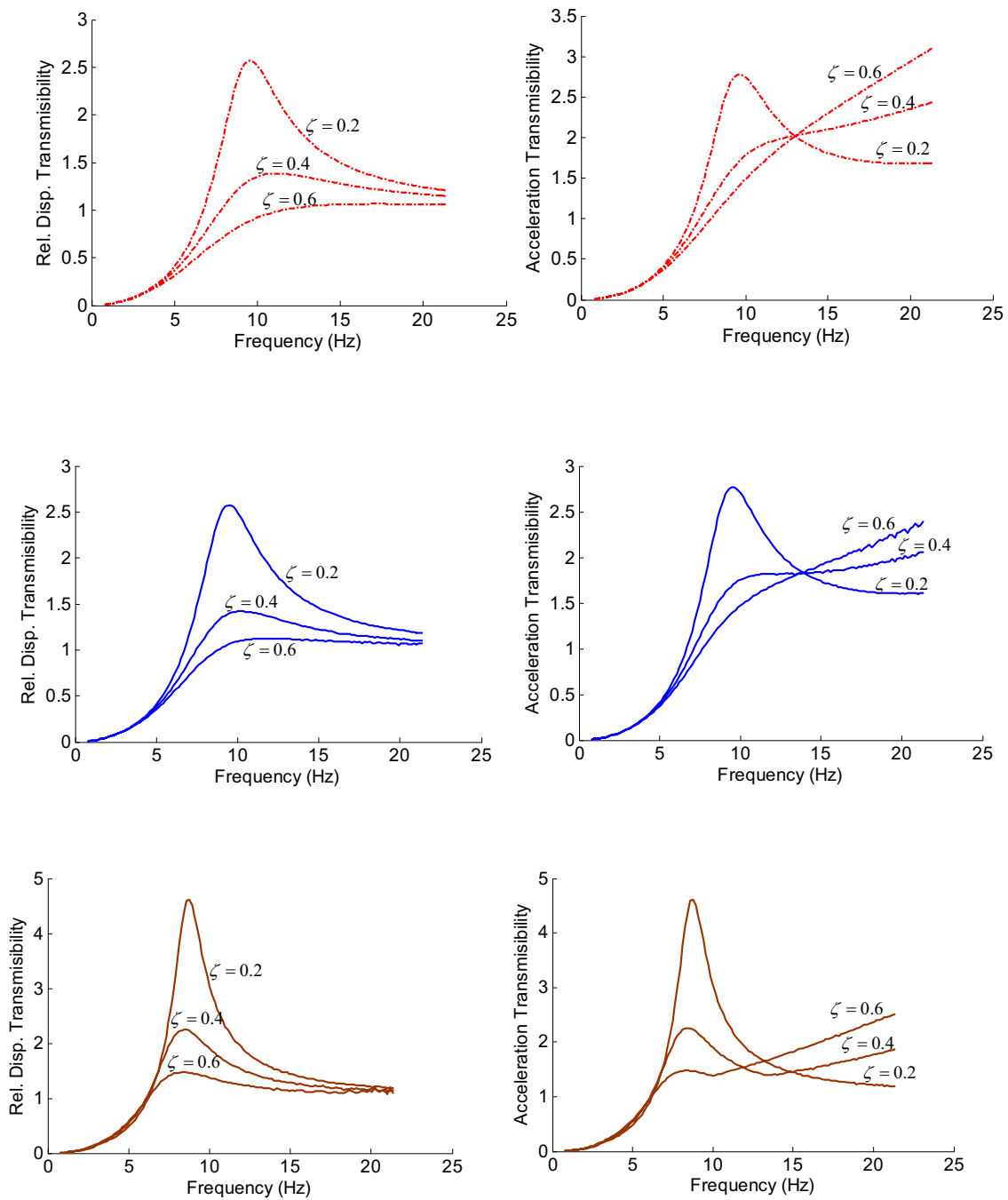
Figure 11: Comparison of passive, Skyhook, and R-S control methods in different damping ratios for a one-degree-of-freedom system simulation. Top: passive system, Middle: Skyhook control method, Bottom: R-S control method.
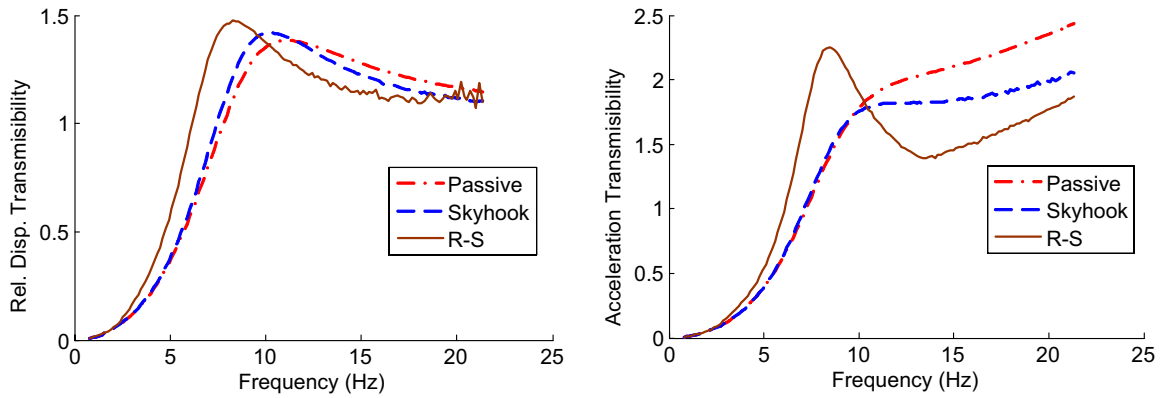
Figure 12: Comparison of the passive system with Skyhook and R-S controlled systems ($\zeta = 0.4$)

1.4.6 Application of Advanced Technologies in Semi-active Control Methods

Although Zadeh developed fuzzy logic in 1965, only in recent years has it been applied to vehicle suspension dynamic control. Among the first application attempts, Al-Holou *et al*. (1996) adopted fuzzy logic to control the vibration of semi-active suspension systems. Although results obtained by fuzzy logic have shown improvement over passive suspension, not much work has been done to compare the results from fuzzy logic controllers with those from other conventional methods (introduced above). In this thesis, a fuzzy logic controller, as well as Skyhook and Rakheja-Sankar controllers, is designed, and results are compared. In addition, since the suspension systems are complex and non-linear in nature, neural network is introduced as a tool to model the properties of an actual semi-active damper.

1.5 Research Motivation, Objectives, and Methodologies

Semi-active suspension systems have shown a significant improvement over the passive systems. Due to this fact, semi-active dampers have been designed and made commercially available; the control strategies have been adopted and implemented to offer superior ride quality to passenger vehicles. However, the technology is still an emerging one, and elaboration and more research work on different theoretical and practical aspects are required. This thesis is an attempt to develop an understanding of some of those aspects, such as the effect of the semi-active dampers response-time on the performance of the control strategies through analytical and numerical methods. On the other hand, the technology has not yet been adopted for heavy vehicles. This attributes to three reasons: first, the un-availability of semi-active actuators (dampers) suitable for peculiar requirements of the heavy and off-road vehicles; second, lack of interest in the manufacturing sector, given that the superior advantages of such systems,

23

for an armored vehicle for instance, are yet to be demonstrated; and third, the possible economical impacts of such systems.

In recent years, research work on improving the semi-active control systems has advanced in four major directions:

- Development of high-performance and low-cost semi-active actuators

- Achieving higher-performance semi-active control methods and algorithms while maintaining the simplicity and cost efficiency of those systems

- Improving the sensing system through the use of integrated sensory structures

- Manufacturing of a high-speed, high-performance, low-cost micro controller

The focus of this thesis is on the first two of these directions.

In this thesis exploring an new technology, a cost-effective semi-active damper that can withstand the punishing, wide-ranging requirements of heavy vehicles is designed, developed, and tested, for the proof of concept. New and innovative damper modeling methods are proposed. Given the data obtained from an armored vehicle – a GPV in fact – the proper control strategies have been developed, and the technical advantages of the technology compared with the passive system have been illustrated. Different aspects of the semi-active controlled systems, such as response-time and frequency-dependent damping, have been analyzed and investigated through analytical methods and numerical studies. Through extensive analytical methods, numerical simulations, and real-time experiments, new control strategies have been proposed, while the simplicity of the conventional control systems has not been altered.

To achieve the research objectives, this thesis makes effective use of different analysis methods, including the nonlinear perturbation techniques, such as method of averaging; numerical studies and simulation processes; and real-time tests and experiments where applicable.

1.6 Thesis Outline

This thesis consists of seven chapters. Chapter 1 provides an insight to the semi-active suspension technology and reviews the background information. It also presents the problem statement and provides a general overview of this research. In Chapter 2, a detailed investigation on the dampers of heavy vehicles is presented. The chapter further discusses the modeling of a passive damper, and validates the

modeling using the empirical data as a basis to develop plans for a new in-house, semi-active damper. Plans to develop and design semi-active dampers are described, and the modeling and prototyping processes are discussed. For proof of concept, the prototype has been tested and the test results are reported. In addition, conventional methods of damper modeling based on the experimental data are discussed, and a new method using the functionality of neural networks to model the dampers is introduced. Finally, to show the performance of the in-house-designed and the prototype dampers, the simulation process is used. The dampers are modeled and their performances are compared with the scaled version of a few commercially available semi-active dampers. Chapter 3 presents an analytical and numerical examination of the on-off semi-active control technique as piecewise linear function and a source of non-linearity in the systems. In this investigation, the method of averaging is adopted to explore the frequency response of semi-active controlled systems at resonance. As a result of nonlinearity, the harmonic frequencies are observed in the frequency response domain. Furthermore, a new method to evaluate the performance of semi-active controlled systems is proposed. In Chapter 4, the idea of the frequency-dependent damping, a generalized version of semi-active damping control, is presented. The analytical method of averaging and numerical simulation are extensively used to analyze the system. A special case, asymmetric damping, is of special interest in this chapter. The effects of asymmetric damping on the suspension performance indexes are investigated. Using the averaging method allows us to analyze the frequency and response-time characteristics of the nonlinear asymmetric system. Optimal damping and stiffness values for the isolator are obtained by minimizing the root mean square (RMS) of the absolute acceleration and the relative displacement as cost functions. The asymmetric damping effects are further used to improve the conventional semi-active controller; to show this, numerical, analytical and experimental data are used and discussed. One aspect of the semi-active controllers that has not been explored in detail in the prior art is the response-time of those systems. Chapter 5 is an attempt to analyse the effects of the semi-active systems response time using numerical simulations, nonlinear analysis, and real-time experiments. A practical method to estimate the proper response-time boundaries for the semi-active controlled systems is proposed. In addition, real-time experiments have been performed on the semi-active controlled systems to find the average response time of the different semi-active actuators. Chapter 6 examines the practical aspect of the semi-active control strategies and proposes applicable control strategies to optimize the vehicle suspension performance. A semi-active neuro-fuzzy control strategy is developed, and the performances are compared with those of the conventional strategies. Using the suspension models presented in the introductory section, a rollover assist controller is also developed, and the performance of the system is

examined using the simulation process. The professional vehicle modeling software, CARSIM, is used in this chapter. Chapter 7 presents the concluding remarks and provides recommendations for future research. Because of the different subject materials presented in this thesis, the literature review related to each chapter is presented at the beginning of that chapter.

Chapter 2

Semi-Active Damper for Heavy Vehicles – Design, Modeling, and Prototyping

"What you need to invent, is an imagination and a pile of junk"

(Thomas Edison)[3]

Modeling of vehicle suspension dampers can range from simple linear models to more complex parametric models. The simplest model is a linear viscous damper, which presents a damping force proportional to the damper velocity (Inman, 2001). Dixon (1999) discusses a parametric model of a dual-tube shock absorber; in this model the force produced by the damper is calculated by determining the fluid pressures. Different nonlinear parametric models of mono-tube dampers have been developed which calculate the fluid pressures based on incompressible fluid flow through valve restrictions (Reybrouck, 1994). Models that are more complex have also incorporated the compressibility of the damper-fluid, resulting in flow rates being no longer proportional to damper velocity (Mollica *et al.*, 1997). The presence of suspended gas in the damper introduces nonlinearity to the fluid-compressibility; this effect has been considered in mono-tube damper models as well (Audenino *et al.*, 1995).

In addition to passive dampers, semi-active damper modeling has also been the centre of attention in recent years. Semi-active dampers with external solenoid valves have been modeled taking into account the flow forces on the valve, but not including variable fluid compressibility (Park and Kim, 2005). Models of the semi-active dampers that take into account the variable fluid compressibility using a constant fluid chamber volume have also been proposed (Kitching *et al.*, 2000). More complex modeling of hydraulic control valves has also been investigated, including variable coil inductance and valve spool dynamics (Elmer and Gentle, 2001) and (Vaughan and Gamble, 1990). Winslow (1947) was the first to patent the MR fluid concept. It was not until the 1980`s that the industrial applications of MR

---

[3] Quoted from: http://www.design.caltech.edu/erik/Misc/design_quotes.html

fluids was developed by industry researchers (Jazar and Golnaraghi, 2002). Peel *et al.* (1996) demonstrated the applicability of MR fluid in vibration isolation. As a follow up, Jolly *et al.* (1996) and Davis (1999) introduced both a mathematical model and a mechanical model by using MR fluids. This subject has resulted in an extensive number of publications. Spencer *et al.* (1997) used the Bouc-Wen hysteresis model to capture the MR damper behaviors – probably the most popular model for MR dampers among the researchers.

   In this chapter, first a passive hydro-pneumatic damper used for the heavy armored and light armored vehicle application is modeled based on a simple linear model and equation (1-17). The damper characteristics are then compared with those of a passenger vehicle damper. Based on the specific requirements for a heavy vehicle, the design constraints are set to develop a new semi-active damper. The design, development of the prototype, modeling of the new semi-active, and finally the tests results are presented. The application of neural networks in semi-active damper modeling is then proposed and discussed. Finally, for the proof of concept, the newly developed damper performance is compared with that of the scaled version of commercially available semi-active dampers.

2.1 Development of a Passive Damper Model and the Model Verification

A commercially available hydro-pneumatic damper is selected and modeled. The damper is manufactured by GKEC[4] (Part No. V-116645) for light armored vehicle applications. Figure 13 is a schematic diagram of a hydro-pneumatic damper, a highly nonlinear device normally used in heavy vehicle applications; the system, categorized as mono-tube damper, is composed of a cylinder containing a gas chamber and two hydraulic fluid chambers (a combination of a gas spring and a passive hydraulic damper). As a result, to model the complete system, two separate models are developed. The first model is intended to capture the gas spring properties and the second model, using equation (1-17) , is intended to model the hydraulic damper. Experimental results are used to validate both models, as well.

---

[4] Due to confidentiality agreements, we are unable to show the detail drawings of the damper in this thesis.

2.1.1 Gas-Spring Model

A gas-spring mechanism, as shown in Figure 14, is simply a cylinder and piston filled with air or nitrogen gas. Considering the initial conditions of the system under the external force F_1 to be P_1, the initial pressure; V_1, the initial volume; and L_1 in equilibrium, the initial position of the piston, then

$$P_1 \times A_1 = F_1 \qquad \text{(2-1)}$$

If the piston is forced to move an absolute displacement, x, then in this new equilibrium point, the governing equation will be

$$P_2 \times A_1 = F_2 + F_1 \qquad \text{(2-2)}$$

Assuming ideal gas properties and, therefore, the perfect gas law, from thermodynamics theory, the following equation will govern:

$$P_1 \times V_1^{\gamma} = P_2 \times V_2^{\gamma} \qquad \text{(2-3)}$$

where γ, the ratio of specific heat, is equal to 1 for an isothermal process and equal to 1.42 if the process is considered adiabatic (Cengel, 1997).
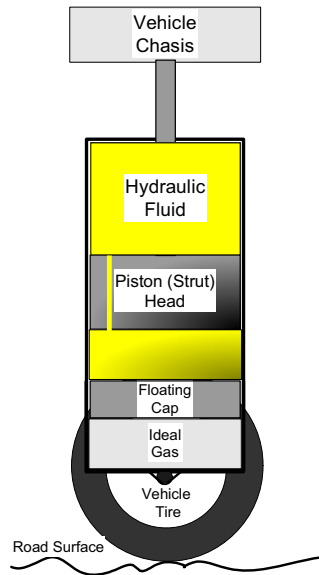
Figure 13: Schematic diagram of a hydro-pneumatic damper

As a result, the equivalent spring force of the gas spring for the isothermal case will be

$$F_2(Isothermal) = \frac{P_1 \times A_1 \times x}{L_1 - x}$$ (2-4)

And for the adiabatic case, the equivalent spring force will be

$$F_2(Adiabatic) = \frac{(P_1 \times A_1) \times ((L_1)^{1.42} - (L_1 - x)^{1.42})}{(L_1 - x)^{1.42}}$$ (2-5)

where $L_1 = \dfrac{V_1}{(\dfrac{\pi D^2}{4})}$
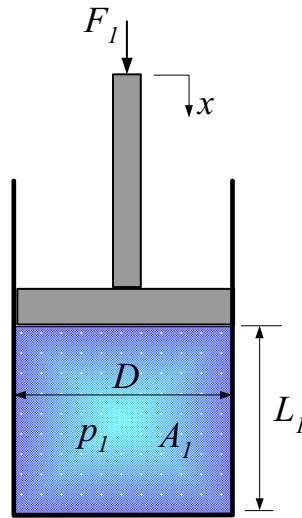
Figure 14: Schematic of the gas-spring system

Figure 15 illustrates the comparison between the two proposed models of gas spring with the same physical parameters and initial conditions. When the piston displacement is small (in the range of 0-0.05 m, the normal range for passenger vehicles), both models follow a similar linear pattern. However, as the piston displacement becomes larger, the case for heavy and off-road vehicles, the nonlinear effects start to dominate, and the models deviate from each other and follow different patterns.
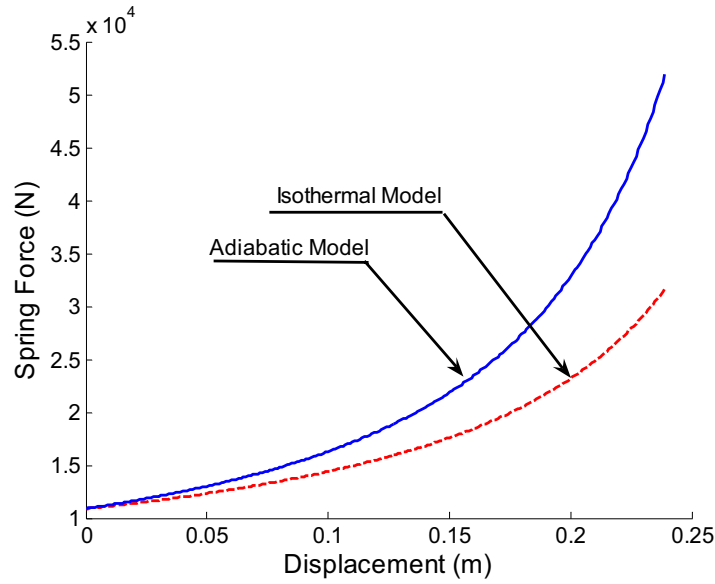
Figure 15: Comparison of adiabatic and isothermal models of spring gas

To validate the model, the physical parameters of the GKEC hydro-pneumatic damper mentioned above were measured. Table 2 summarizes the measured values. Static tests were performed on the hydro-pneumatic damper using an MTS dynamometer; force versus displacement was measured and recorded. Figure 16 compares the test results with theoretical results for the gas spring.

Table 2: Measured physical parameters of GKEC hydro-pneumatic damper

Damper parameter	Measured value
Initial pressure (P_1)	248×10^4 (N/m^2)
Initial Volume (V_1)	0.0011(m^3)
Internal diameter (D)	0.065 (m)
Piston Rod Diameter	0.025 (m)

The test results suggest that the adiabatic model is capable of capturing the gas-spring properties. There is an obvious DC shift between the modeling results and test results. The shift is due to such reasons as friction, errors in initial measurements, and errors in load cell readings.
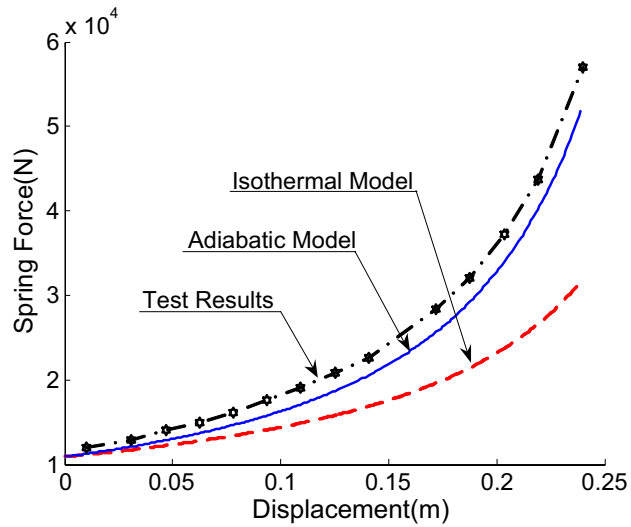
Figure 16: Comparison of experimental results and mathematical models of gas spring

To model the damper side (Eslaminasab *et al.,* 2004) of the hydro-pneumatic damper, the piston (strut) head was first analyzed and modeled. The existing strut head is complicated and contains different sets of spring-valve systems with different operating limits. In addition, the flow passages are different in compression and rebound processes. As a result, the modeling of the damper was divided into four categories. Using the measured physical parameters and equation (1-17), the damping coefficients were calculated and are listed in Table 3.

Table 3: Calculated damping coefficient for the strut head

Item	Damping Category	Speed Limit (m/s)	Calculated damping ratio (kN s/m)
1	Compression - Low speed	$0 < v \le .035$	84.17
2	Compression - High speed	$0.035 < v$	18.50
3	Rebound - Low speed	$0 < v \le 0.075$	97.10
4	Rebound - High speed	$0.075 < v$	14.97

Using these models, a piecewise linear damper model was constructed; the lamped mass model is shown in Figure 17. Based on this model, a series of simulations were performed using the MATLAB/SIMULINK. The real-time experiments were also performed on the hydro-pneumatic damper. The results of numerical simulations and the real-time tests are compared to find out if the simple linear model is capable of predicting the damper behavior. The results are depicted in Figure 18 and Figure 19.
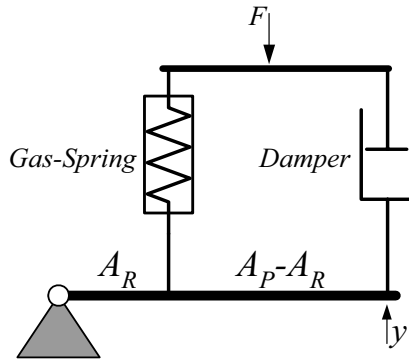
Figure 17: Lumped mass model of hydro-pneumatic damper

In this figure, A_p and A_R are the cross sectional area of the piston and the piston rod respectively.

The tests and the modeling results agree reasonably well; especially in the lower speed ranges (0-0.5 m/s) as illustrated in Figure 19, the model captures perfectly the dampers characteristics. However, in the higher speed ranges (0.5-1.5 m/s) the model loses accuracy, a result attributable to the fact that the simple assumptions on the modeling process are no longer valid in this velocity range. For instance, equation (1-17) is based on the assumption of laminar fluid flow in the damper, and as a result, the modeling loses its credibility as the damper velocity rises. On the other hand, as the velocity rises, the effects of parameters including fluid compressibility and the turbulence in gas spring, which are not of concern in simplified model, change the damper properties significantly.
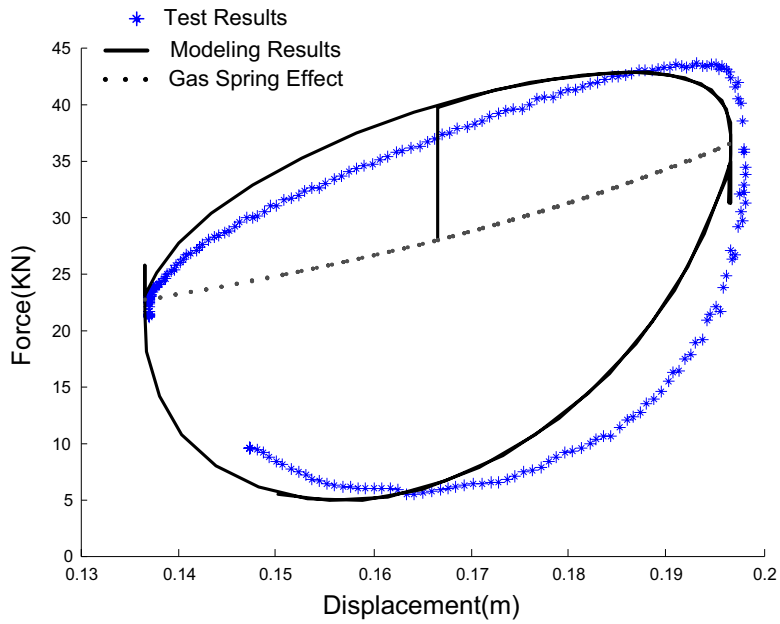
Figure 18: Experimental results versus numerical results for sinusoidal input with maximum velocity of 1.5 *m/s*
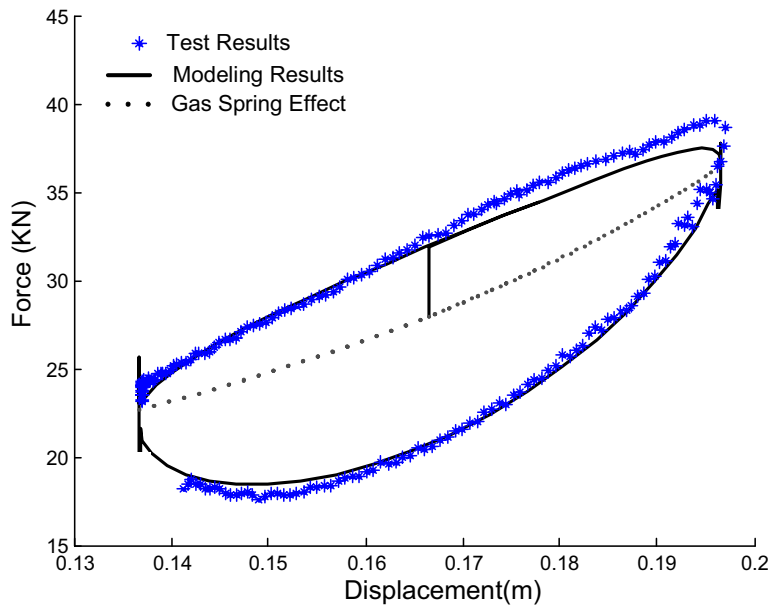
Figure 19: Experimental results versus numerical results for sinusoidal input with maximum velocity of 0.5 *m/s*

The simulation of fluid compressibility effect is shown in Figure 20 (Eslaminasab, *et al.,* 2008). The similarities in force-displacement characteristics of dampers in Figure 18 and Figure 20 confirm that fluid compressibility is a likely source of model deviations in high velocity case.
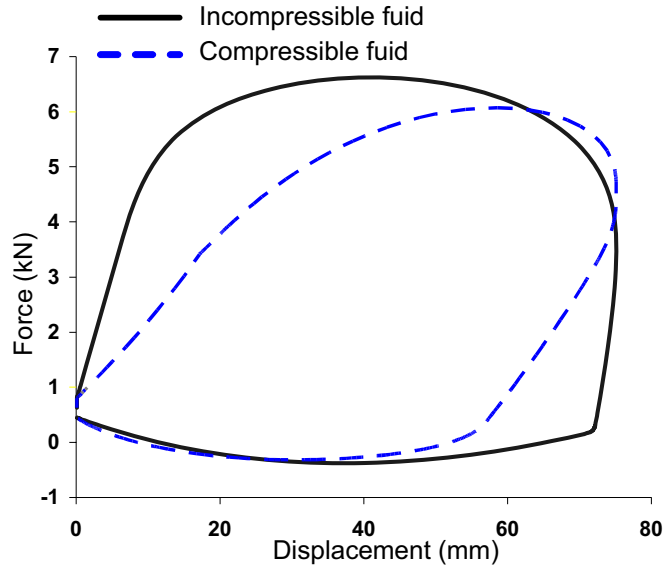
Figure 20 : Effect of fluid compressibility on damper force

This study gives us an insight into the modeling and testing of the heavy vehicle dampers. It also shows the applicability and validity of the modeling process in capturing damper characteristics. In addition, the study shows the force requirements of a heavy vehicle's damper. Based on the numbers shown on Table 3, a typical heavy vehicle damper can produce 18.5 kN and 14.9 kN of damping force in compression and rebound, respectively.

2.2 Development of Semi-Active Dampers for Heavy Vehicle application, Analysis and Prototyping

As stated earlier, the semi-active damper is an essential part of a controllable suspension system. Unfortunately, study of the prior-art has shown there is no commercially available damper for heavy-vehicle applications despite the existence of the technology; therefore, four possible routes were planned to design and develop the semi-active damper; these are as follows: 1) an internal embedded solenoid operated valve semi-active damper, 2) an internal MR operated valve semi-active damper, 3) a full-scale MR semi-active damper, and 4) an external solenoid valve semi-active damper. Among all the design

parameters introduced earlier, two were identified as the most important: cost requirements and force-velocity requirements.

Plan 3 has previously been adopted and manufactured for passenger vehicle applications. However, due to the amount of MR-fluid required for a heavy vehicle damper (nearly 2 liters) compared with that required for a passenger vehicle damper (typically 0.5 liters), and due to the cost of MR-fluids ($600/liter) (Kim *et al.,* 2004), the plan does not meet the very first and most important constraints of the design, and therefore it was abandoned. Plan number 4 has also been successfully implemented for the passenger vehicles. The major challenge was to find a proper solenoid valve capable of handling a flow rate corresponding to the volume of displaced fluid in the damper at its maximum velocity. For heavy-truck and off-road-vehicle applications, this flow rate is much higher than for passenger vehicles.

On the other hand, plans 1 and 2 are innovative and have not been designed or implemented to date. They are cost-effective and easy-to-implement solutions. The internal semi-active valve can be installed in a mono-tube damper as well as a twin-tube damper. Figure 21 depicts the internal valve concept, installed in a mono-tube damper.

Figure 21: Internal valve installed in a mono-tube damper

In the next section, the internal solenoid valve concept, plan 1, is studied in detail. The governing equations are derived and the prototype test results are presented for the proof of concept.

2.2.1 Development of Internal Solenoid Valve Semi-Active Damper

The prototype damper (Kim *et al.,* 2004) was developed based on a unique proportional valve design installed inside a piston with a 63.5-mm (2-1/2") bore and 25.4-mm (1") rod diameter. The prototype uses an existing twin tube damper manufactured by General Kinetics Engineering Corporation (GKEC). Figure 22 shows a cross section of the prototype damper. The semi-active piston 6 is located inside the inner tube "3". The foot valve "9" separates the compression chamber "8" from the reservoir chamber "7". The oil reservoir chamber lies between the inner tube and the outer tube "2" and is separated from the gas chamber "4" by an annular sliding plug called "5". A valve at the end of the gas chamber "1" allows for charging the gas pressure. The foot valve – having a foot valve is the main difference between dual and mono tube dampers – in this damper contains two separate poppet valves for compression and rebound cases. The oil is forced through either the compression path or the extension path of the foot valve depending on flow direction, with the compression direction providing the greater force.

Item no.	Description
1	Gas charge opening
2	Outer tube
3	Inner tube
4	Gas chamber
5	Annular sliding plug
6	Semi - active piston
7	Reservoir chamber
8	Compression chamber
9	Foot valve
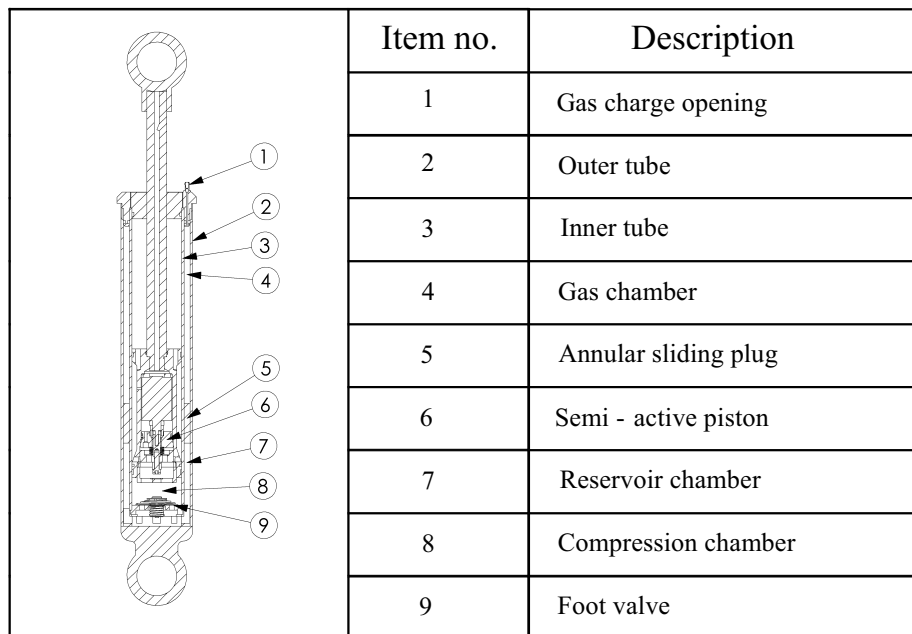
Figure 22: The prototype section view and part list

The semi-active valve is located inside the piston as shown in cross section in Figure 23. The hydraulic fluid path in compression first enters the piston through large holes in the piston cap "17". Next, the fluid passes around the outer edge of the valve disc "15", which is the main flow restriction, and outwards radially through eight holes "14" leading to the space between the piston and the inner

tube "11". Next, the fluid flows along the outside of the piston and through another set of holes at the top of the piston that lead to the extension chamber.

The valve disc is mounted at the end of the valve shaft "12". A seal around the shaft prevents fluid from entering the solenoid chamber, which remains at atmospheric pressure. The solenoid "10" is a push type that exerts a pushing force on its plunger when energized.

The solenoid pushes against the valve shaft to close the valve. The valve spring "13" is located over the valve shaft to assist the solenoid to close the valve.
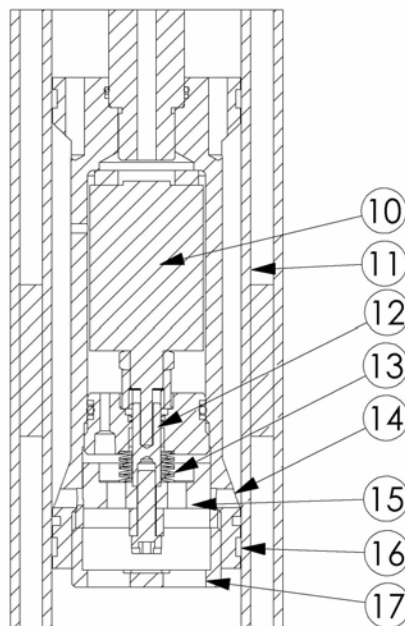
Figure 23: Internal solenoid valve detail

2.2.1.1 Internal solenoid valve concept and modeling

The ultimate goal of the modeling discussed in this section is to find a parametric relation between damper velocity and the solenoid valve current to the damping force such that the performance of the damper could be analyzed and different parameters and parts (such as orifice size or solenoid force) could be fine-tuned. To simplify the modeling process, the model is divided in two parts. In the first part of the modeling, the fluid flow and pressure balance equations for the damper piston are derived. The second part concerns the modeling of the solenoid and the internal valve system inside the piston.

38

Figure 24 shows the free-body diagram of the piston and the applied forces due to the damper movement as a result of an external force (F_{damper}) and generated pressure difference. The equation of motion for the piston is

$$F_{damper} = F_{compression} - F_{extension} + F_{friction} + M\ddot{x} \tag{2-6}$$

where the compression chamber force ($F_{compression}$) is

$$F_{compression} = P_C A_P = P_C \pi R_P^2 \tag{2-7}$$

where P_C is the compression chamber pressure, A_P is the piston area, and R_P is the piston internal radius. The extension chamber force ($F_{extension}$) is

$$F_{extension} = P_E \left(A_P - A_R \right) = P_E \left(\pi R_P^2 - \pi R_R^2 \right) \tag{2-8}$$

where P_E is the extension chamber pressure, A_R is the piston rod area, and R_R is the piston rod radius. Note that both P_E and P_C are gauge pressures.

The friction force ($F_{friction}$) is considered to be of constant magnitude "F_f" and it opposes the motion of the piston.

$$F_{friction} = F_f \left(\frac{|\dot{x}|}{\dot{x}} \right) \tag{2-9}$$

Therefore, equation (2-6) is re-written as

$$F_{damper} = P_C \pi R_P^2 - P_E \left(\pi R_P^2 - \pi R_R^2 \right) + F_f \left(\frac{|\dot{x}|}{\dot{x}} \right) + M\ddot{x} \tag{2-10}$$

To predict the damping force from this equation, the model must determine the fluid pressure in the compression chamber, P_C, and in the extension chamber, P_E.

F_{damper}

x

$F_{extension}$

M

$F_{compression}$ $F_{friction}$
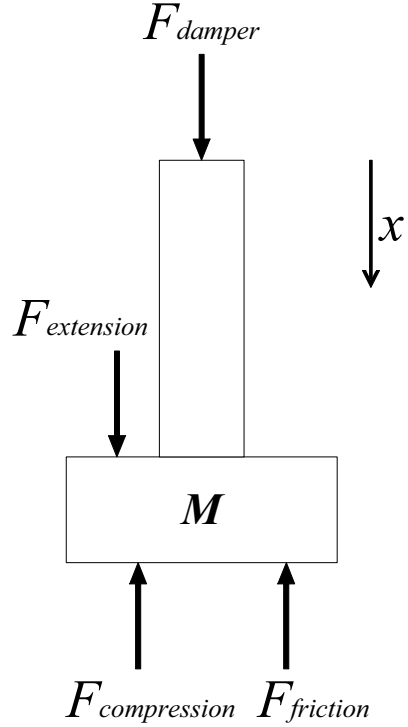
Figure 24: Piston free-body diagram

2.2.1.1.1 The Compression and Extension Chamber Pressures, P_C and P_E

To derive the equations for pressure calculations, the fluid flow inside a twin-tube damper should be reviewed. Figure 25 shows a schematic diagram of this type of damper; there are two different fluid passages. Due to the movement of the piston in x direction, part of the fluid flows from the compression chamber to the extension chamber. The second portion of the fluid flows from the compression chamber into the reservoir through the foot valve. This flow compresses the trapped gas, normally pressurized nitrogen, inside the gas chamber.

The gas chamber pressure (P_{gas}) is calculated based on the adiabatic model (equation (2-5)) as derived and validated in section 2.1.1. As a result, the gas chamber pressure is

$$P_{gas} = P_{0gas} \left(\frac{V_{0gas}}{V_{0gas} - x\left(\pi R_R^{\,2}\right)} \right)^{1.4} \qquad (2\text{-}11)$$

where P_{0gas} is the initial gas chamber pressure, V_{0gas} is the initial gas volume, and x is the piston movement.

40
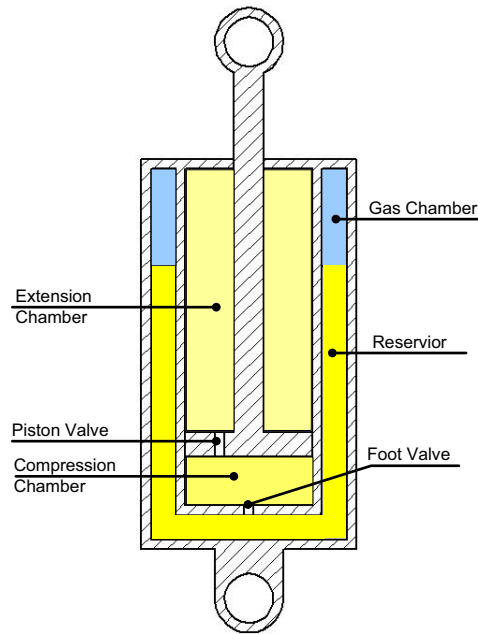
Figure 25: Schematic drawing of a twin-tube damper

The pressure exerted by the gas chamber is opposed directly by the fluid pressure in the reservoir. Therefore, the reservoir pressure (P_{RV}) is assumed equal to the gas pressure:

$$P_{RV} = P_{gas} \tag{2-12}$$

Between the reservoir and the compression chamber, is the foot valve, which provides a substantial proportion of the damping force in most twin-tube dampers (Dixon, 1999). Normally, this type of spring-actuated valve has three operating modes per flow direction: closed, opening, and fully opened. At low velocities, the pressure drop across the valve is small and there is not enough force to open the valve. The valve-closed mode still allows some fluid to pass through small slots in the valve seat. In this mode, the valve acts as an orifice with a fixed area that corresponds to the slots. Generally, the orifice equation relates the flow rate "Q" to the pressure drop across an orifice. For the existing foot valve used in this prototype, this relation has been identified as shown in Figure 26.
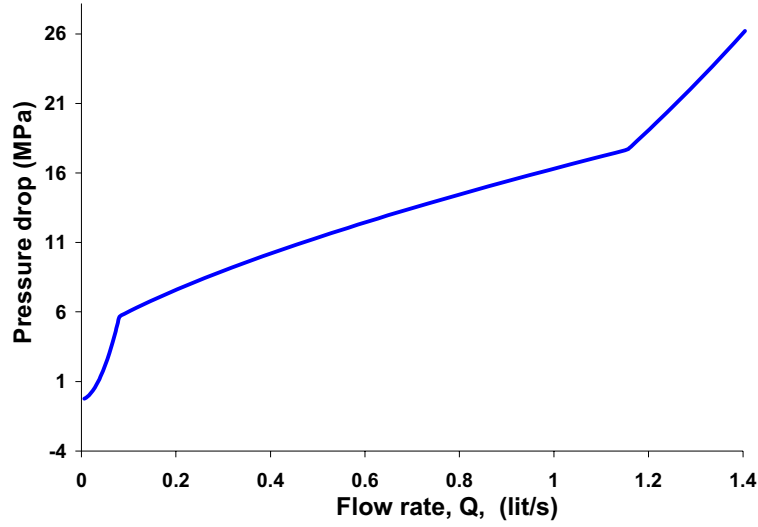
Figure 26: Flow-rate and pressure-drop relation for the prototype foot-valve in compression cycle

This relation can be translated mathematically as

$$Q_{FV} = C_{FV}\Delta P = C_{FV}(P_C - P_{RV})$$
$$\begin{cases} C_{FV} = C_{1FV} & if \quad Q_{FV} \ is \ low \\ C_{FV} = C_{2FV} & if \quad Q_{FV} \ is \ medium \\ C_{FV} = C_{3FV} & if \quad Q_{FV} \ is \ High \end{cases} \qquad \textbf{(2-13)}$$

where Q_{FV} is the foot valve flow-rate and C_{FV} is the foot valve discharge coefficient.

On the other hand, the foot valve floe-rate is equal to

$$Q_{FV} = A_R \dot{x} \qquad \textbf{(2-14)}$$

and as a result of the above equations – that is (2-12), (2-13), and (2-14) – the compression chamber pressure becomes

$$P_C = P_{gas} - \frac{A_R \dot{x}}{C_{FV}} \qquad \textbf{(2-15)}$$

Between the compression chamber and the extension chamber are the piston valve and the internal solenoid valve damper. Considering that the valve is acting like an orifice, the relation between flow-rate and pressure difference can be determined based on the following equation:

$$Q = A_{orifice}C_d\sqrt{\frac{2|\Delta P|}{\rho}} = A_{orifice}C_d\sqrt{\frac{2|P_E - P_C|}{\rho}} \qquad \textbf{(2-16)}$$

where C_d is the orifice discharge coefficient, $A_{orifice}$ is the valve orifice area, ρ is the fluid density, and ΔP is the pressure drop across the orifice. For the internal solenoid valve, if the values for the valve orifice area and the discharge coefficient are determined, then the extension chamber pressure, P_E, can be calculated.

2.2.1.1.2 Internal Solenoid Valve Model

Figure 27 shows the free-body diagram of the valve disc and the applied forces. The major forces acting on the valve disc are

- Pressure force ($F_{pressure}$) due to the pressure difference generated by piston motion
- Fluid flow force ($F_{fluid\ flow}$) due to the fluid direction change and, as a result, change of fluid momentum
- Spring force (F_{spring}) due to the existence of balancing springs
- Force generated by solenoid ($F_{solenoid}$) due to the existence of push type solenoid
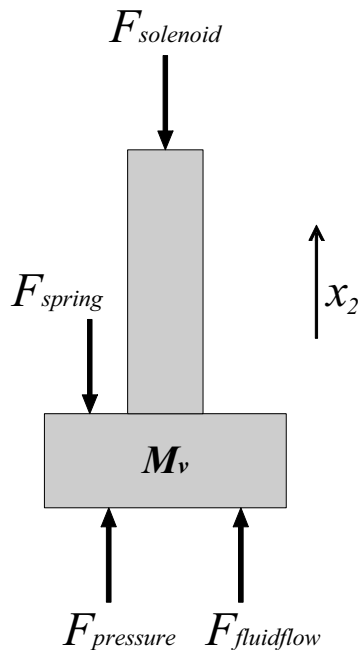
Figure 27: Valve disc free-body diagram

$$F_{spring} + F_{solenoid} - F_{fluidflow} - F_{pressure} + M_v \ddot{x}_2 = 0 \qquad \text{(2-17)}$$

In the next sections, each force is modeled and then the total dynamic valve model is built.

2.2.1.1.2.1 Modeling of Pressure Force ($F_{pressure}$)

To simplify the modeling, it is assumed that the orifice by itself is perfectly made and there is no leaking or gap in the valve while it is fully closed. On the other hand, all the leaks and the pre-set opening in the valve are modeled as a secondary flow pass parallel to the original orifice. In this case, the fluid flow in the orifice region is governed by

$$Q_{TV} = Q_1 + Q_2 \qquad \text{(2-18)}$$

where Q_1 is the portion of the fluid passing through the orifice valve and Q_2 is the fluid passing through the secondary flow pass (due to the possible leakage and the gap).

To develop the equations of the fluid flow through the valve orifice, a closer look at the unique valve disc design is necessary. Due to the force exerted by the valve spring, and the solenoid when it is energized, in the absence of fluid flow the valve disc will be located in its closed position. When the pressure on one side of the valve-disc rises in a compression or extension stroke cycle, a force is being applied; this force should act to open the valve. The valve opening due to the compression or extension cycle force is accomplished through the use of differential areas and the manufactured steps (See Figure 28) on either side of the valve disc.
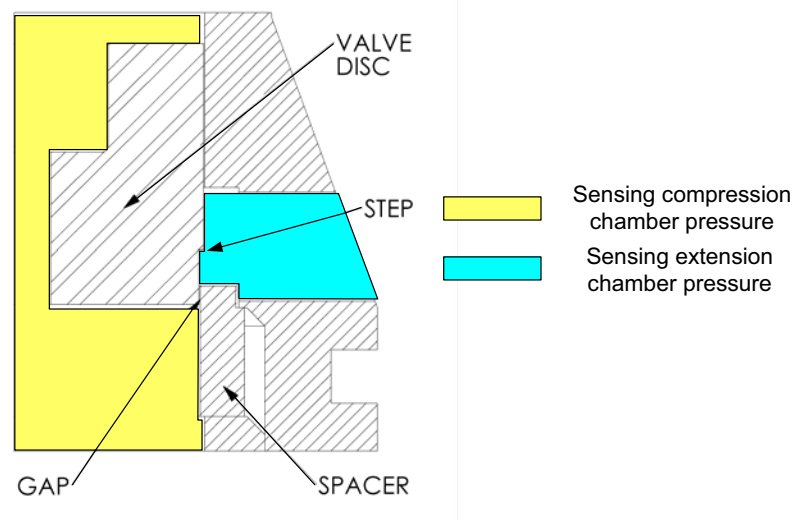
Figure 28: Detailed view of the solenoid valve section (see Figure 23 for the valve assembly)

44

Figure 28 shows a close-up view of the edge of the valve disc and its position relative to the radial holes in the piston. A spacer ring is in place by the piston cap and creates the flow restriction between the disc and the spacer. The small step in the side of the disc is located such that the extension-chamber-side-fluid pressure acts upon it. This design allows pressure build-up on each side of the flow restriction to push the valve open, yet maintains control over the relative strength of that pressure.

The operation of the valve during the compression cycle is as follows: As the damper is compressed, the pressure in the compression chamber builds up relative to the pressure in the extension chamber. The compression chamber pressure acts on both sides of the valve disc (see Figure 28) because of the large holes through it, but it does not act on the outer edge of the disc and the disc step, which is downstream of the flow. The force on the shaft side of the valve disc is equal to the compression chamber pressure, P_C, multiplied by the shaft side area of the valve disc minus the cross-sectional area of the shaft.

$$F_{shaft\_side} = P_C \left(\pi R_{disc\_back}^2 - \pi R_{valve\_shaft}^2 \right)$$
(2-19)

where R_{disc_back} is the radius of the shaft-side of the valve disc and R_{valve_shaft} is the radius of the valve shaft.

The force on the compression chamber side of the valve disc is equal to the compression chamber pressure multiplied by the compression chamber-side area of the valve disc. This area is equal to the shaft side area minus the area taken up by the step on the outer edge of the disc.

$$F_{compression\_side} = P_C \left(\pi R_{disc\_front}^2 \right)$$
(2-20)

where R_{disc_front} is the radius of the compression chamber side of the valve disc.

The area taken up by the step, which is the difference between the back and front areas of the valve disc, is designed to be equal to half of the cross-sectional area of the valve shaft.

$$\pi R_{disc\_back}^2 - \pi R_{disc\_front}^2 = \frac{1}{2} \pi R_{valve\_shaft}^2$$
(2-21)

Therefore the force due to the compression chamber pressure acting on the valve disc to open it is equal to the compression chamber pressure multiplied by half of the cross sectional area of the valve shaft.

$$F_{compression\_pressure} = P_C \left(\pi R_{valve\_shaft}^2 \right) - P_C \left(\pi R_{disc\_back}^2 - \pi R_{disc\_front}^2 \right) == \frac{1}{2} P_C \left(\pi R_{valve\_shaft}^2 \right) \qquad \text{(2-22)}$$

On the extension chamber of the valve, the pressure is acting on the outside edge of the valve disc (see Figure 28). This means that that pressure is applied over the area of the step in order to create a force that tends to open the valve.

$$F_{extension\_pressure} = \frac{1}{2} P_E \left(\pi R_{disc\_back}^2 - \pi R_{disc\_front}^2 \right) = \frac{1}{2} P_E \left(\pi R_{valve\_shaft}^2 \right) \qquad \text{(2-23)}$$

where P_E is the pressure in the extension chamber.

Since the step area is half of the shaft area, both the upstream and downstream pressures are acting over the same area. This means that the net force acting to open the valve due to pressures on either side of the valve can be calculated as the pressure drop across the valve multiplied by half of the valve shaft cross-sectional area, and is always pushing the valve to open.

$$F_{pressure} = \frac{1}{2} \pi R_{valve\_shaft}^2 \left| P_C - P_E \right| \qquad \text{(2-24)}$$

This relation reveals two interesting aspect of the design and modeling. First, it shows that the valve disc will always be pushed in the x_2 direction in both compression and extension cycles. Second, it shows that if the pressures in the compression and extension chambers are known, then the fluid pressure force can be easily calculated.

It is possible to calculate the compression chamber pressure using equations (2-6) to (2-16). To calculate the extension chamber pressure, P_E, an extra relation is required. To do so, using equations (2-18) and (2-16) and considering the fact that the total valve flow "Q_{TV}" is proportional to the damper velocity with the following equation

$$Q_{TV} = \dot{x} \left(\pi R_P^{\,2} - \pi R_R^{\,2} \right) \qquad \text{(2-25)}$$

the equation for Q_1 will be

$$Q_1 = A_{Valve} C_d \sqrt{\frac{2 \left| P_E - P_C \right|}{\rho}}, \quad A_{Valve} = 8 \times \cos^{-1}\left(\frac{r_{hole} - x_2}{r_{hole}} \right) - \left(r_{hole} - x_2 \right)\sqrt{x_2 \left(2 r_{hole} - x_2 \right)} \qquad \text{(2-26)}$$

an equation derived from the geometry of the valve; the number 8 in the equations refers to the 8 holes around the valve, and r_{hole} represents the radius of these holes (refer to item no.14 in Figure 23 above) .

In addition, the equation for Q_2 becomes

$$Q_2 = A_2 C_d \sqrt{\frac{2|P_E - P_C|}{\rho}}, \ A_2 = \pi R_{equivalent}^2 \qquad \text{(2-27)}$$

where $R_{equivalent}$ is the equivalent orifice radius for the secondary flow passes, including the valve gap (Figure 28) and any possible leakages.

2.2.1.1.2.2 Modeling of other forces ($F_{fluid\ flow}, F_{spring}, \ F_{solenoid}$)

The fluid force "$F_{fluid\ flow}$" is generated as a result of the change in the direction of fluid flow as well as the change of momentum,. The magnitude of this force is calculated using the following equation:

$$F_F = \rho Q_{TV} v_{Fluid} \cos(\theta) \qquad \text{(2-28)}$$

in which the angle θ is the change in fluid direction, which is considered to be 69° for the regular orifice (McCloy and Martin, 1980). For the case of the internal valve, and because of the many unknowns about the fluid characteristics, the fluid force is assumed to be negligible and is not considered in the equations.

The spring force "F_{spring}" is modeled as a linear force which produces a force proportional to the valve displacement.

$$F_{spring} = k_v x_2 \qquad \text{(2-29)}$$

where k_v is the valve spring stiffness. The stiffness of the spring used in the valve is a variable, which has to be selected based on the valve modeling and the valve geometry.

The force generated by solenoid "$F_{solenoid}$" is a function of the selected solenoid for this application and will be given by the solenoid manufacturer; the selection of a proper solenoid for this application is one of the main goals of the simulation and modeling.

2.2.1.2 Internal solenoid valve simulation

It is possible to predict the valve behavior and to determine the unknown parameters of interest using equations (2-6) to (2-27) in a series of simulations. There are many parameters in the simulation process, some of which are pre-set and/or the known physical parameters mentioned in Table 4. On the other hand, the goal of the modeling and simulation is to determine a few of the unknown parameters of the system using trial and error effort. Such parameters include the solenoid valve disc springs, solenoid force, and the gap size (refer to Figure 28).

47

Table 4: The internal solenoid valve damper parameters

Item	Notation	Description	Value
1	A_P	piston area	0.00315(m²)
2	R_P	piston internal radius	0.0317(m)
3	A_R	piston rod area	0.00051(m²)
4	R_R	piston rod radius	0.0127(m)
5	$P_{0\,gas}$	initial gas chamber pressure	1379(kPa)
6	$V_{0\,gas}$	initial gas volume	0.0019(m²)
7	C_{FV}	foot valve discharge coefficient	Varies (As shown in Figure 26)
8	C_d	orifice discharge coefficient	0.6
9	ρ	fluid density	875 (kg/ m³)
10	R_{valve_shaft}	radius of the valve shaft	0.0048(m)
11	r_{hole}	radius of valve holes	0.0032(m)
12	M	piston and rod mass	4.0(kg)
13	M_v	valve disc and valve shaft mass	0.1(kg)

The damper model is numerically simulated using Matlab Version 7. The program is developed to simulate a typical test done on a damper dynamometer and it displays the results. In the program, the constant system parameters (mentioned in Table 4) were first initialized. In addition, the test conditions including the input displacement amplitude and peak velocity were initialized. The program runs a series of simulations at different peak velocities. Each simulation consists of one compression/extension cycle of the damper starting from the fully extended position under a sinusoidal input displacement. The simulation inputs are the damper displacement and the damper velocity as follows:

$$x = -A\cos(\omega t) + A_0 \tag{2-30}$$

$$\dot{x} = A\omega\sin(\omega t) \tag{2-31}$$

The simulation process starts with the calculation of the gas chamber pressure (equation (2-11)) and continues with the calculation of the pressure drops across each valve by finding the differences between the pressures already solved. Then the flow rates through the valves are calculated by solving equations (2-25) to (2-27). The damper force is then calculated using equation (2-10) with the calculated pressures

and acceleration. An offset weight is also added to the damper force that allows the simulation to match previously recorded test data in which load cell measurements contain an offset due to the weight of the damper. Figure 29 shows a sample of the simulation results.
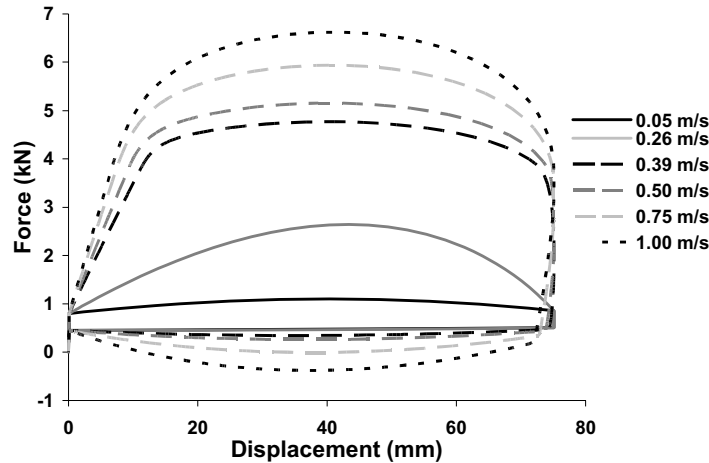
Figure 29: A sample of simulation results

In this figure, each curve represents a different forcing frequency with a different peak velocity, clearly showing the differences in damping force in compression and extension. The extension force is much smaller than the compression force. During the various simulations, other parameters of interests were changed and different outputs of the system were constantly controlled. For instance, to find a proper design value for the gap size, simulations were performed with different gap sizes and an acceptable range was determined. Figure 30 shows one of these simulations while the gap size was pre-set to zero. In this case, as seen from the figure, the valve disc experienced a large displacement at the start of the simulation cycle and it took a long time (nearly 50 seconds) for the valve disc to settle, which is an undesired behavior.
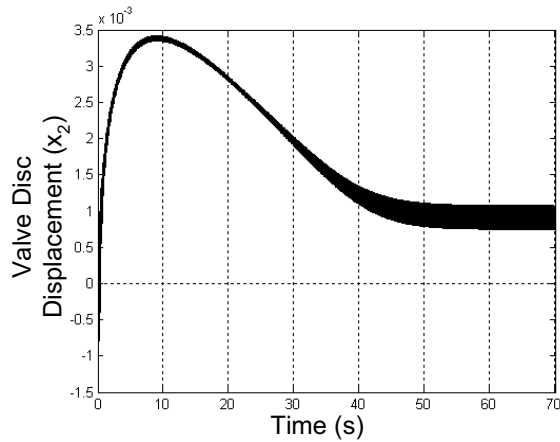
Figure 30: Valve disc displacement while the gap is pre-set to zero

The other goal of the simulation and modeling, as discussed above, is to find out the force of the solenoid and the valve disc spring required to control the valve position. To calculate this value, a series of simulation was performed in which the valve disc was set to be fixed ($x_2 = $ constant). Figure 31shows a sample of these simulations for the case where x_2 is equal to 0.5 mm and the gap is set to be 0.2 mm. As shown, the maximum spring and solenoid force is estimated to be around 450 N and 200 N in the compression and rebound cycle, respectively.
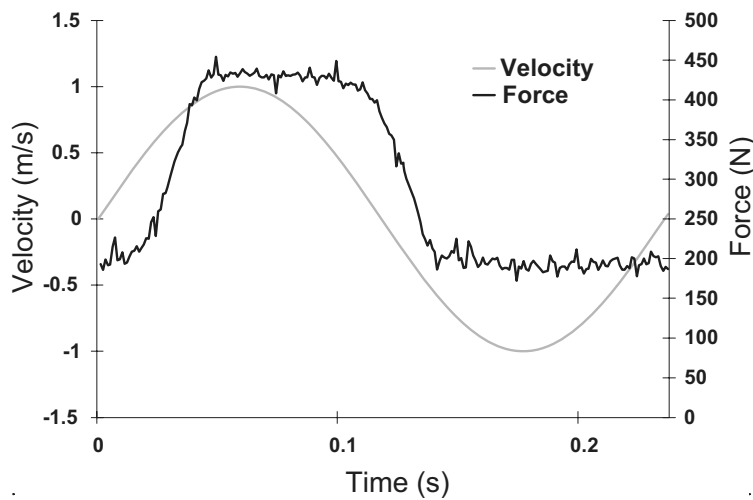
Figure 31: A sample of damper-simulation results showing the required solenoid force

It is possible to calculate the gap size and the range of the solenoid and the valve spring forces using the simulation results. Because the solenoid and valve disc springs should be ordered externally however, a set of tests were designed and performed to confirm the outcome of the simulations and to finalize the required solenoid and valve spring properties.

2.2.1.3 Internal solenoid valve load cell experiments

As described earlier, the damper model is divided into several states to facilitate identification of the variation of the piston-valve discharge parameter. The testing of the damper is similarly divided into several tests. Each test records the force produced by the damper while the piston valve is set in place at a particular opening displacement. This testing process provides information similar to that which could be measured using a dedicated hydraulic flow bench. Unfortunately, the equipment for a hydraulic flow bench test of this scale was not accessible at the time of this research and, as a result, this innovative method of testing was designed and performed. The measured damper force can be used to determine the discharge coefficient of the piston valve; however, the force exerted against the valve disc due to the pressure drop and the flow momentum would remain unknown. In order to measure this force, a special load cell mount was designed which allowed a small load cell to be placed inside the piston to measure the flow forces. The load cell used was a Sensotec model 53 miniature-compression load cell with a load range of up to 2200 N. This load cell achieves a maximum non-linearity of ±0.25% full scale, a maximum hysteresis of ±0.3% full scale, and a maximum non-repeatability of ±0.1% full scale. This particular load cell has a calibration factor of 1.869 mV/V at 2200 N with an excitation of 10.0 Volts DC. The load cell was mounted inside a steel housing having the same size and shape as the solenoid. The load cell and housing system is shown in a cross section in Figure 32.

The testing was performed at the General Kinetics Engineering Corp. test laboratory in Brampton, Ontario. The damper was tested on an MTS damper dynamometer with a maximum velocity of 2.5 m/sec and a maximum load of 89 kN, connected to a MTS Test Star II controller. The gas chamber was charged to a pressure of 1379 kPa. A static test of the damper was performed to measure the effects of compressing the gas chamber on the damper force. In the static test, the damper was manually compressed by increments of 10 mm and the damper force was recorded. This test was used to compare the actual damper force with the force predicted by the formula for the compression of an ideal gas, as in equation (2-11).

The dynamic test program tests the damper at various velocities. This program specifies a series of sinusoidal compression and extension strokes of the damper with constant amplitude of 75 mm. The damper is excited at seven different frequencies from 0.21 Hz to 4.25 Hz. The time, displacement, velocity, and load measured were recorded at a frequency of 600 times per cycle.
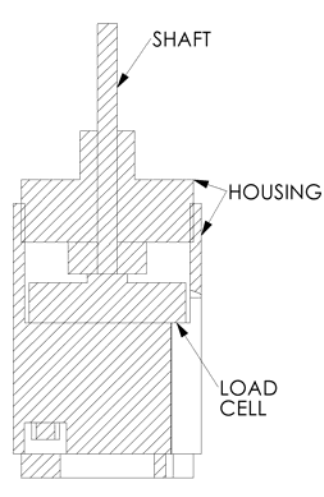
Figure 32: Cross sectional view of the miniature load cell installed inside the damper

The expected outcomes of these experiments are as follows:

- To validate the modeling and simulation results by comparing them with the damper output force.

- To measure the required solenoid force range under working conditions

- To verify the outcome of equation (2-24), stating that the valve disc will always be pushed in x_2 direction in both the compression and the extension cycle.

To perform the tests, the piston valve disc and valve shaft were held in place between the load cell shaft and a setscrew threaded through the piston cap. The position of the valve disc was adjustable by the addition of shim discs between the valve shaft and the valve disc. When a stack of shims 1.524 mm tall is installed in the valve, the valve position is equal to that achieved when the valve is resting against the uncompressed valve springs (valve-closed position). A range of 1.524 mm in valve opening is therefore achievable. This distance covers the useful valve operating range. Tests conducted covered this operating range in 0.254-mm steps.

Figure 33 shows a sample of the results and the simulation results obtained while the valve was fixed in mid-range position. The results show perfect agreement even in high velocities. On the other hand, the results show that the damper is capable of generating a maximum damping force of 16 kN in compression cycle at 1 m/s velocity. This is in the same ranges of forcing expected for a heavy-vehicle damper.
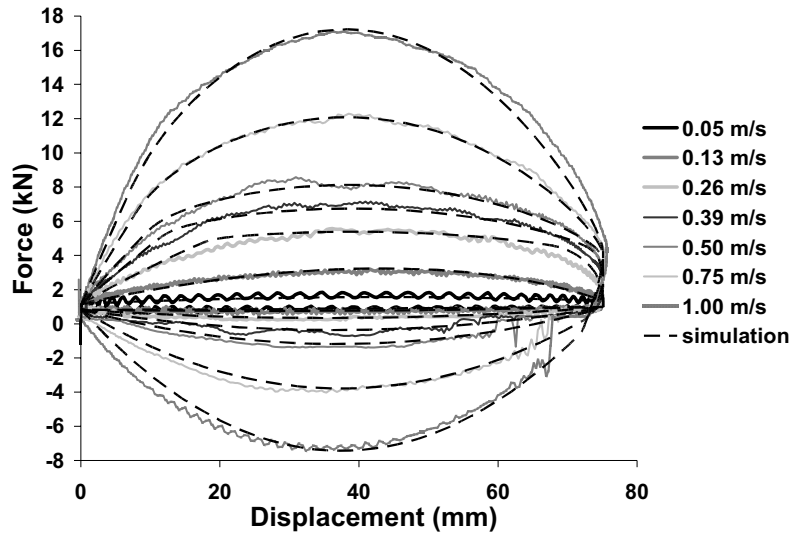
Figure 33: Comparison of the experiment and simulation results, while a 0.508 mm spacer is installed (valve is half-open)

The results of the internal load cell measurements recorded during these tests show how much force will be applied to the spring and solenoid when it is in a particular position and the damper is under various excitations. The variation in this load as the damper undergoes a compression and extension cycle can be seen by plotting the valve force versus time during a compression and extension cycle as well as versus position, as shown in Figure 34. The valve load in extension increases steadily as the valve is closed, and is much smaller than the valve loads in compression. The compression loads show a drop in valve force when the valve is near the middle position. The results not only provide a good estimate of the required force, that is a maximum of 350 N, but also indicate that the force applied to the valve disc is always positive (in x_2 direction).

Using these results and the simulation process, the unknown parameters have been finalized and a final prototype has been developed. The solenoid chosen to be used in the prototype piston valve is a 1-

1/2-inch diameter tubular push type solenoid, model number S-22-150-HF, made by Magnetic Sensor Systems. Its coil specifications were selected to match the 28 vDC 4 Amp power supply to be used in testing. The coil uses 24 AWG wire and has a resistance of 7.4 ohms. The selected spring comprises eight disc springs in series, each with a stiffness of approximately 1635 kN/m. Together, the stack of springs has a stiffness of approximately 204 kN/m. The resultant force of the valve springs and the solenoid is shown in Figure 35 for different solenoid charge currents.
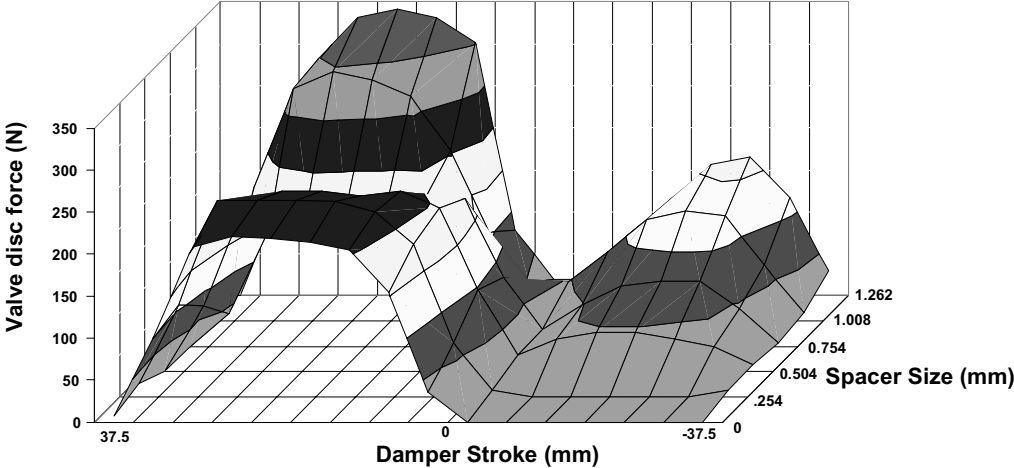
Figure 34: Valve disc force under operating condition versus different spacer sizes
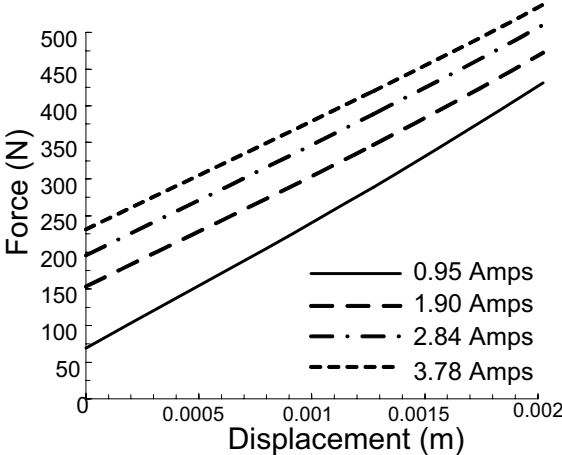
Figure 35: Resultant force of valve-disc springs and the solenoid

2.2.1.4 Internal solenoid valve damper prototype tests

The final internal solenoid damper prototype was tested using again the test apparatus discussed in the previous section. Each test was repeated in different velocities and while the solenoid was charged with different applied currents ranging from 0 to 1.7 Amp. Figure 36 shows the summary of the test results. As depicted, the damper is capable of producing forces up to 35kN while the solenoid applied current is 1.7 Amp in both compression and extension cycles.
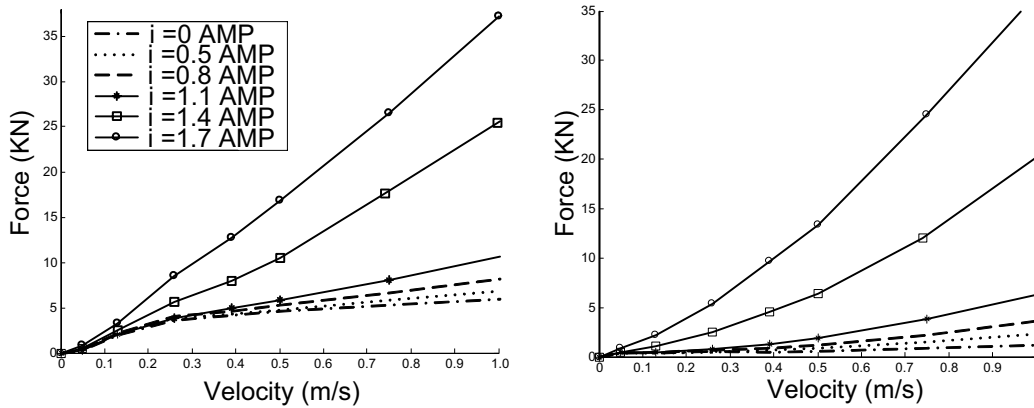
Figure 36: Damping versus velocity for different input currents in compression cycle (left) and extension cycle (right)

2.3 Application of Neural Networks in Semi-Active Damper Modeling

Figure 37 shows a general lumped mass parameter representation of a damper. For simplicity, in most cases the force-velocity of a damper would be modeled as a linear dashpot ($F_{damper} = c\dot{x}$) only.
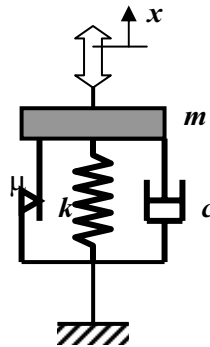
Figure 37: A lumped model of a damper consisting of nonlinear damper and spring elements together with dry friction and an inertia effects

55

In an actual damper however, the force-velocity relationship is not linear. A spring element is normally added to the simple pure dashpot model ($F_{damper} = c\dot{x} + kx$) to account for the following:

- Presence of bushings at attachment location of a damper to the chassis of suspension

- The effect of pressurized gas chamber

- The oil compressibility due to gas emulsification

As briefly discussed above, to date, different methods and mathematical approaches have been employed to model and to identify damper characteristics. As the main goal of the modeling in this thesis, and in general in suspension control application, is to implement different semi-active dampers mapped in a feed-back control loop using the experimental results, neural networks are proposed and designed to approximate the mappings (Eslaminasab *et al.,2007*). This method is much faster than the conventional methods in the modeling process and it captures the damper's behaviors such as nonlinearities more accurately. To incorporate the neural networks in the simulations, the training is done offline and the networks with the trained parameters are used online for control implementation. This technique is desirable to allow for control implementation in real time without having to worry about the computation cost required for implementing the neural-network-learning algorithms.

Due to the asymmetric nature of these dampers, two different networks are designed and trained independently for each damper. These networks use the velocity and current as input and output the damping force. Initially, two different types of neural network were considered: Radial Basis Function (RBF) and Multi-layer Perceptron (MLP). The MLP neural network produced the better results and, hence, it is adopted for the purpose of control development and validation in this thesis. The MLP networks have two inputs: one hidden layer with 40 nodes and one output layer. Forty-eight sets of data were used for offline training purposes. Figure 38 depicts the neural network approximation of the internal solenoid valve damper as well as the approximation error. The results reveal how accurately the neural networks mimic the actual dampers characteristics.
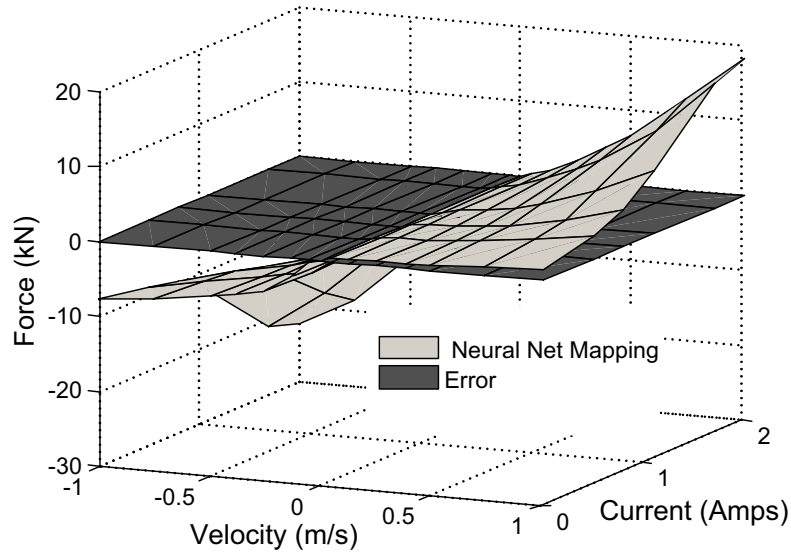
Figure 38: Neural net approximate mapping of the internal solenoid valve damper damping- force and the approximation error

2.4 Comparative Study on the Performance of Different Semi-Active Dampers

In this section, the performances of the two newly developed semi-active dampers are compared with two of commercially available semi-active dampers – a total of four different semi-active dampers. The first damper is a semi-active MR damper made by Delphi Corporation and used in the Delphi Magneride suspension system. This particular damper is commercialized and used in different passenger vehicles including the Cadillac-SRX; this damper will be referred to as the generic MR damper hereafter. The second damper is a semi-active external solenoid valve, manufactured and commercialized by Tenneco Inc. and used in various vehicle suspension systems such as in Volvo-S60R; this damper will be referred to as the generic external valve damper. The third damper is the in-house prototype of an internal solenoid valve (as described in previous sections), designed and developed for research purposes. The fourth damper is an external solenoid valve damper designed and manufactured by General Kinetics Engineering Corporation (GKEC) for heavy-vehicle applications as a parallel approach to this research. This study does not reflect the performance of the selected commercialized dampers while installed on the existing vehicle models – namely Cadillac SRX and Volvo S-60R – nor is it seeking such comparisons. Due to their availability and high performance characteristics, these dampers have been

selected as a baseline for comparing the new products. To eliminate any confusion arising from this matter, these selected dampers will be called by generic names throughout the thesis.

The dampers were tested on an MTS damper dynamometer with a maximum velocity of 100 in/sec and a maximum load of 20,000 lbf connected to a MTS Test Star II controller. The MTS machine was equipped with a 0-100-kN rate load cell and an internal LVDT to measure the relative displacements. A data acquisition system together with a workstation was used to record and save the test data. Figure 39 shows the test bed set up used to measure the damper's transferred force in different velocity ranges and for different input currents to characterize the damper's capabilities. The objective of these tests was to investigate the variable damping capabilities of the dampers. Using an adjustable power supply, several tests were carried out on these semi-active dampers. A summary of the test results of the damper's force-velocity for a given current are presented in Table 5.

Figure 39: Test design
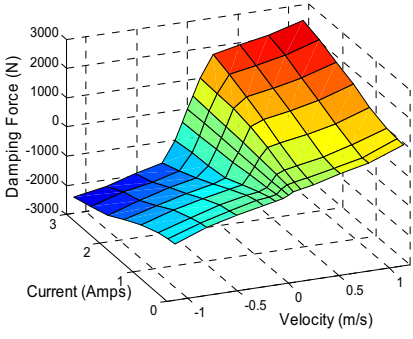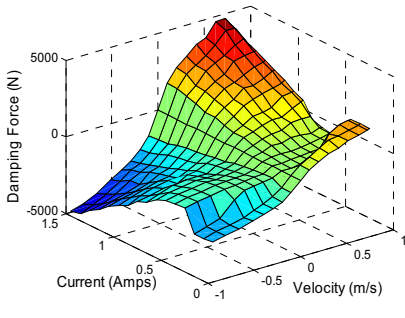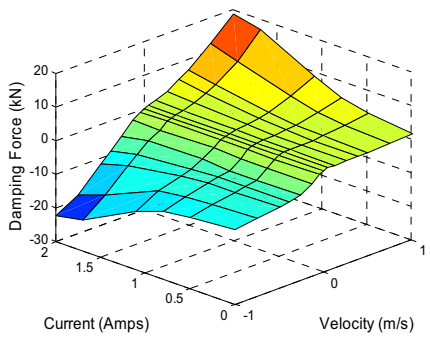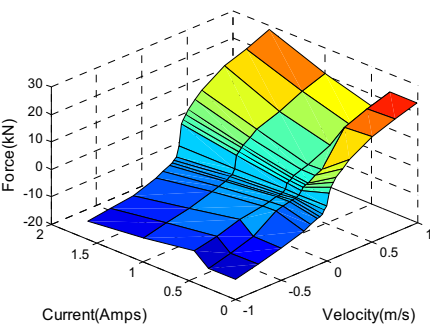
The MLP neural networks, as proposed in the previous section, have been used to model the four dampers using the test results. Figure 40 shows a sample of the modeling and the approximation error. Among all four dampers introduced above, only two are specifically designed for the high damping and force requirements of heavy vehicles. To compare the mapping of the two other dampers, a scaled version of the test data was used in the simulation process.

58

The main goal of this section is to compare the effectiveness and the performance of the newly developed damper's unique mapping, in a feed back control loop, while conventional semi-active controllers (as discussed in Chapter 1) are in place to optimize the ride comfort and road handling performance indexes (see section 1.2.4.1 and 1.2.4.2) . To simulate the system properly, a 1DOF quarter-car model, as shown in Figure 2-a, was modeled in Matlab$^{®}$/Simulink. The model parameters used in this simulation were obtained from a heavy vehicle system and are listed in Table 6. To control the desired outputs – acceleration and displacement transmissibility – a feedback control loop was designed based on the conventional control strategies defined in equations (1-20) and (1-24) . Figure 41 depicts the simulation process.

$^{®}$ MATLAB is the registered trademark of MathWorks Inc.

Table 5: Dampers test result summary

Damper Name	Shape	Test Results
Generic MR Damper		
Generic External Valve Damper		
Internal Solenoid Valve Damper		
GKEC External Valve Damper		
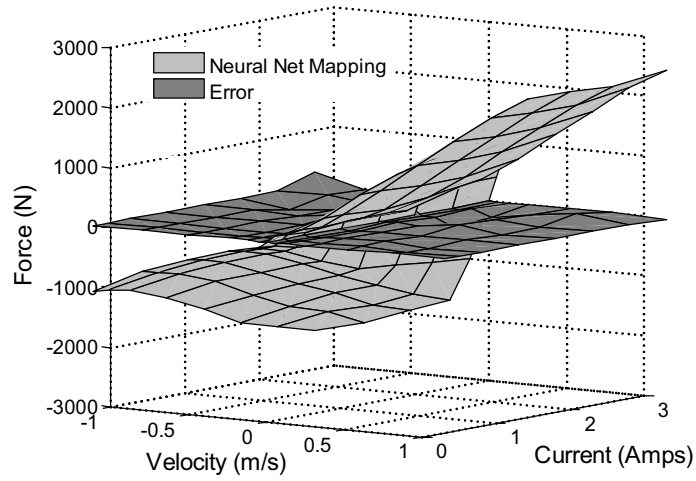
Figure 40: Neural network approximate mapping of the Generic MR Damper and the approximation error

Table 6: Simulation Data

System parameter	Value
Sprung mass - m (kg)	2000
Stiffness- k (N/m)	55000
Damping- c (Ns/m)	Variable

To perform the numerical analysis, a harmonic input $y = A\,sin(\omega t)$ is applied as the road induced vibration to the system. The amplitude of excitation is set to 0.05 m and the frequency range is 0-5 Hz. The simulation results are obtained and discussed in frequency domain.
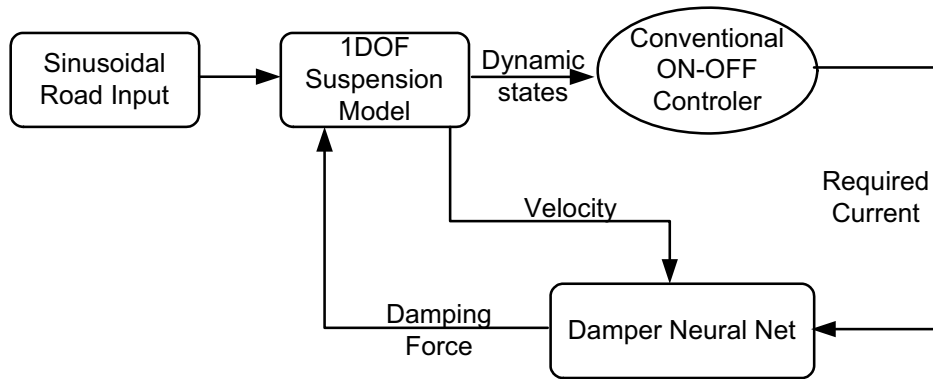
Figure 41: Simulation diagram

2.4.1 Simulation Results

Figure 42 shows a comparison of the newly designed internal valve damper together with the conventional semi-active control methods and passive system. As expected, the semi-active controlled damper is capable of improving the systems performance. The results of this study and the test results presented in the previous section provide sufficient evidence to prove the relevance and applicability of this newly designed damper for heavy-vehicle applications. Further, the performance of the four dampers are compared in Figure 43 and Figure 44, where the conventional R-S control method and Skyhook control method are implemented in a feed-back state control loop system. As depicted in theses figures, the performances of the systems using the two newly designed dampers are in the exact same range as the commercially available semi-active dampers chosen for this study.
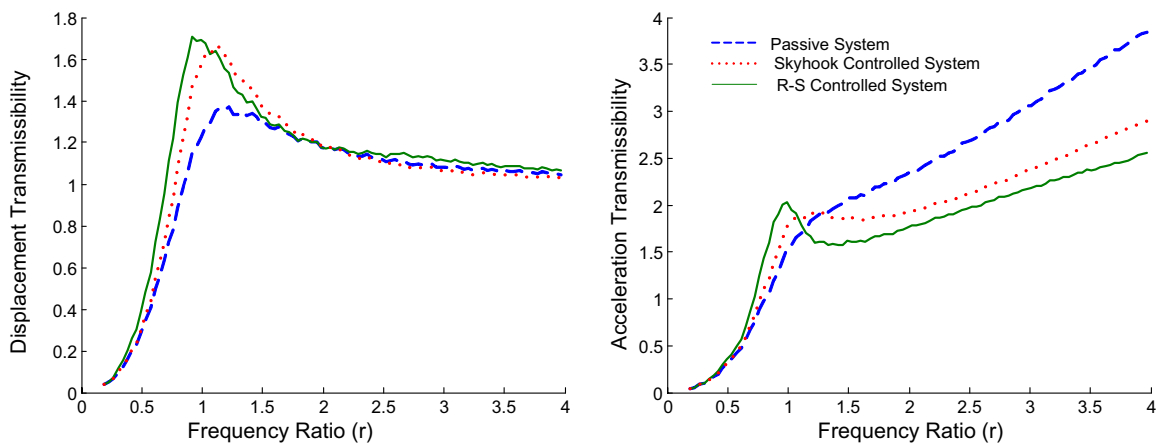
Figure 42: Internal valve damper performance with and without conventional on-off controllers
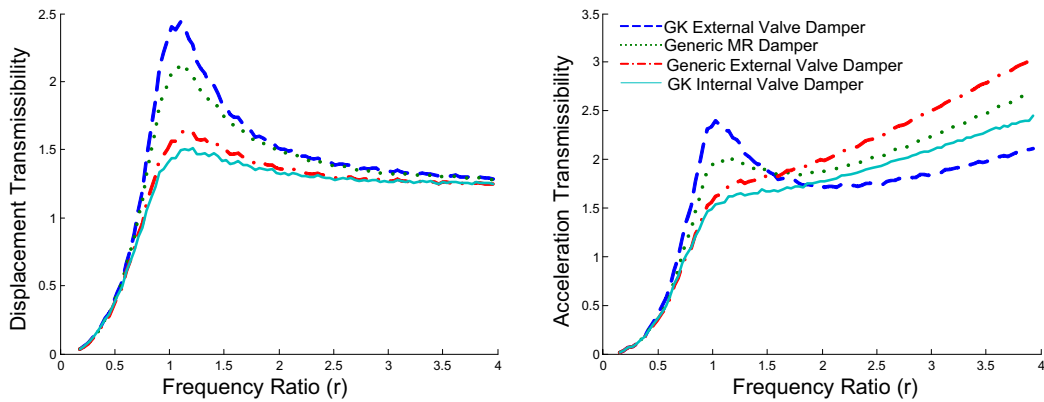
Figure 43: Comparison of different dampers' performance when the system is controlled with R-S method
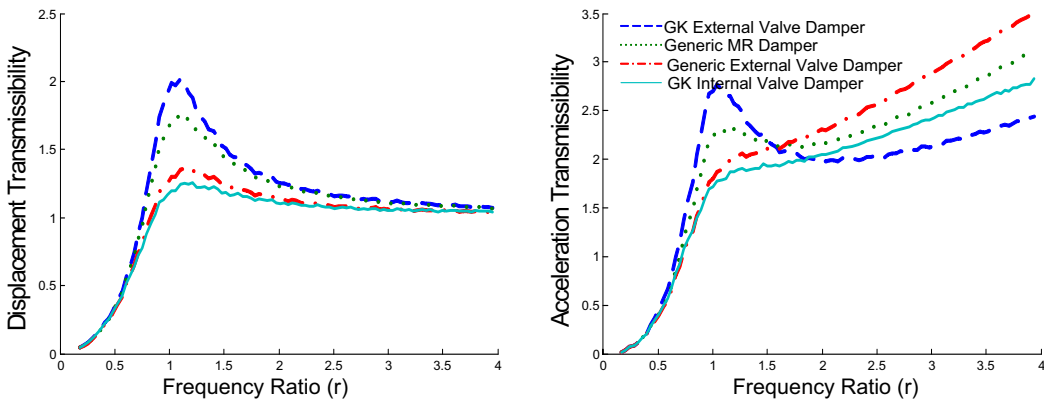
Figure 44: Comparison of different dampers' performance when the system is controller with Skyhook method

Although many other important parameters enter into the design and manufacture of dampers such as reliability, lifetime, configuration, the main concern of the study presented in this section is to provide a proof of concept for the applicability of the new semi-active damper technology in heavy-vehicles systems. In the case of industrial production of such dampers, other design parameters should be studied in detail.

2.5 Conclusions

In this chapter, a heavy-vehicle passive damper is analyzed, tested, and modeled. The model is further verified using the test results. The existing gas spring, a highly nonlinear system, has been mathematically modeled, and an adiabatic model is proposed for the modeling process. The test results prove that the proposed model is capable of predicting the gas spring behavior. Furthermore, the plans

for development of a semi-active damper for heavy-vehicle applications are set, and this newly designed system has been modeled, prototyped and tested. Two commercially available semi-active dampers have been selected as the benchmark, and the performance of the newly developed semi-active damper is proven to be at an acceptable level. In addition, the application of neural networks in modeling and mapping the semi-active dampers is proposed and successfully implemented.

Chapter 3

Nonlinear Analysis of Switched Semi-Active Controlled Systems

"We need to stop treating nonlinear systems like monsters"

(Dr. Eihab Abdel-Rahman)[5]

As stated in the first chapter, semi-active suspension systems offer significant improvement in ride comfort and road handling performance of ground vehicles. Also because of size, weight, price, and performance advantages, these systems have generated more interest than either the active or the passive systems. One interesting aspect of all on-off semi active control strategies is that they introduce nonlinearities into the system by adding discontinuities. Although by definition these systems are still piecewise linear, it is important to investigate the effect of these added nonlinearities. Since the source of nonlinearity is the step change in damper force, the acceleration response will have a discontinuity (Alanoly and Sankar, 1986). In recent years, Shen (2005) used the nonlinear approach to find a closed form solution for the conventional on-off control strategies to compare the performance of those systems. However, this study does not present a practical method for performance characterization. Unfortunately, a direct nonlinear analysis of the semi-active systems and the need for a global performance characterization is seldom discussed in literature.

In this chapter, the nonlinearity of on-off semi-active control strategies is discussed, and the nonlinear analysis methods are used to explore the problem. A method to characterize the performance of these systems is also established. In addition, the possibility of adverse effects of this nonlinear phenomenon on ride comfort quality of vehicles is discussed.

3.1 The Nonlinearity of Semi-active Control Methods

A simple approach to explore the effects of added nonlinearities due to on-off control strategies is to use the Fourier transform to analyze the output of a simple 1DOF-based excited system under a sinusoidal excitation. In order to highlight the nonlinear problem due to the on-off semi-active controlled system,

---

[5] Quoted from Faculty of Engineering Annual Report 2006, University of Waterloo; publication no. 40065122.

consider a 1DOF system (equation (1-3)) in which the damping ratio, ζ, – and ultimately the damping force – is controlled by R-S control strategy (equation (1-24)). Figure 45 shows the time domain responses – that is Relative displacement, Relative velocity, Damping force, and Mass absolute acceleration – of a 1DOF system under a sinusoidal excitation. As expected, the steady state responses of the system are also sinusoidal. On the other hand, as depicted in Figure 46, the time domain outputs of a 1DOF system controlled by R-S control strategy are not sinusoidal. Moreover, as expected, because of the discontinuities of the damping force, the mass acceleration has discontinuities as well. These effects are translated as the existence of nonlinearity in the system. In a frequency domain presentation of the problem, Figure 47 compares the frequency contents of the output signal (Mass acceleration ($\ddot{x}$)) for the passive system and the system controlled by a conventional on-off (R-S) control method based on the mathematical simulation results. As illustrated in this figure, the on-off control method introduces new frequency contents to the system's output while reducing the amplitude of vibrations at excitation frequency. In some cases, this might be an important design factor, for instance in cases where the human body is the subject to the vibration since the human body is sensitive to both vibration frequencies and amplitude (ISO 2631-1974). As pointed out by ISO, the human's body is most sensitive to vibration with frequencies ranging from 4 Hz to 8 Hz. As depicted in Figure 48, the added nonlinearity effects in a suspension system may generate an undesired output frequency if the excitation frequency is below 2.6 Hz. This might be considered as an unwanted and/or disturbing phenomenon and should be addressed as a design factor.

On the other hand, the performance characterization in vibration control and particularly in suspension control subject is based mainly on the frequency response analysis of the system's outputs (in terms of acceleration transmissibility and/or displacement transmissibility). For instance, the performance indexes derived in chapter one (equations (1-12), (1-13), (1-15), and (1-16)) are based on the assumption that the system's outputs are sinusoidal. The Frequency Response Function (FRF) method also requires linearization of the system's mathematical model – a practice commonly used in the prior art (Bendat and Piersol, 1980). Table 7 describes possible linearization techniques (Eslaminasab and Golnaraghi, 2007) for a 1DOF system under sinusoidal excitation with the frequency of excitation "ω", resulting in sinusoidal response of the system, some of which has been described in the literature. Among all the methods described, the so-called "ω method" is the most commonly used method.
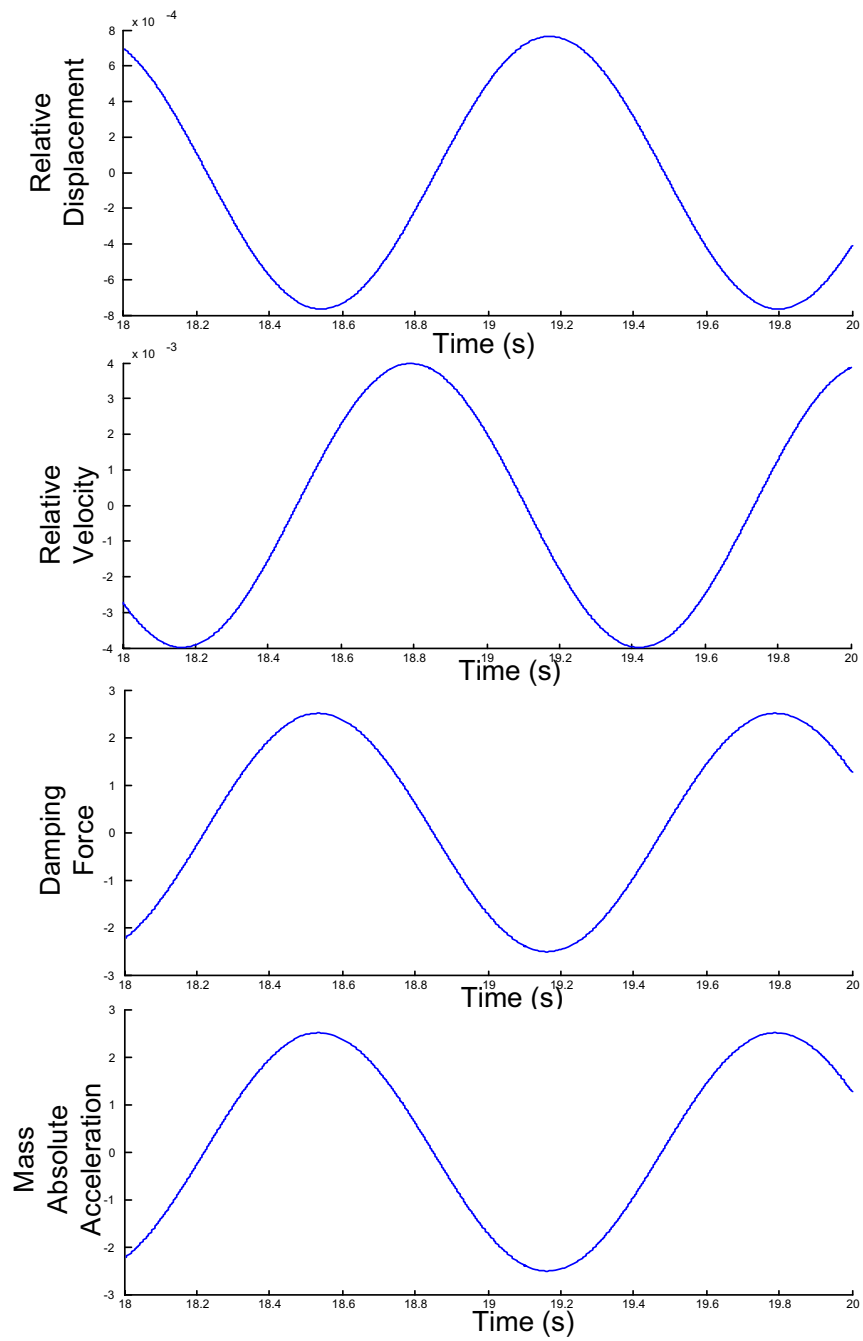
Figure 45: Sample of a 1DOF system outputs
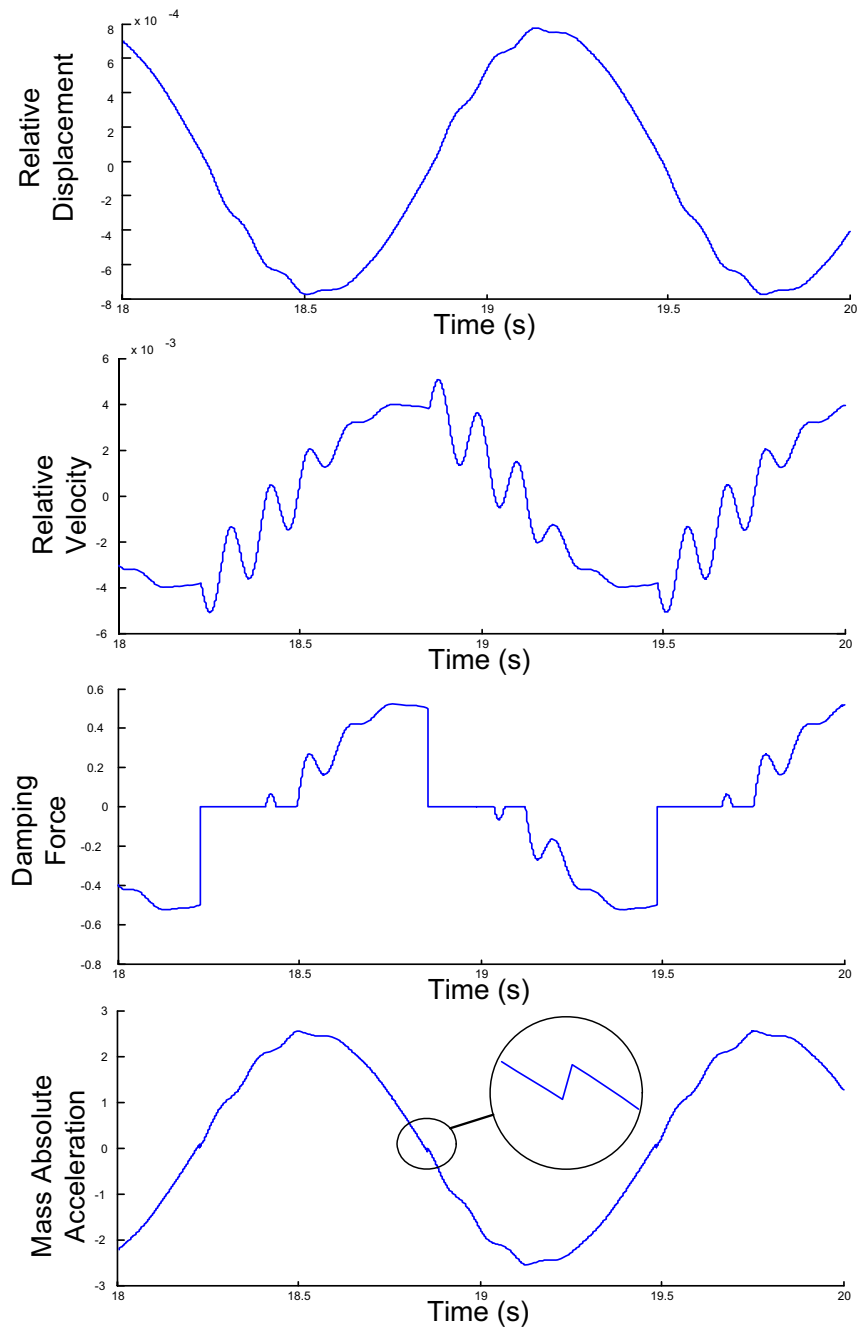
Figure 46: Sample of an R-S controlled 1DOF system outputs
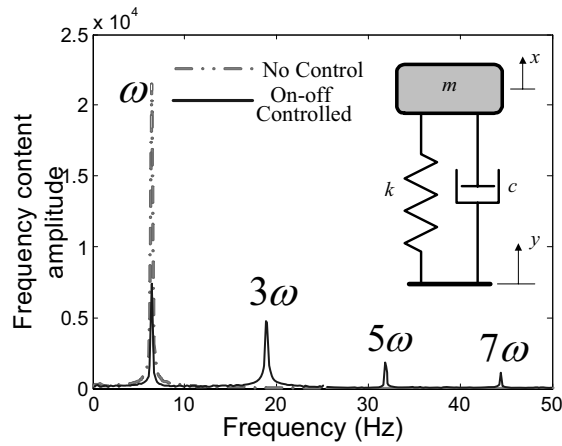
Figure 47: Comparison of the system's output-frequency-content values with and without on-off controller
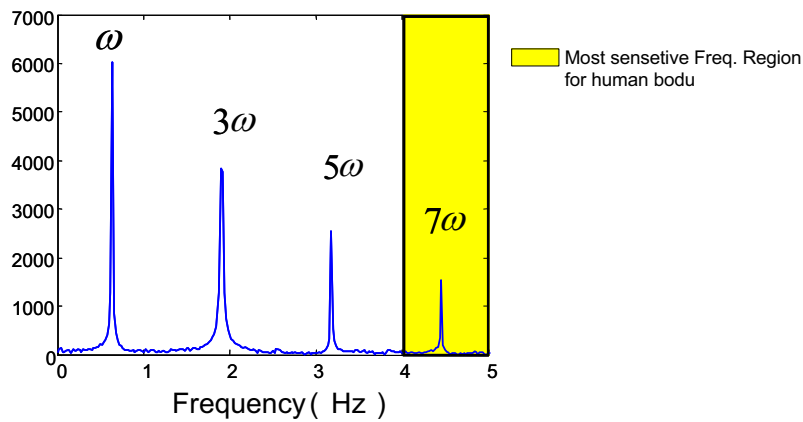
Figure 48: The adverse effect of semi-active controlled system on ride comfort quality

Table 7: Some possible outputs based on the linearization methods[6]

Item	Method	Output of the system is assumed :
1	ω	$x = A_1 \sin(\omega t + \phi)$
2	3ω	$x = A_2 \sin(3\omega t + \phi)$
3	$\omega + 3\omega$	$x = A_1 \sin(\omega t + \phi) + A_2 \sin(3\omega t + \phi)$
4	Max-Max	$x = A_{max} \sin(\omega t + \phi)$

---

[6] Where A_1 and A_2 are the corresponding amplitude obtained from FRF analysis and A_{max} is the maximum amplitude of the multi frequency system in steady state obtained from time domain analysis.

To investigate the existence of this nonlinear phenomenon in practice, a 1DOF system test bed (for the system details and the instrumentation refer to Chapter 6) was used. The system was excited using various sinusoidal base excitations with different amplitudes and frequencies. The test bed was equipped with two accelerometers to record the base and the mass acceleration. The semi-active damper of the system was controlled using R-S control method. The control method was implemented using the Matlab/XPC Target real time package. Figure 49 shows a sample of the out put results. As depicted in this figure, the existences of higher harmonics are evident.
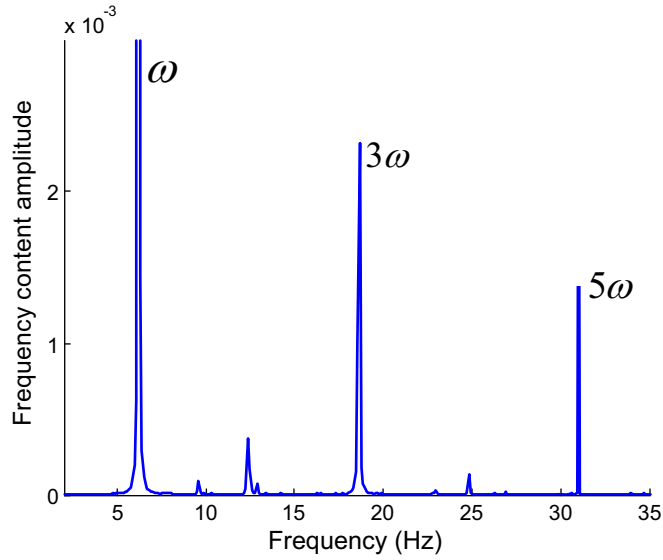
Figure 49: Test results confirming the added nonlinearity of on-off-semi-active controllers. Figure represents the frequency content of a 1DOF mass acceleration

To highlight the issue of performance characterization method and the importance of this issue, consider a passive 1DOF system, as modeled in Chapter 1, under a sinusoidal base excitation ($y = Y\sin(\omega t)$). If the purpose of the study is to measure the effect of a change in one of the system's parameter (e.g. damping ratio) on the systems performance using the suspension performance indexes, the task is easy because the output of the system in steady state is known to be in the form of $x = A_1 \sin(\omega t + \phi)$ and $\ddot{x} = -A_1 \omega^2 \sin(\omega t + \phi)$, where A_1 is (Inman, 2001)

$$A_1 = \frac{Y}{\sqrt{(\omega_n^2 - \omega^2)^2 + 4\zeta^2 \omega_n^2 \omega^2}}$$

(3-1)

70

As a result, it is possible to calculate and compare the transmissibility functions for any given damping ratio.

Now consider an unknown nonlinear 1DOF system whose output has been identified to be in the form of (this is the case for the on-off semi-active controlled systems)

$$x = \sum_{1}^{n} A_n \sin((2n-1)\omega t + \phi_n)$$ (3-2)

$$\ddot{x} = -\sum_{1}^{n} A_n (2n-1)^2 \omega^2 \sin((2n-1)\omega t + \phi_n)$$ (3-3)

To calculate and compare the transmissibility functions as defined in equations (1-11) and (1-14), either the equivalent maximum amplitudes must be determined or a new performance index should be introduced. For instance, Alanoly and Sankar (1986) defined and used the ratio of root mean square (RMS) value of the response acceleration to the RMS-value of the input acceleration as the acceleration transmissibility.

In this thesis, using the original transmissibility definitions, for the harmonic base excitation case, a new method (to be named "Max-Max method") is proposed and used to find the equivalent maximum amplitudes. In this method, the output of the system is considered to be sinusoidal, having the same frequency as the input with its amplitude equal to the maximum value of the (multi-frequency) output at steady state in time domain (see Figure 50). In the next section, using the analytical method of averaging, this method is compared with the few other possible choices and is shown to be an effective way to solve this issue.
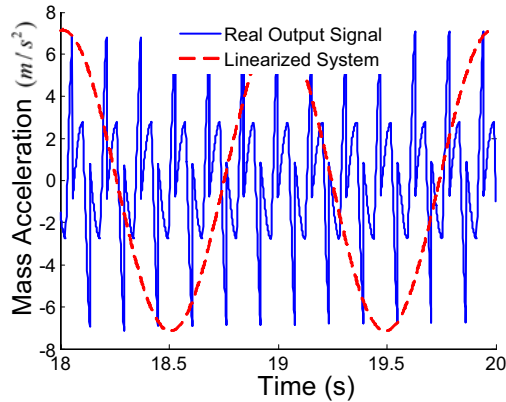
Figure 50: Illustration of Max-Max method

71

3.2 Analytical Method of Averaging and Semi-Active Controlled Systems

When the semi-active on-off controlled damping force is regarded as a piecewise linear force, the characteristics of the conventional semi-active control methods can be determined using the nonlinear dynamics analytical method, the method of averaging. With this analytical approach, a closed form solution for the system frequency response can be obtained. The analytical method of averaging is introduced in this chapter and is frequently used in the next chapters as well. This method provides an easy and efficient way to study the performance of the semi-active controlled systems. The results obtained from the averaging method are verified with the numerical method and are used to validate the Max-Max method proposed in the previous section.

The method of averaging (developed by Bogoliubov and Mitropoloski (Wei-Chau, 2006)) is introduced and discussed through the application of the method into the analysis of the 1DOF R-S controlled system.

The equation of motion for a 1DOF R-S controlled system under a harmonic base excitation is (Ref. to Chapter 1 for details)

$$\ddot{x}_r + 2\zeta_s \omega_n \dot{x}_r + \omega_n^2 x_r = Y\omega^2 \sin(\omega t)$$

$$\zeta_s = \begin{cases} \zeta_{max} & (x-y)(\dot{x}-\dot{y}) \le 0 \\ \zeta_{min} & (x-y)(\dot{x}-\dot{y}) > 0 \end{cases}$$

$$\zeta_{min} = \beta\zeta_{max}, \quad 0 \le \beta \le 1$$

$$(3\text{-}4)$$

In order to analyze the effect of the nonlinearity with the averaging method, it is necessary to transform the equations to a time scaled form. Considering that the base excitation of the system, "y", is sinusoidal ($y = Y \sin(\omega t)$), the time scaled equation of motion will be

$$r^2 x_r'' + x_r + 2\zeta_s r x' = Yr^2 Sin(\tau)$$

$$\zeta_s = \begin{cases} \zeta_{max} & (x-y)(\dot{x}-\dot{y}) \le 0 \\ \zeta_{min} & (x-y)(\dot{x}-\dot{y}) > 0 \end{cases}$$

$$\zeta_{min} = \beta\zeta_{max}, \quad 0 \le \beta \le 1$$

$$(3\text{-}5)$$

The parameters in this equation are "$r = \omega/\omega_n$", frequency ratio, "$(\ )' = d(\ )/d\tau$", and the time scaling parameter "$\tau = \omega t$".

Introducing a new parameter, ε ($0 < \varepsilon < 1$), and considering that the damping and the non-linearities are small, the equation of motion will be

$$r^2 x_r'' + x_r = -\varepsilon(2\zeta_s r x_r' - Y r^2 \, Sin(\tau))$$

$$\zeta_s = \begin{cases} \zeta_{max} & (x-y)(\dot{x}-\dot{y}) \leq 0 \\ 0 & (x-y)(\dot{x}-\dot{y}) > 0 \end{cases} \tag{3-6}$$

Although this nonlinear system may have other periodic solutions such as second and third sub/super harmonics, we consider the solution of the above equation for the main resonance case, in polar coordinates, to be in the form:

$$x_r = a_r(\tau)\cos(\phi(\tau))$$

$$\phi(\tau) = \tau + \varphi(\tau) \tag{3-7}$$

And as a result, the first and second derivatives of x_r with respect to τ will be

$$x_r' = a_r'(\tau)\cos(\phi(\tau)) - a_r(\tau)\varphi'\sin(\phi(\tau)) - a_r(\tau)\sin(\phi(\tau))$$

$$x_r'' = -a_r'(\tau)\sin(\phi(\tau)) - a_r(\tau)\cos(\phi(\tau)) - a_r(\tau)\varphi'\cos(\phi(\tau)) \tag{3-8}$$

On the other hand, if the nonlinear parts are negligible (i.e. ζ), then the solution of equation (3-6) is

$$x_r = a_r \cos(\phi(\tau))$$

$$\phi(\tau) = \tau + \varphi \tag{3-9}$$

As a result, the first and second derivatives of x_r with respect to τ will be

$$x_r' = -a_r \sin(\phi(\tau))$$

$$x_r'' = -a_r \cos(\phi(\tau)) \tag{3-10}$$

Comparing equations (3-9) and (3-10), we get

$$a_r'(\tau)\cos\phi(\tau) - a_r(\tau)\varphi'(\tau)\sin\phi(\tau) = 0 \tag{3-11}$$

Substituting equations (3-9) and (3-10) into equation (3-6) and solving the resulting equation together with the equation (3-11) for $a_r'(\tau), \varphi'(\tau)$, we get

73

$$\frac{d(a_r)}{d(\tau)} = -\frac{1}{r^2}\Big(\big(r^2 a_r \cos(\phi) - a_r \cos(\phi)\big)$$
$$+2\zeta_s \varepsilon r a_r \sin(\phi) + y r^2 \varepsilon \sin(\tau)\big)\sin(\phi)\Big)$$

(3-12)

$$\frac{d(\varphi)}{d(\tau)} = -\frac{1}{r^2 a_r}\Big(\cos(\phi)\big(r^2 a_r \cos(\phi) - a_r \cos(\phi)\big)$$
$$+2\zeta_s \varepsilon r a_r \sin(\phi) + y r^2 \varepsilon \sin(\tau)\big)\Big)$$

(3-13)

From these equations – that is (3-12) and (3-13) – it is seen that $a_r'(\tau), \varphi'(\tau)$ are small, which implies that $a_r(\tau)$ and $\varphi(\tau)$ change slowly with τ over one period. Therefore, as an approximation, the right side of these equations can be replaced by their averaged values (Wei-Chau, 2006). The general averaging operator is

$$Ave(f) = \lim_{T \to \infty} \frac{1}{T} \int_{\tau}^{\tau+T} (f)\, d\tau$$

To implement the method of averaging to equations (3-12) and (3-13), first we need to redefine the R-S control rules in terms of the polar coordinates (a, φ) which are used in the analysis. Recall from equation (3-9) that the system's response is considered to be in the form of "$x_r = a_r \cos(\phi(\tau))$". Therefore, the polar R-S control rules are

$$\zeta_s = \begin{cases} \zeta_{max} & 0 \le \phi < \dfrac{\pi}{2} \\[2mm] \beta \zeta_{max} & \dfrac{\pi}{2} \le \phi < \pi \\[2mm] \zeta_{max} & \pi \le \phi < \dfrac{3\pi}{2} \\[2mm] \beta \zeta_{max} & \dfrac{3\pi}{2} \le \phi < 2\pi \end{cases}$$

(3-14)

Averaging the equations above over the period of $\phi = [0, 2\pi]$ results in:

$$\bar{a}_r' = -\frac{1}{2} Y \cos(\varphi) + \int_0^{\frac{\pi}{2}} \frac{-2a_r \sin^2(\phi)\zeta_{max}}{r}\, d\phi + \int_{\pi}^{\frac{3\pi}{2}} \frac{-2a_r \sin^2(\phi)\zeta_{max}}{r}\, d\phi +$$
$$\int_{\frac{\pi}{2}}^{\pi} \frac{-2a_r \sin^2(\phi)\beta\zeta_{max}}{r}\, d\phi + \int_{\frac{3\pi}{2}}^{2\pi} \frac{-2a_r \sin^2(\phi)\beta\zeta_{max}}{r}$$

(3-15)

$$\bar{\varphi}' = -\frac{1}{2}\frac{-r^2 a_r + a_r + Yr^2 \sin(\varphi)}{r^2 a_r} + \int_0^{\frac{\pi}{2}}\frac{-\sin(2\phi)\zeta_{\max}}{r}d\phi + \int_{\pi}^{\frac{3\pi}{2}}\frac{-\sin(2\phi)\zeta_{\max}}{r}d\phi +$$

$$\int_{\frac{\pi}{2}}^{\pi}\frac{-\sin(2\phi)\beta\zeta_{\max}}{r}d\phi + \int_{\frac{3\pi}{2}}^{2\pi}\frac{-\sin(2\phi)\beta\zeta_{\max}}{r}$$

<div align="right">(3-16)</div>

where "$\overline{*}$" represent the average value. By calculating the integrals, the final averaging results will be:

$$\bar{a}_r' = \frac{-a_1\zeta_s\beta - a_1\zeta_s\beta - a_1\zeta_s - a_1\zeta_s - 2Yr\cos(\varphi)}{4r}$$

<div align="right">(3-17)</div>

$$\bar{\varphi}' = \frac{a_1 r\zeta_s\beta - a_1 r\zeta + a_1 r\zeta_s\beta - a_1 r\zeta_s}{2r^2\pi a_r}$$

$$+\frac{-r^2\pi a_r + \pi a_r + \pi Yr^2\sin(\varphi)}{2r^2\pi a_r}$$

<div align="right">(3-18)</div>

Solving these equations for the steady state where $\bar{a}_r'(\tau) = 0$, $\bar{\varphi}'(\tau) = 0$, we find the averaged equation for the amplitude and phase of the relative displacement. To find the parameters of interest, (η, λ), to compare the analytical and simulation results, it is necessary to find the averaged value for the absolute acceleration, $\ddot{x}(t)$, through the following relations:

$$x = \bar{a}_r \cos(rt + \bar{\varphi}) + Y\sin(\omega t)$$
$$x = a\cos(rt + \theta)$$
$$a = \sqrt{(\bar{a}_r)^2 + (Y)^2 + 2\bar{a}_r Y\cos(\bar{\varphi})}$$

<div align="right">(3-19)</div>

and

$$\lambda = 2\pi r^2 \left| \frac{1}{\sqrt{A+B+C+D+E+F+G+H}} \right|$$

where:

$A = -8\zeta_s^2 r^2 \beta + 4\zeta_s^2 r^2 \beta^2 + 8\zeta_s^2 r^2$

$B = 4\zeta_s^2 r^2 + 4\pi^2 - 8\zeta_s^2 r^2 \beta$

$C = 4\zeta_s^2 r^2 \beta^2 - 16\zeta_s^2 r^2 \beta + 8\zeta_s^2 r^2 \beta^2 + 4\zeta_s^2 r^2$

$D = \zeta_s^2 \pi^2 r^2 \beta^2 + 8\zeta_s \pi r + 4\zeta_s^2 \pi^2 r^2 \beta$

$E = 2\zeta_s^2 \pi^2 r^2 \beta - 8\zeta_s \pi r \beta - 8\zeta_s \pi r - 8\zeta_s \pi r^3$

$F = 8\zeta_s \pi r^3 \beta + 8\zeta_s \pi r^3 \beta + \zeta_s^2 \pi^2 r^2 + \zeta_s^2 \pi^2 r^2 \beta^2$

$G = 2\zeta_s^2 \pi^2 r^2 \beta^2 + 2\zeta_s^2 \pi^2 r^2 \beta + 2\zeta_s^2 \pi^2 r^2 + \zeta_s^2 \pi^2 r^2$

$H = 8\zeta_s \pi r - 8\zeta_s \pi r^3 - 8\pi^2 r^2 + 4r^4 \pi^2$

(3-20)

As a result, the acceleration transmissibility is

$$\eta = r^2 \left| \sqrt{(\lambda^2 + 1 \pm 2\lambda \cos(\varphi))} \right|$$

(3-21)

To ensure the averaging method results match the numerical simulations results, let us consider $\beta = 1$. In this particular case, the results derived from the averaging method should be equal to the theoretical results obtained from equations (1-12) and (1-15). As indicated in Figure 51, the results closely match.

Using the result obtained from the method of averaging, Figure 52 depicts the comparison of the acceleration transmissibilities obtained using the proposed methods in Table 7 and the averaging method results. The figure shows that in the neighborhood of the natural frequency (where the averaging method results are most accurate), the averaging results are close to the so-called "Max-Max method" results proposed and used in this thesis as a basis for the comparison of acceleration and displacement transmissibility.
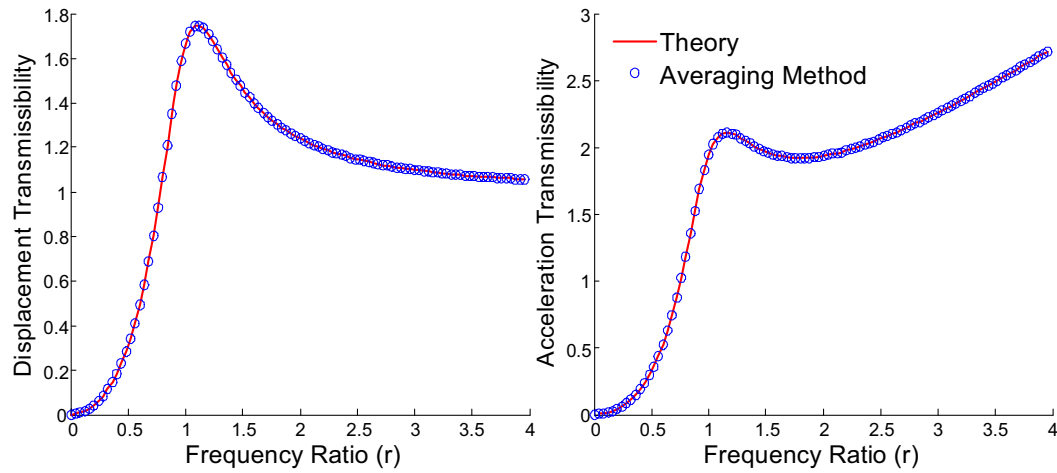
Figure 51: Comparison of the averaging method and the theoretical results for a passive system using simulation data presented in Table 1
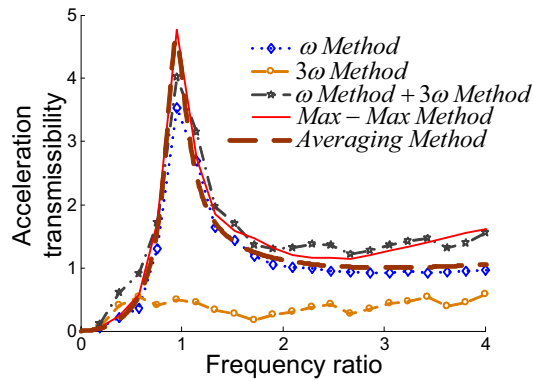
Figure 52: Comparison of the averaging results with those of other proposed methods for an R-S controlled system

3.3 A New Controller to Eliminate the Added Nonlinearities Effect

The existence of the excitation frequency harmonics in a semi-active controlled system might be harmful or considered an unwanted phenomenon in many applications. For instance, as discussed before, in the case of the human body being the subject of those vibrations, then it is important to eliminate the counter effect of the added nonlinearity when the higher harmonics fall in the 4-8 Hz region. Because the source of this effect has been identified as the semi-active damper discontinuous force, possible changes to eliminate these force discontinuities is a viable option to eliminate the effect.

While studying and performing numerical and experimental studies on the issue of response time of semi-active dampers (refer to Chapter 5 for details), it was clear that if the response time of a semi-active damper increases, the added nonlinearity effect diminishes. This observation initiates the idea of this new controller.

A typical diagram that describes the implementation of conventional semi-active controllers in a 1DOF system is depicted in Figure 53.
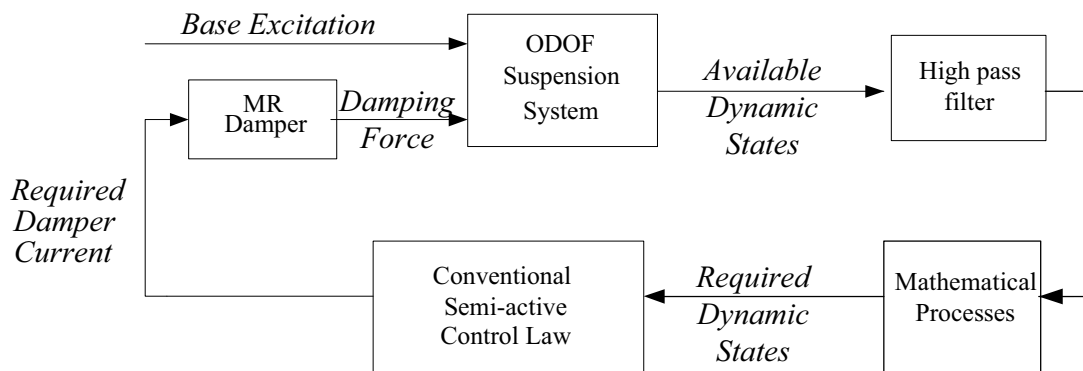
Figure 53: Typical 1DOF system conventional semi-active control implementation

To eliminate the added nonlinearity effects, the controller put out signal (semi-active damper input current) will be filtered using a response-time (e^{-at}) shape filtering. The modified controller implementation is depicted in Figure 54. Using this filtering process, the shape of the actual damper input current signal changes as shown in Figure 55.
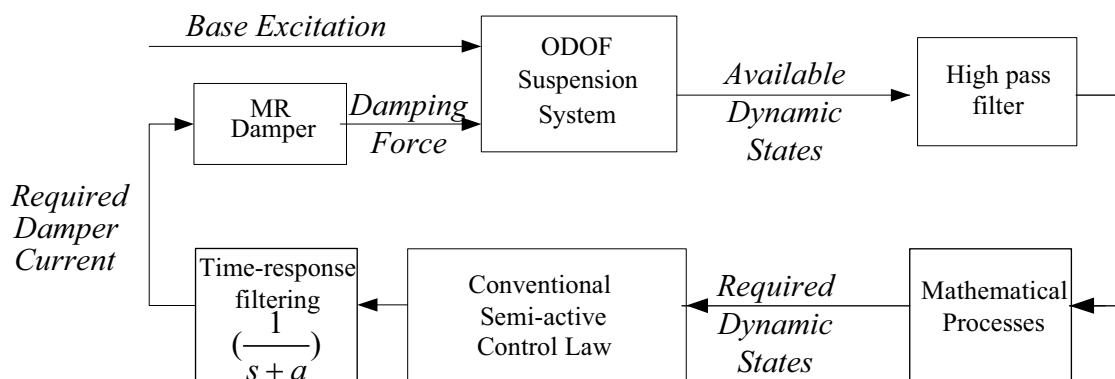
Figure 54: Modified 1DOF system conventional semi-active control implementation
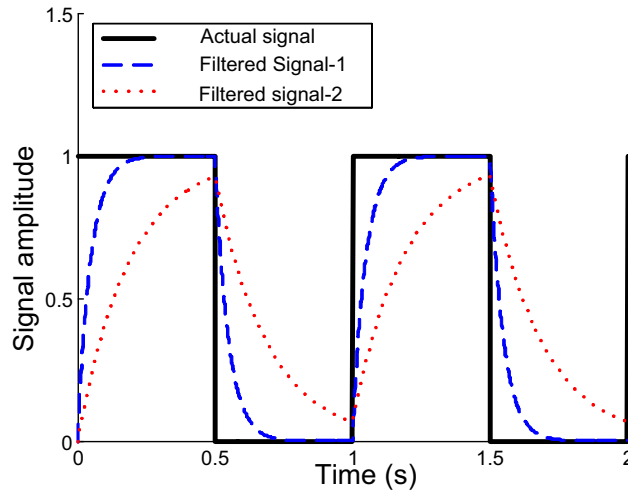
Figure 55: Actual and filtered signal with different "a" values

Note that depending on the application, the filtering process might be required just for a certain time if the switching frequency is below or above a certain value. For instance, when using a suspension system where the goal is to eliminate the harmonics in 4-8 Hz region, the filtering is required if the excitation frequency is in the 1.3-2.6 Hz region. This is implemented in the actual control algorithm using a simple switching process.

To show the effectiveness of the proposed system, a series of simulations were performed and the effect of the proposed control system was observed. Figure 56 shows a sample of those simulation results. As shown, the proposed system eliminates the added nonlinearities effectively. It is important to mention that this process will deteriorate the performance of the semi-active control systems (this subject is discussed in more detail in Chapter 5) to some extent and, as a result, each case should be studied individually and the proper filtering parameter (*a*) determined. This process is also dependent on the response time of the actual semi-active actuator used in the system. If the response time of the device is large, there might be no need to add a physical controller to the system. The lower the response time of the actuator, the greater is the need for this modified system.
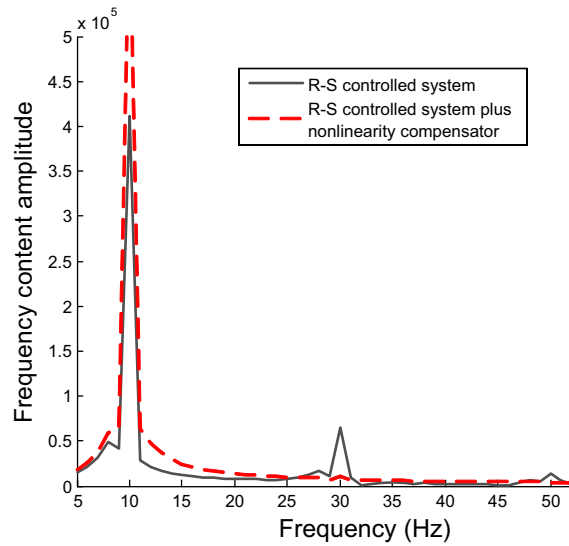
Figure 56: Comparison of the systems response using the new controller to compensate the added nonlinearities with the conventional R-S controlled system

3.4 Root Mean Square (RMS) Comparison Index

The Root Mean Square (RMS) is a useful means to summarize and evaluate the performance of a suspension system and its control strategies. As Hrovat (1997) states, the simple RMS of the acceleration is a satisfactory measure of the ride comfort. In addition, to address the issue, the RMS has been used by many researches in this field, including Hrovat (1997), Ahmadian (1999), Shen (Shen et al., 2006), and Cole (2001). As stated in Chapter 1, in a 1DOF system, there exists an inherent conflict between the acceleration and displacement transmissibility. Usually, this means that in the system operating range, reducing the acceleration results in higher displacement transmissibility. This, in turn, results in two unwanted phenomena in the suspension system. First, the system – dampers or springs – is pushed to its stroke limits (end of the stroke), resulting a hard stop experience. Second, the high displacement transmissibility can result in poor road handling. As a result, to compare the performances of such systems it is practical to compare the RMS of the acceleration transmissibility with the RMS of displacement transmissibility. In the frequency domain, the RMS of a discrete function "f" over a frequency range of r_{min}, r_{max} is calculated based on the following:

80

$$RMS(f) = \sqrt{\frac{1}{(r_{max} - r_{min})} \sum_{r_{min}}^{r_{max}} f^2 \Delta r}$$

(3-22)

in which Δr is the frequency steps.

The corresponding formula for a continues{{continuous?}} function " f " over a frequency range of r_{min}, r_{max} is calculated based on the following:

$$RMS(f) = \sqrt{\frac{1}{(r_{max} - r_{min})} \int_{r_{min}}^{r_{max}} f^2 dr}$$

(3-23)

The RMS is used in the next chapters to compare the performances of different control strategies.

3.5 Conclusions

In this chapter, a different aspect – probably the most neglected aspect – of the semi-active on-off control strategies, the added nonlinearity effect, is introduced and analyzed. The issues of higher harmonics and performance index are discussed in details. A new method to analyze, calculate, and compare the performances of the semi-active controlled systems is proposed. The analytical method of averaging is introduced and used to analyze the conventional semi-active controlled system, namely R-S controlled system. In addition, using the method of averaging results, the applicability and performance of the proposed linearization method are discussed. Moreover, the issue of the higher harmonics is described in detail using numerical simulation analysis. The existence of the phenomena is then confirmed using experimental results. Further, a new controller based on observations of actual test data is proposed, to eliminate the effects of added nonlinearities. This new controller is implemented in numerical simulations, and its applicability and effectiveness are confirmed.

Chapter 4

Effects of Asymmetric Damping on Suspension Performance Indexes and Semi-Active Suspension Control Methods

As described in the previous chapters, on-off semi-active suspension control strategies for suspension systems control the damping ratio of the system through a state-feedback-control. Although these control strategies might use different states and control rules, the resultant controlled system will be a frequency-dependent damping system. In general, even passive systems in some cases can be categorized as the frequency-dependent damping systems. In this chapter, the frequency-dependent asymmetric damping systems are analyzed and studied. The effect of asymmetry on system responses is studied through numerical simulations and the analytical method of averaging. In addition, in this chapter the method of averaging and the RMS optimization procedure (defined in this chapter) is used to analyze the effect of the asymmetric damping on the optimal damping values in passive systems; the method is used to create a design guide for the asymmetric isolator parameters. The effect of asymmetry on the conventional semi-active systems is also studied and the method for the optimal design of asymmetric semi-active systems is discussed.

4.1 Effects of Asymmetric Damping on Vibration Isolation Properties of Suspension System

As stated already, vibration isolators are used to reduce the magnitude of motion or force transmitted from a vibrating source to vibration-recipient bodies. Such recipients might be a foundation, a structure, or even a human body. Despite the advancements in vibration control using active and semi-active systems, passive vibration isolators are still widely used in different industrial applications because of their simplicity and low cost. In this section, we investigate an asymmetric one-degree-of-freedom vibration isolator – an important area in practice because all hydraulic dampers are asymmetric in nature. As discussed previously, because of the non-linearity of this system and because of asymmetric damping discontinuities, analytical methods of averaging and numerical simulation are used to analyze the system's frequency and time-domain response characteristics.

   The equation of motion for a 1DOF system with asymmetric damping is formulated as

$$\ddot{x}_r + 2\zeta\omega_n\dot{x}_r + \omega_n^2 x_r = Y\omega^2 \sin(\omega t)$$

$$\zeta = \begin{cases} \zeta_{reb} & (\dot{x} - \dot{y}) \geq 0 \\ \zeta_{com} & (\dot{x} - \dot{y}) < 0 \end{cases} \tag{4-1}$$

$$\zeta_{com} = \Gamma\zeta_{reb}$$

where ζ_{reb} and ζ_{com} are damping ratios in rebound and compression cycles, respectively. Typically, the automotive industry requirement for a good damper is to acquire a higher damping ratio in rebound than in compression, meaning $0 \leq \Gamma \leq 1$.

The effect of asymmetric damping should be analyzed and studied in more detail for two main reasons: first, to optimize the system parameters properly, and second, to find any possible counter effect of the asymmetric damping into the system's properties. To do this, the numerical simulations are used. To get the closed form equations for displacement transmissibility, λ, and acceleration transmissibility, η, through mathematical analysis, the method of averaging (Wei-Chau, 2006), as described in the previous chapter, is also deployed in this section, while the results are used in the optimization procedure in the next section.

Figure 57 shows a sample comparison of the 1DOF system with a symmetric passive and an asymmetric (for this case $\Gamma = 0.7$) passive damper based on the numerical simulation results. As seen in this figure, the asymmetric damper can effectively reduce the acceleration transmissibility at high frequencies.
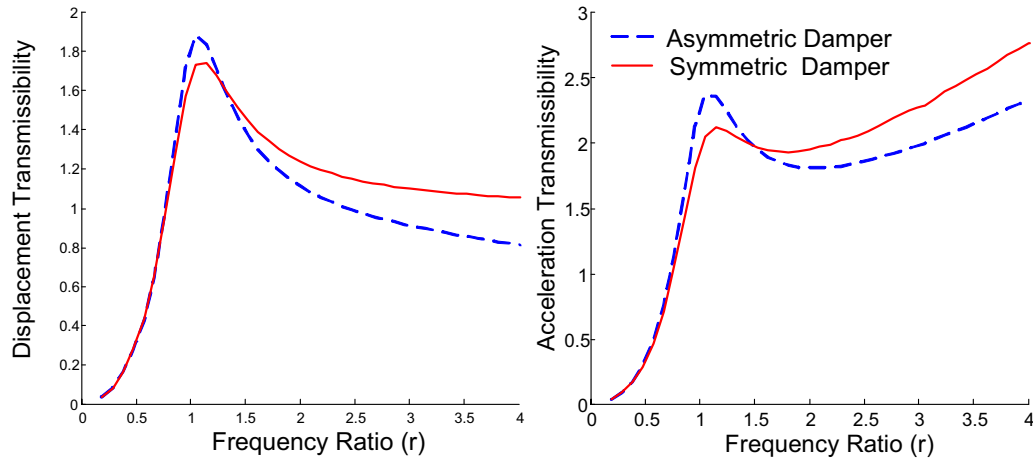
Figure 57 Comparison of symmetric and asymmetric damper performance

Another interesting aspect of the asymmetric damping is a phenomenon called "dynamic-fixed-point" in this thesis. This phenomenon is described through a close look into the time-domain responses of the symmetric and asymmetric damped systems. Consider a 1DOF symmetric system with the properties mentioned in Table 8. The systems response (x_r) under a sinusoidal-based excitation ($0.05\sin(\omega t)$) with the excitation frequency of 15 Hz is shown in Figure 58.

Table 8: Simulation data

System parameter	Value
Sprung mass - m (kg)	2000
Stiffness- k (N/m)	55000
Damping ratio- ζ (Ns/m)	0.7
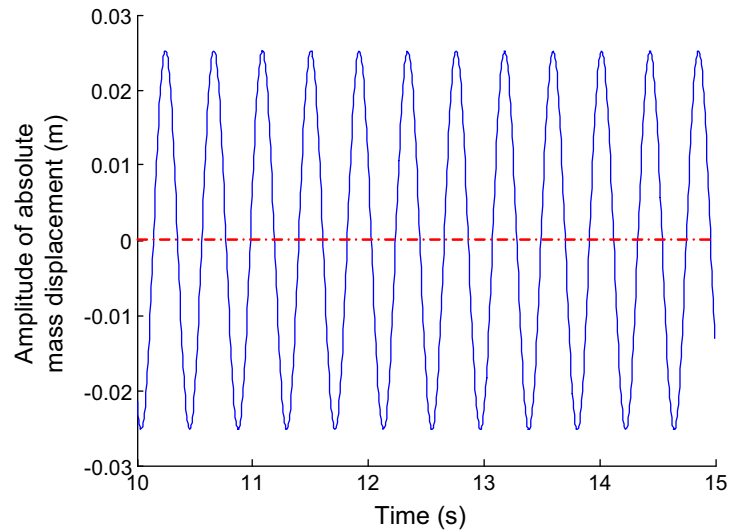
Figure 58: Sample of a 1DOF symmetric system response to base excitation input

As expected, in the steady state the mass vibrates around its static fixed point with the same frequency as the base excitation input frequency with amplitude of 0.025 m. Now consider the same system with asymmetric damping properties. For example, consider $\Gamma = 0.7$, which means $\zeta_{reb} = \zeta_{symmetric} = 0.7$ and $\zeta_{com} = \Gamma\zeta_{symmetric} = 0.49$. Figure 59 shows the asymmetric system's response to the base excitation input.

As depicted in this figure, at steady state the mass vibrates around a shifted point (at nearly -0.02 m) instead of the static fix point of $x_0 = 0$.
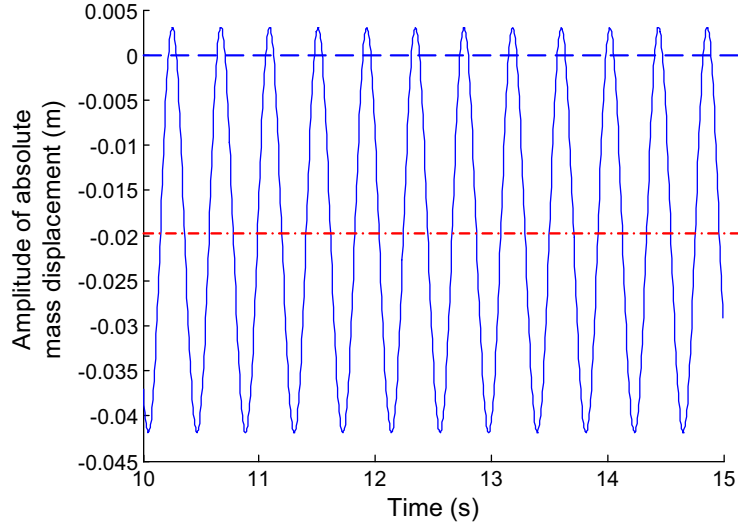
Figure 59: Sample of a 1DOF asymmetric system response to base excitation input

This behavior can be explained through a simplified force analysis on the asymmetric system. A sample of the damper output force in such systems is shown in Figure 60. Assume that the response of the system is in the form

$$x_r = A\sin(\omega t + \phi)$$

(4-2)

and as a result, the relative velocity is

$$\dot{x}_r = A\omega\cos(\omega t + \phi)$$

(4-3)

The asymmetric damping force will be

$$F_d = \begin{cases} F_{reb} = 2\zeta_{reb}\sqrt{km}\dot{x}_r & (\dot{x} - \dot{y}) \geq 0 \\ F_{com} = 2\Gamma\zeta_{reb}\sqrt{km}\dot{x}_r & (\dot{x} - \dot{y}) < 0 \end{cases}$$

(4-4)

This asymmetric force could be treated as the combination of a symmetric force and a discontinuous force as

$$F_d = F_{com} + \begin{cases} F_{reb} - F_{com} & (\dot{x} - \dot{y}) \geq 0 \\ 0 & (\dot{x} - \dot{y}) < 0 \end{cases}$$

(4-5)

85

If we replace the second part of the forcing with its average as a simplification, then the asymmetric system can be considered a symmetric system plus an additional force as

$$F_d = F_{com} + (2\zeta_{reb}\sqrt{km})(1-\Gamma)(A\omega)\,sign(|\dot{x}_r|)$$

(4-6)
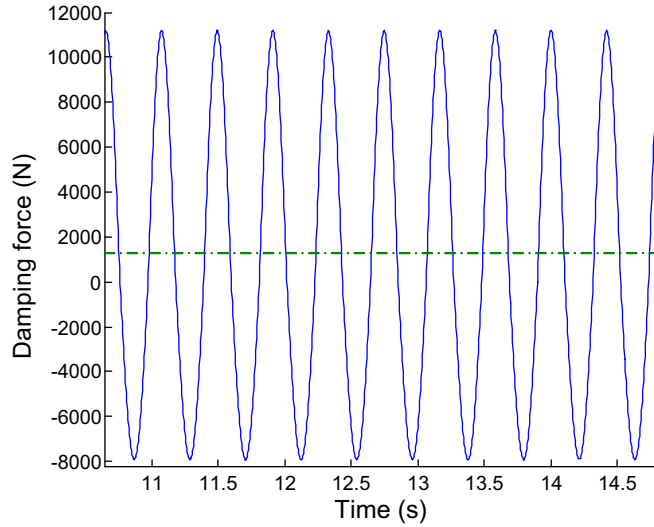
Figure 60: Sample of a 1DOF asymmetric system damping force

As a result, while there exists a relative velocity in the system, the additional force will cause a deflection in the system that can be approximated as

$$x_{d0} = \frac{(2\zeta_{reb}\sqrt{km})(1-\Gamma)(A\omega)\,sign(|\dot{x}_r|)}{k}$$

(4-7)

For instance, for the simulation case presented here, the dynamic fix point is calculated to be $x_{d0} = 0.198$, which a close approximation of the simulation results shown in Figure 59.

The understanding and analysis of this effect is important in the design and implementation of both passive and semi-active suspension systems for the following reasons:

- This phenomenon in reality causes a lower height for the vehicle body, meaning less clearance. This in turn has a positive effect on the stability of the vehicle.

- Lowering the suspension system, on the other hand, will result in a smaller damper stroke in one direction. For instance, if a regular damper has 10 cm of stroke (5 cm in rebound and 5 cm

86

in compression) and if the suspension deflection due to the asymmetry is around 2 cm (as seen for the sample case presented above), then the total damper clearance in the compression stroke is reduced to 3 cm, perhaps causing a hard stop if this parameter is not considered in the design parameters.

- In addition to the above, the understanding of this phenomenon is of extreme importance in the implementation of semi-active controlled system. To clarify, this assumes the R-S control strategy will be implemented in a suspension system. Based on the control strategy (equation (1-25)), to implement the control R-S method, the direction (sign) of relative velocity and displacement of the suspension system must be determined. In a symmetric system, it is easy to determine the directions based on the time domain response of the system, which could be provided with sensory information. For an asymmetric system, however, this is not the case. As shown in Figure 59, due to the shift in the system's fix point, the direction (sign) of the system states must be determined using a different method such as signal filtering. The implementation of high-pass filters is a common practice to eliminate such effects (Smith, S., 2003). This method has been adopted and implemented in the experimental studies of this thesis.

It is important to note that it is possible to treat an asymmetric damping system as a regular average system – the term "regular average" is used here to prevent any confusion between the "Analytical Method of Averaging" and "arithmetic averaging," meaning that the asymmetric system modeled as mentioned in equation (4-1) can be modified as

$$\ddot{x}_r + 2\zeta\omega_n\dot{x}_r + \omega_n^2 x_r = Y\omega^2 \sin(\omega t)$$

$$\zeta = \begin{cases} \zeta_{Ave} & (\dot{x} - \dot{y}) \geq 0 \\ \zeta_{Ave} & (\dot{x} - \dot{y}) < 0 \end{cases}$$

$$\zeta_{Ave} = \frac{\zeta_{com} + \zeta_{reb}}{2}$$

(4-8)

Although this averaged system might be used in many cases, as shown in Figure 61, there will be an error in the calculated system's response depending on the damping ratio and the asymmetry ratio. In addition, use of the regular averaged system will eliminate the non-linear effects of the damping discontinuity, a point discussed in detail in the previous chapter.
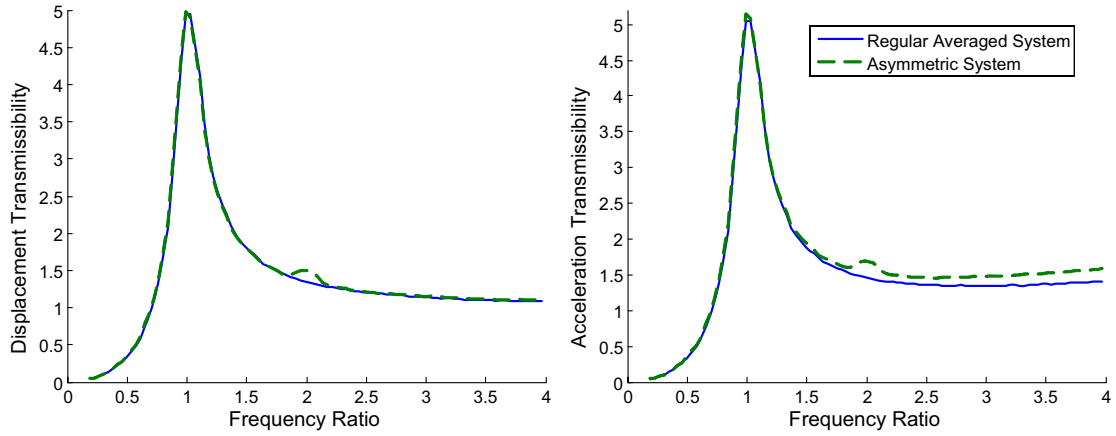
Figure 61: The comparison between asymmetric damping system and the equivalent regular averaged system

4.1.1 Analytical Analysis of Asymmetric Damping System Using Method of Averaging

The method of averaging, as described in Chapter 3, is employed in this section for the analytical study of the asymmetric system properties and to find a closed form solution for the parameters of interests: displacement transmissibility, λ, and acceleration transmissibility, η.

As stated before, in order to analyze the effect of the nonlinearity with the averaging method, it is necessary to transform the equation of motion (Equation (4-1)) to a time-scaled form. The transformed equation of motion is[7]

$$r^2 x_r'' + x_r = -\varepsilon(2\zeta_s r x_r' - Yr^2 Sin(\tau))$$

$$\zeta_s = \begin{cases} \zeta & (\dot{x} - \dot{y}) \geq 0 \\ \Gamma\zeta & (\dot{x} - \dot{y}) < 0 \end{cases} \tag{4-9}$$

Although this nonlinear system might have other periodic solutions such as second and third sub/super harmonics, we consider the solution of equation (4-9) for the main resonance case to be in the form

$$x_r = a_r(\tau)\cos(\phi(\tau))$$

$$\phi(\tau) = \tau + \varphi(\tau) \tag{4-10}$$

Following the mathematical steps described in Chapter 3:

---

[7] The notations used in this section are the same as notations used in Chapter 3 unless otherwise noted.

$$\frac{d(a_r)}{d(\tau)} = -\frac{1}{r^2}\left(\left(r^2 a_r \cos(\phi) - a_r \cos(\phi)\right.\right.$$
$$\left.\left. +2\zeta_s \varepsilon r a_r \sin(\phi) + yr^2\varepsilon \sin(\tau)\right)\sin(\phi)\right)$$

(4-11)

$$\frac{d(\varphi)}{d(\tau)} = -\frac{1}{r^2 a_r}\left(\cos(\phi)\left(r^2 a_r \cos(\phi) - a_r \cos(\phi)\right.\right.$$
$$\left.\left. +2\zeta_s \varepsilon r a_r \sin(\phi) + yr^2\varepsilon \sin(\tau)\right)\right)$$

(4-12)

The asymmetric system equation – (4-9) – is redefined in terms of the polar coordinates (a,φ). Therefore, the transformed equations are

$$r^2 x_r'' + x_r = -\varepsilon(2\zeta_s r x_r' - Yr^2\,Sin(\tau))$$

$$\zeta_s = \begin{cases} \zeta & 0 \le \phi < \dfrac{\pi}{2} \\[2mm] \Gamma\zeta & \dfrac{\pi}{2} \le \phi < \pi \\[2mm] \Gamma\zeta & \pi \le \phi < \dfrac{3\pi}{2} \\[2mm] \zeta & \dfrac{3\pi}{2} \le \phi < 2\pi \end{cases}$$

(4-13)

averaging equations (4-11) and (4-12) over the period of $\phi = [0, 2\pi]$,

$$\bar{a}_r' = \frac{-a_1\zeta_s - a_1\zeta_s\Gamma - a_1\zeta_s - a_1\zeta_s\Gamma - 2Yr\cos(\varphi)}{4r}$$

(4-14)

$$\bar{\varphi}' = \frac{a_1 r\zeta_s - a_1 r\zeta + a_1 r\zeta_s\Gamma - a_1 r\zeta_s\Gamma}{2r^2\pi a_r} + \frac{-r^2\pi a_r + \pi a_r + \pi Yr^2\sin(\varphi)}{2r^2\pi a_r}$$

(4-15)

Solving these equations for the steady state where $\bar{a}_r'(\tau) = 0$, $\bar{\varphi}'(\tau) = 0$, we find the averaged equation for the amplitude and phase of the relative displacement. To find the parameters of interest, (η), it is necessary to find the averaged value for the absolute acceleration, $\ddot{x}(t)$.

$$x = \bar{a}_r \cos(rt + \bar{\varphi}) + Y \sin(vt)$$
$$x = a\cos(rt + \theta)$$
$$a = \sqrt{(\bar{a}_r)^2 + (Y)^2 + 2\bar{a}_r Y\cos(\bar{\varphi})}$$

(4-16)

and

$$\lambda = \left|\frac{x-y}{y}\right| = 2\pi r^2 \left|\frac{1}{\sqrt{A+B+C+D+E+F+G+H}}\right|$$

where:

$A = -8\zeta_s^2 r^2 + 4\zeta_s^2 r^2 + 8\zeta_s^2 r^2 \Gamma$

$B = 4\zeta_s^2 r^2 \Gamma^2 + 4\pi^2 - 8\zeta_s^2 r^2 \Gamma^2$

$C = 4\zeta_s^2 r^2 \Gamma^2 - 16\zeta_s^2 r^2 \Gamma + 8\zeta_s^2 r^2 \Gamma + 4\zeta_s^2 r^2$

$D = \zeta_s^2 \pi^2 r^2 \Gamma^2 + 8\zeta_s \pi r \Gamma + 4\zeta_s^2 \pi^2 r^2 \Gamma$

$E = 2\zeta_s^2 \pi^2 r^2 \Gamma^2 - 8\zeta_s \pi r \Gamma - 8\zeta_s \pi r - 8\zeta_s \pi r^3 \Gamma$

$F = 8\zeta_s \pi r^3 \Gamma + 8\zeta_s \pi r^3 + \zeta_s^2 \pi^2 r^2 \Gamma^2 + \zeta_s^2 \pi^2 r^2$

$G = 2\zeta_s^2 \pi^2 r^2 \Gamma + 2\zeta_s^2 \pi^2 r^2 + 2\zeta_s^2 \pi^2 r^2 \Gamma + \zeta_s^2 \pi^2 r^2$

$H = 8\zeta_s \pi r - 8\zeta_s \pi r^3 - 8\pi^2 r^2 + 4r^4 \pi^2$

(4-17)

As a result, the acceleration transmissibility is

$$\eta = \left|\frac{\ddot{x}}{\omega_n^2 Y}\right| = r^2 \left|\sqrt{(\lambda^2 + 1 \pm 2\lambda\cos(\varphi))}\right|$$

(4-18)

To ensure that the averaging method results match the numerical simulation results, let us consider $\Gamma = 1$. In this particular case, the results, derived from the averaging method should match the theoretical results obtained from equations (1-12) and (1-15). Figure 62 indicates how closely the results match.
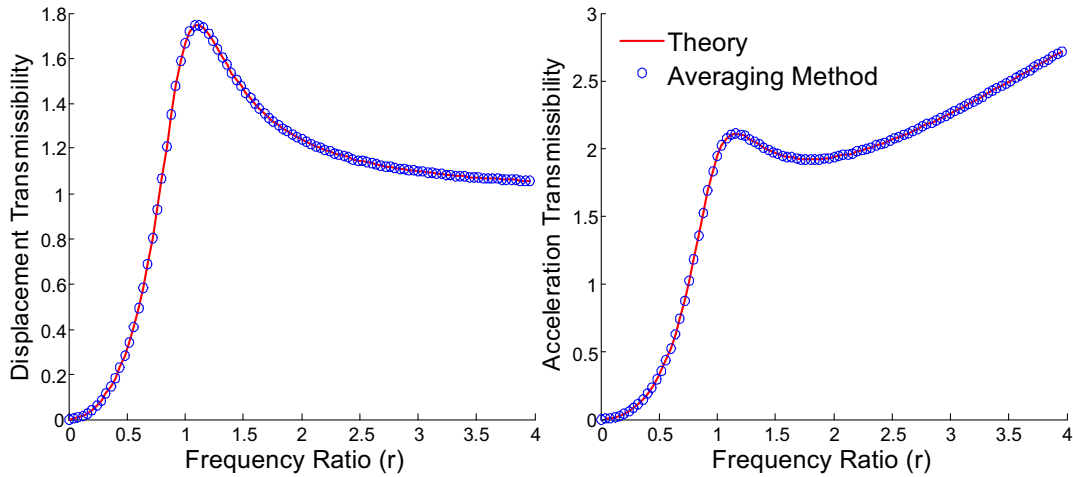
Figure 62 Comparison of the averaging method and the theoretical results for a passive system

4.2 RMS Optimization of a 1DOF System with Asymmetric Damping

As Snowden (Snowden, 1979) states, the reduction of the absolute acceleration, representing the transmitted force, is an important goal of vibration isolators and, in particular, suspension design. A vibration isolator reduces the absolute acceleration by permitting a deflection of the isolator. The relative deflection is a measure of the clearance, known as the working space in the isolator. The clearance should be minimized because the physical constraints in the mechanical design (Narimani, 2004). However, as stated in the previous chapters, these two parameters are in conflict in the operating domain of the vibration isolator.

Depending on the application requirements, various optimization techniques are available; in other words, there is no universally accepted method that can be applied to all cases and ensure the best isolation. This reality explains why the optimization of vibration isolation systems acquired considerable attention in both the past century and the present (Narimani, 2004). Nakhaie Jazar (Nakhaie Jazar *et al.*, 2003) studied, discussed, and compared traditional methods in linear mount optimization. Later, they introduced a new method of optimization for a base excited 1DOF system. Their method is based on the minimization of the acceleration transmissibility with respect to the relative displacement transmissibility. They found an optimal curve on the RMS of Absolute acceleration-RMS(λ) plane. In their optimization study, they considered a linear symmetric damping, as the linearity of the system enabled them to approach the problem analytically (Nakhaie Jazar *et al.*, 2003). Given the analytical approach presented in the previous section, the RMS optimization approach, developed by Nakhaie Jazar (Nakhaie Jazar *et al.*, 2003), is adopted for an asymmetric non-linear system.

4.2.1 Optimization Procedure

In this thesis, the optimum stiffness and damping ratio, values of the asymmetric isolator, are obtained using a cost function in the frequency domain. In this case, the cost function is defined by using the RMS of the average acceleration transmissibility and the RMS of displacement transmissibility over the frequency range of 0-20 Hz; the frequency range for the optimization is based on the optimization application, and for this case, the range is selected due to the suspension isolation application. The definition of the RMS of a function, h(ω), over the range of ω=0-20 Hz based on the equations (3-22) and (3-23) is

91

$$RMS(h(\omega)) = \sqrt{\frac{1}{40\pi} \int_0^{40\pi} h(\omega)^2 d\omega}$$

(4-19)

and in a discrete sense

$$RMS(h(\omega)) = \sqrt{\frac{1}{(40\pi)} \sum_0^{40\pi} h(\omega)^2 (\delta\omega)}$$

(4-20)

where $\delta\omega$ is the frequency change steps.

Applying the procedure for a 1DOF symmetric system, as shown in Figure 63 (Arzanpour *et al.*, 2006), in the RMS(Absolute acceleration)-RMS(λ), the line of minima is the optimum values for the 1DOF linear isolator. If the limit values for RMS of either acceleration or displacement are known, then it is possible to find the optimum-damping ratio for a certain isolating system.

To optimize the design parameters of the asymmetric vibration isolator, RMS of acceleration transmissibility, R, is defined as a function of RMS of displacement transmissibility, ρ, using ζ, ω_n, and Γ as parameters applying the results obtained from the method of averaging. It is important to note that for consistency, in this procedure the RMS of the non-dimensional index "acceleration transmissibility (as defined in equation (1-11))" is used, whereas the procedure defined by Nakhaie Jazar (Nakhaie Jazar *et al.*, 2003) uses the RMS of absolute acceleration, which has the dimension T^{-2}.
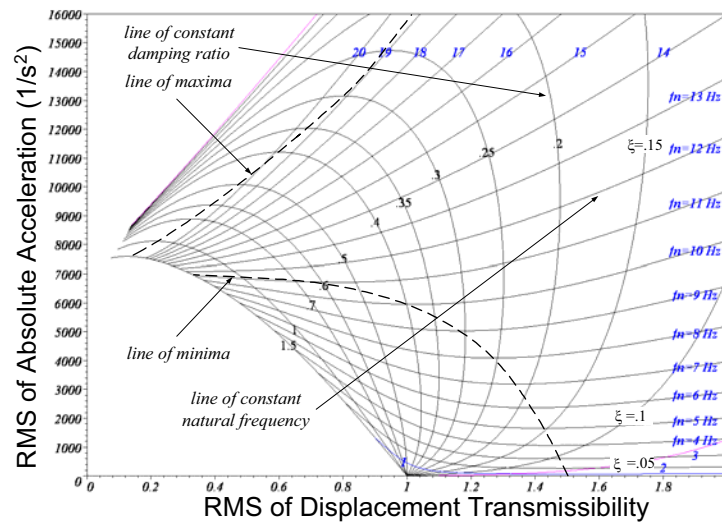
Figure 63: RMS optimization results for a symmetric 1DOF system (Arzanpour *et al.*, 2006)

To make sure that the optimization procedure based on the method of averaging results returns proper results consider the cases where $\Gamma = 1$ (note that $\Gamma = 1$ is the linear symmetric case). It can be seen from Figure 64 that using the method of averaging closed form results and the optimization procedure, the function $R(\rho)$ has a minimum for constant values of natural frequencies (as we expected). A comparison of these results with the results presented by Nakhaie Jazar (Nakhaie Jazar *et al.*, 2003) and (Arzanpour *et al.,* 2006) depicted in Figure 63 reveals that for the two sample cases presented in Figure 64, both methods return the same optimum damping, that is around 0.15 and 0.25 for the systems with 5 Hz and 8 Hz natural frequencies respectively.
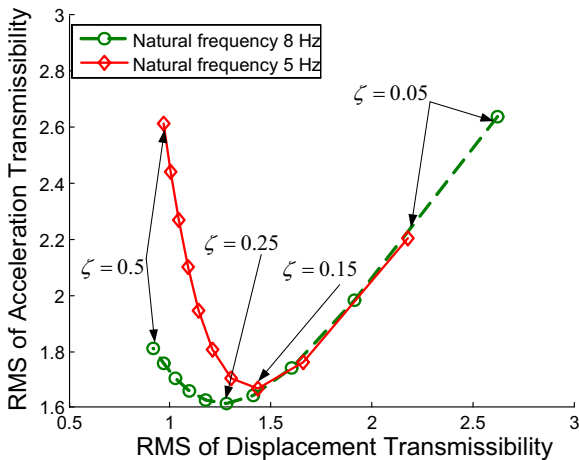
Figure 64: RMS optimization results for an asymmetric 1DOF system while $\Gamma = 1$

The advantage of using the results obtained with the method averaging on the other hand is to implement the procedure into realistic and practical cases where the dampers are asymmetric. Figure 65 and Figure 66 show the results of the optimization for the cases where $\Gamma = 0.8$ and $\Gamma = 0.4$, respectively.
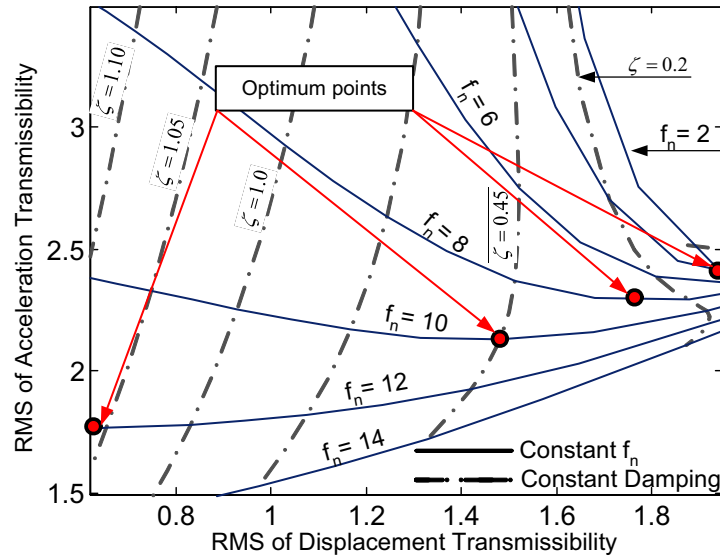
Figure 65: Contour curves for the function $R = f(\rho)$ **and the optimum damping points for the case:** $\Gamma = 0.8$
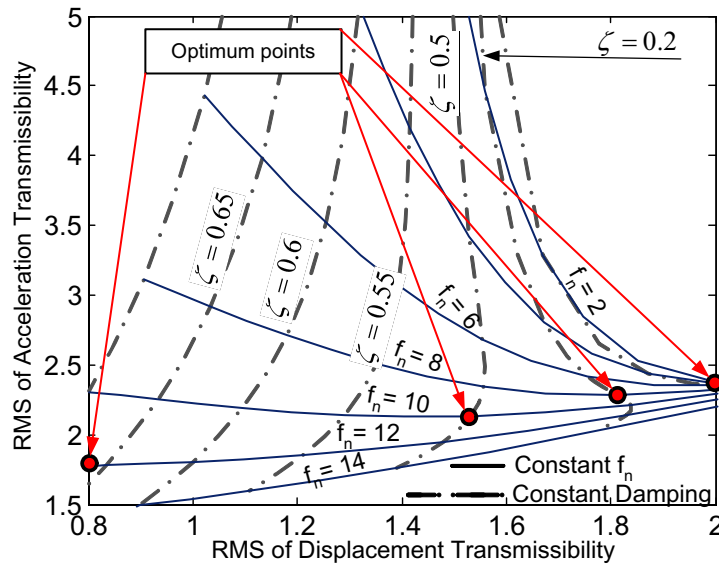
Figure 66: Contour curves for the function $R = f(\rho)$ **and the optimum damping points for the case:** $\Gamma = 0.4$

From these figures, which can be obtained for any natural frequency and Γ value, the optimum-damping ratio of the asymmetric vibration isolators can be found using the averaging method and the RMS optimization procedure if the limit value of RMS of either acceleration or displacement is known.

One interesting aspect of the asymmetric vibration isolator optimization is the shift in optimum damping ratio. For instance, in Figure 65, the case in which $\Gamma = 0.8$, the optimum-damping ratio for the system with natural frequency of $f_n = 10$, is $\zeta = 0.45$, while in Figure 66, the case in which $\Gamma = 0.4$, this optimum point is $\zeta = 0.5$.

On the other hand, as depicted in Figure 67, the results show that in the low damped systems ($\zeta = small$), regardless of the systems' natural frequency, R is a linear function of ρ.
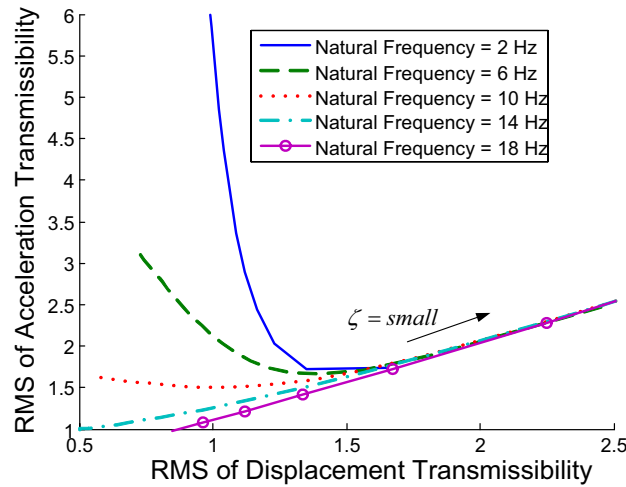
Figure 67: Effect of systems' natural frequency on R-ρ relation

4.2.1.1 Time Domain Examples

The verification of the optimization results can be examined by studying the behavior of the system for the optimal parameters. The goal of the example presented in this section is to compare the optimization results for the asymmetric system with results for a symmetric system, not to validate the optimization procedure. There are many analysis and examples in the prior art to support the performance of the optimization procedures (Nakhaie Jazar *et al*., 2003) and (Arzanpour et al., 2006).

Consider two asymmetric 1DOF systems with the properties listed in Table 9. The damping ratio of system-1is obtained using the RMS method for a symmetric case ($\Gamma = 1$). On the other hand, the damping ratio of system-2 is the optimized damping point using the RMS method for the asymmetric system for the case $\Gamma = 0.3$. Figure 68 (on the top) shows the response of the two systems to an arbitrary step input.

Table 9: 1DOF systems properties for the example

System parameter	System 1	System 2
Natural Frequency	10 Hz	10 Hz
Asymmetry factor (Γ)	0.3	0.3
Optimal damping ratio (obtained using the RMS method)	0.4	0.6

As depicted in this figure, the response of the system-2 with the optimized damping ratio reduces the mass absolute acceleration and relative displacement of the system. As shown, the maximum amplitudes are reduced in both graphs for the optimized system. In addition, the settling time is much smaller for the optimized system.
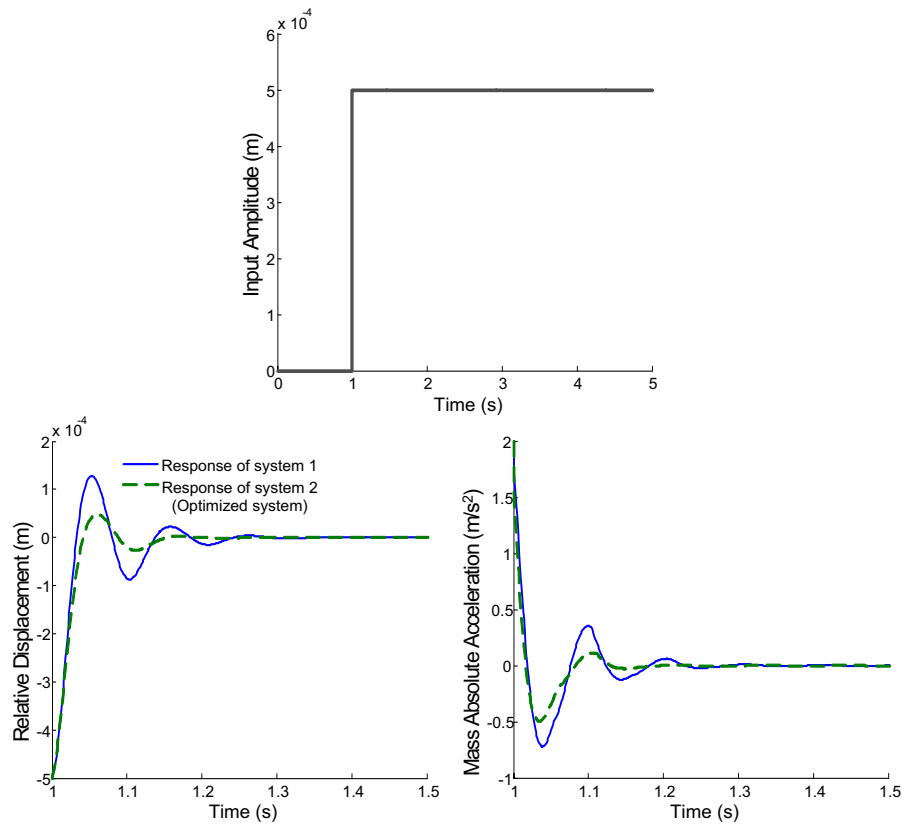
Figure 68: Comparison of the responses of two asymmetric systems with and without optimized damping ratio (Top: input signal, Bottom: systems' responses)

96

4.3 Conclusion

In this chapter, the effect of asymmetric damping in 1DOF quarter car model has been analyzed and the effect of asymmetry on the suspension performance indexes has been explored. The concept of dynamic fix point of the system because of damper asymmetry has also been explained and established. Using the method of averaging descried earlier in Chapter 3, a closed form solution for the 1DOF asymmetric system and the parameters of interest has been obtained. Further, the RMS optimization method has been implemented to the asymmetric system parameters, and the optimized damping ratio has been obtained. In addition, the necessity of having a high-pass filtering in semi-active suspension control implementation has been investigated using the asymmetric damping analysis and the dynamic fix point concept.

Due to similarities among the semi-active control systems and the passive asymmetric damping systems, the application of the asymmetry concept in conventional control strategies has been considered. This topic is discussed and analyzed in detail in Chapter 6.

Chapter 5

Response-time of the Semi-Active Controlled systems

Given advancements in the vibration control strategies and controllable actuator manufacturing, the semi-active actuators (dampers) are finding their way as an essential part of vibration isolators, particularly in vehicle suspension systems. As briefly discussed before, currently available semi-active damper technologies can be divided into two main groups. The first uses controllable electromagnetic valves; the second uses magnetorheological (MR) fluid to control the damping characteristics of the system.

Despite different semi-active control methods and the type of actuators used, the response-time (delay) is an important practical aspect of all hydro-mechanical computer controlled systems. The actuator – in this thesis, the controllable damper – usually introduces the longest response time in a hydro-mechanical computer controlled system.

This chapter investigates the effect of response-time in an on-off controlled suspension system equipped with semi-active dampers. A 1DOF quarter car system (as described and modeled in Chapter 1) mainly is used for the purpose of this study. Numerical simulations and analytical techniques are employed to explore the issue. The performance of the system as a function of systems' response time is then analyzed and discussed. Specifically, the effect of the response time on the performance of a 1DOF suspension system controlled by conventional on-off control strategies such as Skyhook and Rakheja-Sankar (R-S) is studied. Finally, the test method and test results measuring the response-times of a number of semi-active dampers are presented.

Unfortunately, a review of the literature has shown that a detailed description of the response time of the semi-active dampers is seldom given and the methods of computing the response time are not discussed in detail (Koo, J. *et al.,*2006). In the research work by Koo, J. *et al.*(2006), a comprehensive study on the MR damper response-time has been presented. However, the effect of the response-time on the overall performance of the semi-active controlled system is not discussed, nor is the response-time of the solenoid valve controlled semi-active dampers studied.

5.1 Response-time and Semi-Active Controlled System Model

The response-time of an electro-mechanical system is affected by the inductance in the system (normally a coil). In order to determine the electrical response-time of the system, it can simply be considered a circuit consisting of a resistor and an inductor in series (Elmer and Gentle, 2001). The current response through the circuit when a step voltage is applied can be calculated as

$$I = \frac{V}{R}\left[1 - e^{\frac{-tR}{L}}\right]$$

(5-1)

where I is the applied current, V is the voltage, R is the resistance, and L is the inductance of the system.

In the case of a semi-active dampers, assuming the damping ratio, ζ, is a function of the current, I, and assuming the overall response-time of the damper can be modeled in the form of the electrical response time, then

$$\frac{\zeta}{\zeta_0} = 1 - e^{-\alpha t}$$

(5-2)

where α is determined through the real time testing of the semi-active damper, and ζ_0 is the final value of the damping due to the controller output.

Figure 69 shows a typical semi-active on-off controlled system's command signal in the ideal case (zero response-time) and in the real case where the response-time exist. Although there is no universally accepted definition for the response-time, in the literature different values have been suggested for response-time calculations. In this thesis, as shown in Figure 69, response-time is defined as "the required time for the actual signal to reach 90% of the required (command) signal."

Considering the response-time, the original equation of motion for a 1DOF semi-active R-S controlled system (equation (1-25)) will be in the form of

$$\ddot{x}_r + 2\zeta\omega_n\dot{x}_r + \omega_n^2 x_r = Y\omega^2 \sin(\omega t)$$
$$\zeta_s = \begin{cases} \zeta_{max}(1 - e^{-\alpha t}) + \zeta_{min}\ e^{-\alpha t} & (x_r)(\dot{x}_r) \leq 0 \\ \zeta_{min}(1 - e^{-\alpha t}) + \zeta_{max}\ e^{-\alpha t} & (x_r)(\dot{x}_r) > 0 \end{cases}$$
$$\zeta_{min} = \beta\zeta_{max} \qquad 0 \leq \beta \leq 1$$

(5-3)

and the original equation of motion for a 1DOF semi-active Skyhook controlled system (equation (1-19)) will be

$$\ddot{x}_r + 2\zeta\omega_n\dot{x}_r + \omega_n^2 x_r = Y\omega^2 \sin(\omega t)$$

$$\zeta_s = \begin{cases} \zeta_{min}(1-e^{-\alpha t}) + \zeta_{max} e^{-\alpha t} & (\dot{x})(\dot{x}_r) < 0 \\ \zeta_{max}(1-e^{-\alpha t}) + \zeta_{min} e^{-\alpha t} & (\dot{x})(\dot{x}_r) \geq 0 \end{cases} \tag{5-4}$$

$$\zeta_{min} = \beta\zeta_{max} \qquad 0 \leq \beta \leq 1$$
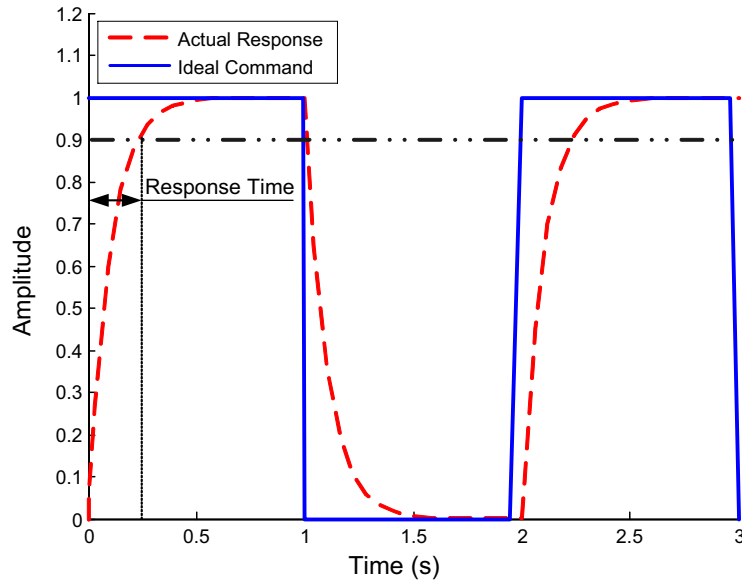
Figure 69: Comparison of the actual and ideal command signals

In the above equation, the controllable damping ratio (ζ_s) switches between a high value (ζ_{max}) and a low value (ζ_{min}).For the case, where $t \to \infty$, the controllable damping ratio approaches the original values suggested by equations (1-19) and (1-25).

5.2 Effects of Semi-Active Dampers Response-Time on the Suspension Performance Indexes

In this section, using these models and the numerical simulation and analytical analysis, the effect of the response-time on the suspension performance indexes is studied.

5.2.1 Numerical Analysis

In this section, the suspension performance indexes of the conventional semi-active controlled system using the proposed models (section 5.1) are assessed through numerical simulation. The results are also compared with those of the ideal (zero response-time) system to investigate the effect of time response on the performance of conventional control techniques.

Matlab®/Simulink tools were used to carry out the numerical simulations. The model parameters for the simulations are listed in Table 10. The results are obtained and discussed in frequency domain.

In all the numerical simulations, the modified case of the control techniques is considered, where the damper (virtually) produces no damping force in the low state ($\beta = 0$).

Table 10: Numerical simulation parameters

System parameter	Value
Sprung mass - m (kg)	2,000
k (N/m)	55,000
c (Ns/m)	varies
α (1/s)	varies

Figure 70 shows and compares the performances of an R-S controlled semi-active system with different pre-set values of the damper response-time (α). As shown, the performance of the system with 1 ms of response-time is close to that of the ideal system (zero response-time). As the response-time increases to 2 and 5 ms, in higher frequency region ($r > 1$) the acceleration transmissibility exhibits higher values (worse performance), while, interestingly, the displacement transmissibility stays nearly at the same level in the same frequency region. While the time response of the system continues to increase, for instance to 10 ms, the system's acceleration transmissibility is much higher and, at the same time, the displacement transmissibility is higher. Interestingly, as the response-time rises, the behavior of both acceleration and displacement transmissibility of the system changes dramatically. The patterns of those changes are also altered. As shown in Figure 70, when the response-time is equal to 20 ms in the higher frequency region, nearly at the point where $r \approx 1.25$ the acceleration transmissibility exhibits lower values (better performance). Even in the higher frequency region, the recorded values for

the acceleration transmissibility falls below the ideal system (zero response-time). This effect will be discussed in detail.

Figure 71 illustrates the same comparison for a 1DOF semi-active system, controlled by the Skyhook method. The phenomena described for the R-S controlled system could be found in this system as well. However, the acceleration transmissibility of Skyhook controlled system appears to be more sensitive to the response-time of the semi-active damper in the higher frequency region ($r > 1$) than the R-S controlled system. Interestingly, for the case where the response-time is 20 ms, the dramatic change in the acceleration transmissibility pattern is noticed as well.
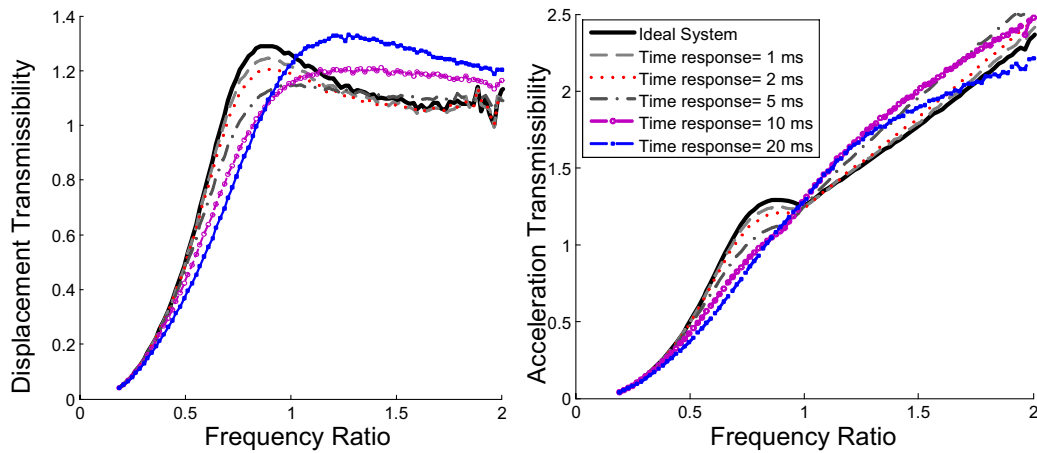
Figure 70: Comparison of the response-time effect on the performance of R-S controlled system
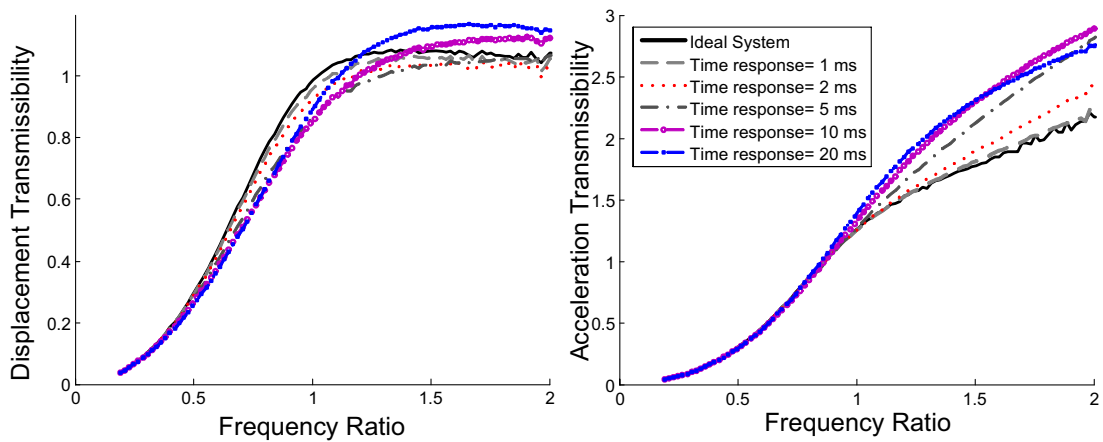
Figure 71: Comparison of the response-time effect on the performance of Skyhook controlled system

The dramatic changes in the higher frequency region, for high response-time (20 ms in this case) of the semi-active dampers, described above, can be explained using Figure 72. When the frequency of the command signal is high (the left drawing of Figure 72), the system with high response-time never reaches the required (commanded) value, or at least never exceeds 90% of the required value for a certain amount of time; as a result, the system acts completely differently and the trend gets distorted. However, the same system with the same response time is able to reach the commanded value – or realistically exceed 90% of the commanded value for a certain amount of time – if the command frequency is lower (see right drawing of Figure 72)
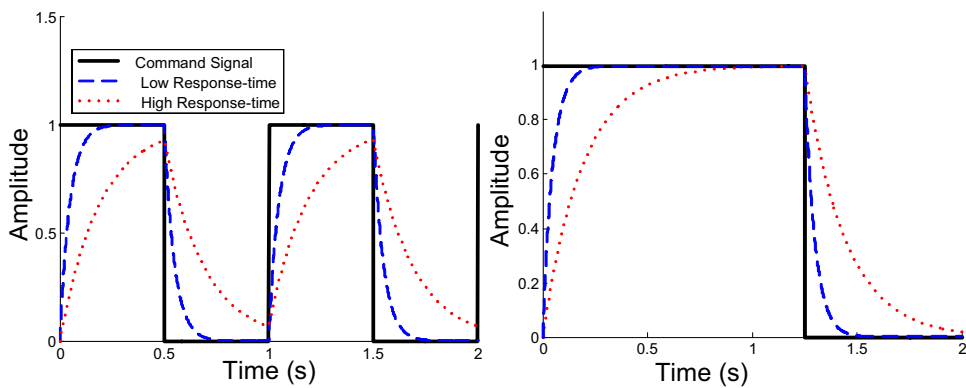
Figure 72: Effect of response time on the semi-active damper output in different frequencies (Left): High switching frequency, (Right): Low switching frequency

As a result, it is important to find the proper limits for the command-switching frequency and the response time of the semi-active damper such that the performance of the system remains at an acceptable level over the entire working region. Unfortunately, there is no global answer for this problem because the command signal frequency is a function of control algorithm, so, as a result, this should be analyzed separately for each case. For instance, consider the R-S control strategy used to control a suspension system. Under a pure sinusoidal base excitation with a certain frequency, ω, and due to the control strategy laws (equation (1-25)), Figure 73 illustrates the switching sequence and switching frequency.
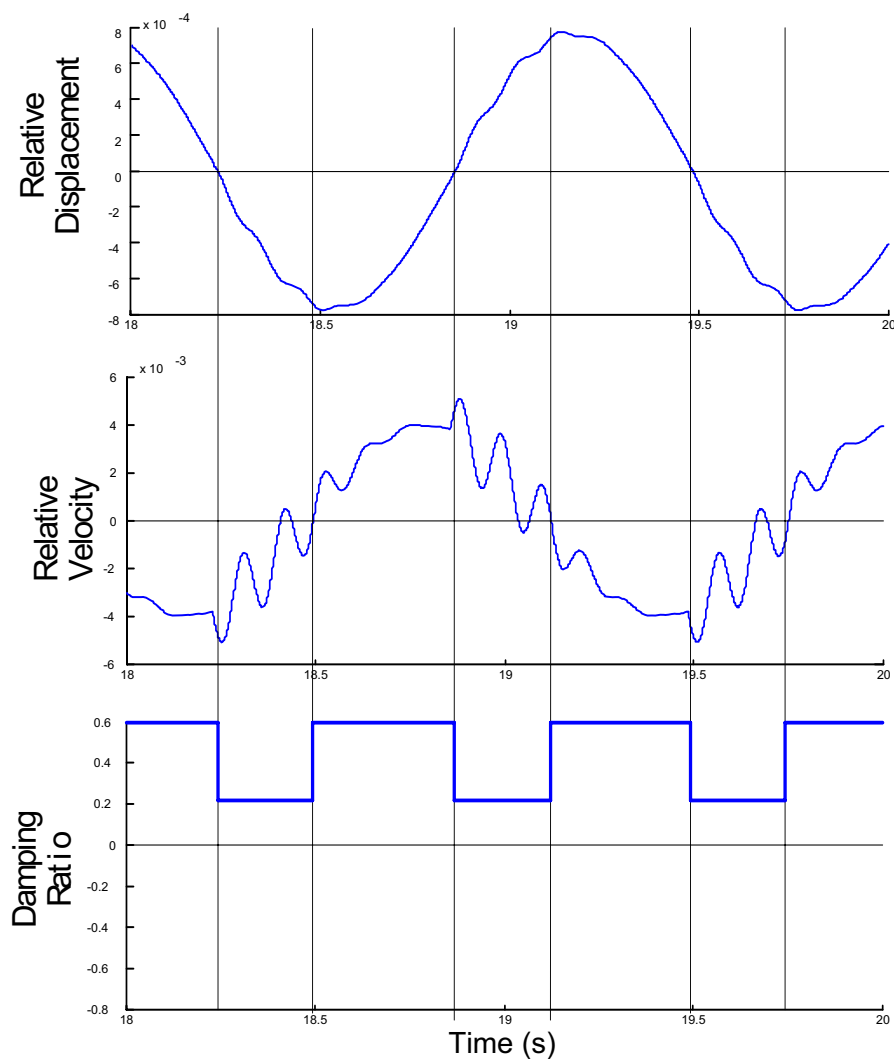
Figure 73: Relation between excitation frequency and the R-S controller switching frequency

As shown in this figure, the switching frequency will be twice the excitation frequency. For this application (Vehicle Suspension), this in turn could be translated as 0-40 Hz (as the road-induced vibrations are normally considered to be in the range of 0-20 Hz). To explain the matter clearly, a new term "Effective-time" is defined. The effective-time is described in Figure 74 and can be mathematically expressed as

$$Effective\,time = \frac{T}{2} - response\,time \qquad\qquad \textbf{(5-5)}$$

From the system's design point of view, the effective time should be determined based on a cost-performance analysis. The effective-time is the duration where the signal reaches, and stays at or above, a certain threshold (in this case 90% of the command). If the effective-time of the system is determined using the switching frequency of the system, it is possible to find the response-time boundary. Following the previous example and considering that the effective time of the system is zero, then the response-time boundary will be

$$0 \le response\,time \le (\frac{T}{2} = 12.5 \ ms)$$

which means that the response time of a proper semi-active device for a suspension system control using R-S strategy should be in this range.
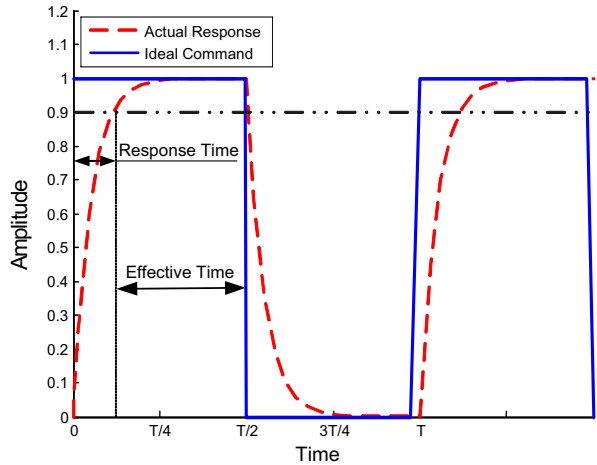
Figure 74: Definition of signal effective time

In section 5.2.3, based on the experimental results, the measured response-time of some conventional semi-active dampers are presented.

5.2.2 Analytical Method of Averaging

To explore the semi-active on-off controlled systems and the effect of response time of the semi-active dampers, through mathematical analysis the method of averaging as described in Chapter 3 is deployed. As stated previously, to analyze the response time of the semi-active dampers, each control technique should be treated separately. In what follows, the semi-active system controlled using the R-S technique is analyzed.

As stated before, in order to analyze the effect of the nonlinearity with the averaging method, it is necessary to transform the equation of motion (equation (5-4)) to a time scaled form. The transformed equation of motion is[8]

$$r^2 x_r'' + x_r = -\varepsilon(2\zeta_s r x_r' - Yr^2 \, Sin(\tau))$$

$$\zeta_s = \begin{cases} \zeta_{max}(1-e^{-\alpha t})+\zeta_{min} \, e^{-\alpha t} & (x_r)(\dot{x}_r) \le 0 \\ \zeta_{min}(1-e^{-\alpha t})+\zeta_{max} \, e^{-\alpha t} & (x_r)(\dot{x}_r) > 0 \end{cases}$$

$$\zeta_{min} = \beta \zeta_{max} \quad 0 \le \beta \le 1$$

$$\text{(5-6)}$$

Following the mathematical steps described in Chapter 3:

$$\frac{d(a_r)}{d(\tau)} = -\frac{1}{r^2}\Big((r^2 a_r \cos(\phi) - a_r \cos(\phi)$$

$$+2\zeta_s \varepsilon r a_r \sin(\phi) + yr^2 \varepsilon \sin(\tau))\sin(\phi)\Big)$$

$$\text{(5-7)}$$

$$\frac{d(\varphi)}{d(\tau)} = -\frac{1}{r^2 a_r}\Big(\cos(\phi)(r^2 a_r \cos(\phi) - a_r \cos(\phi)$$

$$+2\zeta_s \varepsilon r a_r \sin(\phi) + yr^2 \varepsilon \sin(\tau))\Big)$$

$$\text{(5-8)}$$

The asymmetric system equation, equation (4-9), is redefined in terms of the polar coordinates (a,φ). Therefore, the transformed equations are

---

[8] The notations used in this section are the same as notations used in Chapter 3 unless otherwise stated.

$$\zeta_s = \begin{cases} \zeta_{max}(1-e^{-(\alpha/\nu)\tau})+\beta\zeta_{max}\ e^{-(\alpha/\nu)\tau} & 0\le\phi<\dfrac{\pi}{2} \\[2ex] \beta\zeta_{max}(1-e^{-(\alpha/\nu)\tau})+\zeta_{max}\ e^{-(\alpha/\nu)\tau} & \dfrac{\pi}{2}\le\phi<\pi \\[2ex] \zeta_{max}(1-e^{-(\alpha/\nu)\tau})+\beta\zeta_{max}\ e^{-(\alpha/\nu)\tau} & \pi\le\phi<\dfrac{3\pi}{2} \\[2ex] \beta\zeta_{max}(1-e^{-(\alpha/\nu)\tau})+\zeta_{max}\ e^{-(\alpha/\nu)\tau} & \dfrac{3\pi}{2}\le\phi<2\pi \end{cases} \qquad \textbf{(5-9)}$$

Averaging equations (5-7) and (5-8) over the period of $\phi=[0,2\pi]$ and solving these equations for the steady state where $\bar{a}_r'(\tau)=0$, $\bar{\varphi}'(\tau)=0$, we find the averaged equation for the amplitude and phase of the relative displacement. To find the parameters of interest, (η,λ), it is necessary to find the averaged value for the absolute acceleration, $\ddot{x}(t)$, using the following mathematical relations

$$\begin{aligned} x &= \bar{a}_r\cos(rt+\bar{\varphi})+Y\,sin(vt) \\ x &= a\cos(rt+\theta) \\ a &= \sqrt{(\bar{a}_r)^2+(Y)^2+2\bar{a}_r Y\cos(\bar{\varphi})} \end{aligned} \qquad \textbf{(5-10)}$$

To ensure that the averaging method results match the numerical simulation results, consider $e^{-(\alpha/\nu)\tau}=0, \beta=1$ (passive system). In this particular case, the results, derived from the averaging method, should match the theoretical results obtained from equations (1-12) and (1-15). Figure 75 indicates how closely the results match.
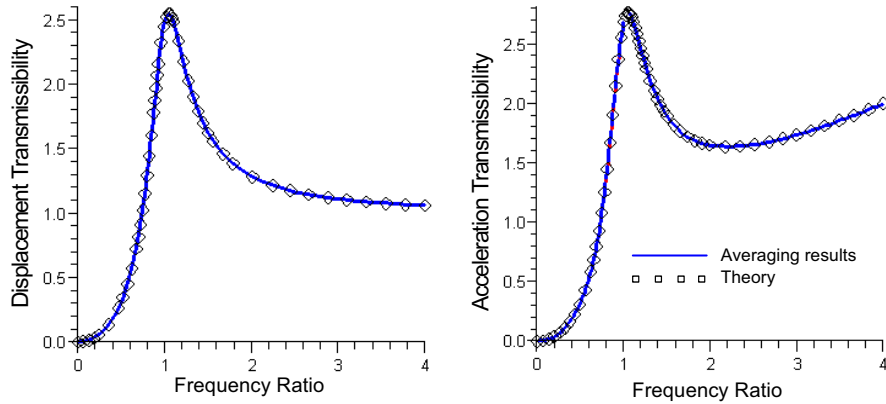
Figure 75: Comparison of the averaging method and the theoretical results

The method of averaging provides the analysis results much faster than the numerical simulations method. Figure 76 shows a sample of the averaging method results comparing the performance of a passive system with that of the R-S controlled systems (for the case where $\beta = 0$) having 1 ms and 5 ms of response-time. As in the numerical simulation results, as expected, the analytical results show that a higher response time results in higher acceleration transmissibility in the higher frequency regions.
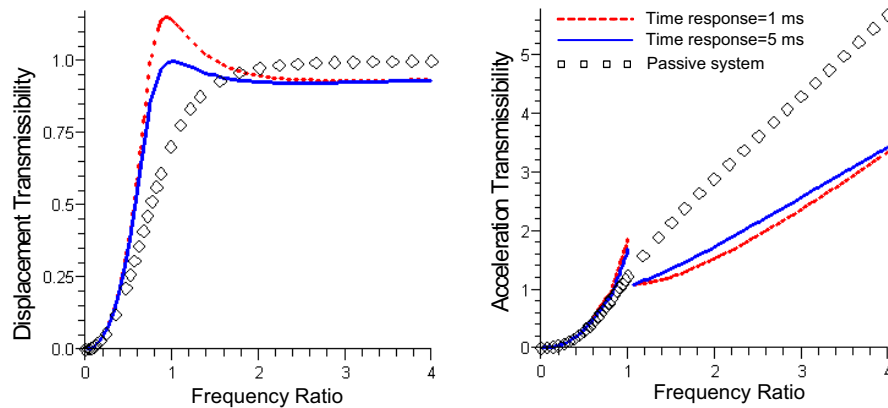
Figure 76: Results obtained by the method of averaging

One shortcoming of the averaging method adopted in this section is that it is unable to show the effect of the high frequency command signal on the system performance. The results obtained from the method of averaging are valid, while the response-time is in the acceptable boundaries, as discussed earlier in this chapter.

5.2.3 Experimental Results and Response-Time Measurements

In this section, the actual response-time of few commercially available, semi-active dampers are tested and presented. The main goals of this section are first, to gain a sense of the actual response time of the semi-active dampers; and second, to compare the test results (the total response-time) and the electrical response-time calculated based on equation (5-1).

To perform the tests, an MTS damper dynamometer with a maximum velocity of 100 in/sec and a maximum load of 20,000 lbf connected to a MTS Test Star II controller was used. The MTS machine was equipped with a 0-100 kN rate load cell and an internal LVDT to measure the relative displacements. To implement the current control system, MATLAB/XPC target was adopted and used.

The main advantage of MATLAB/XPC target is to provide real time control, while at the same time, it calculates the average response-time of the control process algorithm and hardware. The system sampling frequency was set to 2000 Hz. At this frequency, the resolution of the results are 0.5 ms.

In order to evaluate the response-time of the semi-active dampers, an input signal had to be chosen that would ensure constant velocity across the damper. The importance of maintaining a constant velocity becomes clear by considering the force due to the damper. For example, if a sine wave were chosen as the input, the damper force would vary continuously according to the changing velocity of the input. Because the only concern is the change in damper force due to the activation of the signal, the force change due to the velocity complicates the analysis. For this reason, the most appropriate signal that satisfies the constant velocity condition is a triangle wave. Figure 77 shows the input signal used in this study (Koo, J. *et al.,* 2006).
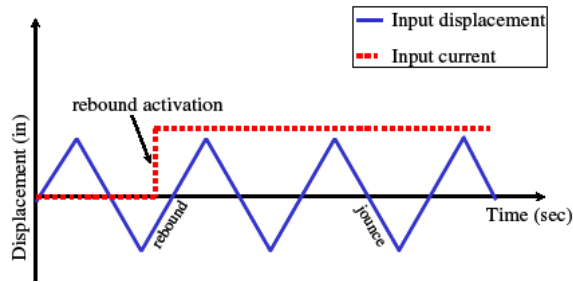
Figure 77: Illustration of proposed constant velocity input (Koo, J. *et al.,* 2006)

Many tests have been performed on different available semi-active dampers. The dampers in question are those shown in Table 5, excluding the last one (GKEC External Valve Damper). Figure 78 shows a sample of tests performed on the internal valve solenoid damper to measure the response-time of the semi-active damper. The calculated average response time based on the test results was recorded as 14 ms. To find the electrical response time of the system, the inductance of the solenoid was measured with an inductance meter and found to be approximately 16 milli-Henrys. The coil resistance is 7.4 ohms. Therefore the current reaches 90% of its steady state (response time) value after 5.0 ms. In addition, the XPC-target system shows an average response-time of 1.4 ms for the current control process. This means that the total electrical response time is 6.4 ms – nearly half of the overall result of 13.5 ms. Table 11 summarizes the results of the response measurement tests.
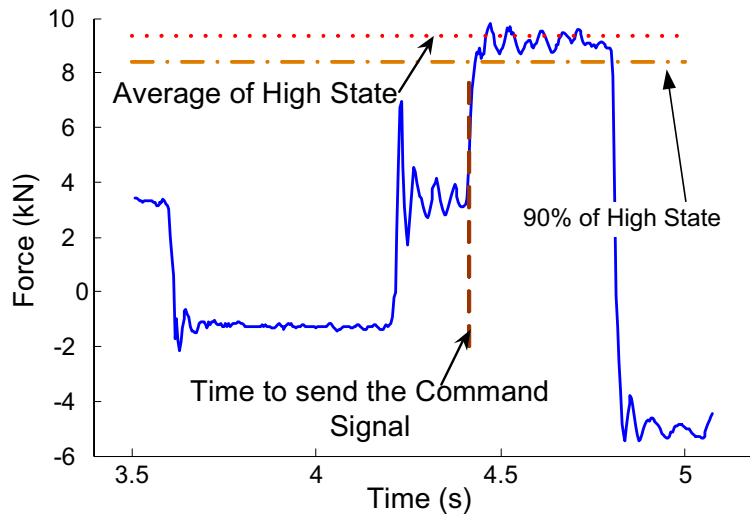
Figure 78: Sample test result to measure the semi-active damper response-time

Table 11: Response-time measurement results based on 10 different tests (ms)

Damper Type	Average Response time	Min. Recorded Response time	Max. Recorded Response time	Electrical Response time
Generic MR	10.0	8.5	14.0	2.3
Generic External Solenoid Valve	12.5	9.0	15.0	3.6
Internal Solenoid Valve	13.5	10.0	16.5	5.0

Given the results presented in Table 11 and the response-time boundary calculated in the previous section (12.5 ms), both generic MR damper and generic external solenoid valve damper are completely suitable for use on the vehicle suspension system, while the internal solenoid valve damper still needs improvement.

5.3 Effect of the Response Time on Nonlinearity of the Semi-Active Controlled Systems

As discussed in Chapter 3, the existence of the excitation frequency harmonics in a semi-active controlled system might be considered as an unwanted phenomenon in many applications. The source

of this effect has been identified as the semi-active damper discontinues force. While studying and performing numerical and experimental studies on the issue of response-time of semi-active dampers, it was observed that if the response-time of semi-active dampers is high, the added nonlinearity effect diminishes. This observation initiates the idea of the new controller to compensate the undesired effects of the switching system, as discussed in Chapter 3. The analysis in this chapter illustrates that such controller will have a counter-effect on the overall performance of the suspension control strategies. As a result, a detailed cost-performance analysis should be performed to analyze the inclusion of such device into the semi-active controlled systems. In addition, the inherent semi-active actuator's response time might be sufficient to eliminate or at least weaken such effects in real-life systems.

5.4 Conclusion

In this section, the effects of the response time of semi-active dampers on the performance of the suspension performance indexes are studied. Numerical simulations and the analytical method of averaging are used to study the effect of the response time on the overall performance of the semi-active, on-off controlled system. It is shown that the longer response time of semi-active damper will result in the higher acceleration transmissibility of the system.

In addition, it is discussed that for a semi-active on-off controlled system, it is important to set and to find the proper limits for the switching frequency of command signal as well as the response time of the semi-active dampers. A simplified and practical method is then presented and, based on suspension requirements, the response-time boundary is calculated. The boundary is calculated such that the performance of the controlled system remains at an acceptable level on the entire predicted working domain.

Moreover, the response time of three different semi-active dampers are measured and compared. Test results are used to confirm the difference between the electrical and overall response times of a semi-active damper. This study advances the existing state of the art in semi-active suspension control.

Chapter 6

Semi-Active Suspension Control System for Ride Comfort, Road Handling, and Rollover Stability

As stated in the thesis introduction, in general, there are three broad classifications of suspension systems: passive, active, and semi-active. Each of these suspensions has different advantages and disadvantages. Passive suspensions are the common systems currently available in most vehicles. These systems are composed of conventional components including springs and dampers (with fixed properties).

As Segel (1993) notes, the earliest attempt to improve ride comfort using controllability of active suspension systems appeared in 1961. Regarding the active suspension, different control methods, for instance optimum control, have been discussed in the literature to control the active systems (Esmailzadeh and Bateni, H., 1992a&b,), (Shannon and Venderploeg, 1989), and (Yue *et al.*, 1989,). Amongst various models proposed, the optimum control was one of the most interesting topics. Hrovat (1997) surveys the applications of optimal control technique to the design of active suspensions. He also uses the normalized root mean square (RMS) of the acceleration versus tire and suspension deflection as a global measure of the performance. Esmailzadeh *et al.* (1996) used LQR method for an active suspension system and showed that optimal control enhances both handling and ride comfort. Yu and Grolla (1998) used LQG to control a suspension system by tuning the weighting parameters, based on different conditions. Kim *et al.*(1999) proposed an LQG shaped control in which the weighting coefficient is expressed as a function of the excitation frequency. Amongst other control methods, Son and Isik (1996) adopted fuzzy logic control.

Regarding the semi-active suspension systems, many different methods have been adopted for their design and control (Crosby and Karnopp, 1973), (Carter, 1998), (Mc Manus *et al.*, 2002), and (Ahmadian and Marjoram, 2000).

The literature describes the adoption of many different models and techniques to address the issue of suspension control. Brennan and Alleyne (2000) utilized a simulation test-bed, where a scaled model of

112

a vehicle was tested on a 4 ft × 8 ft treadmill capable of reaching a top speed of 15 miles/hour. The main thrust of this research was on driver-assisted controls (DAC) rather than roll control. In another model, Sampson and Cebon (2003) investigated a technique to enhance roll stability by applying active anti-roll torques to truck suspensions. They introduced a stabilizer active roll control system which leads the vehicle into corners such that the centre of the sprung mass shifts inboard of the vehicle centre-line to contribute to a stabilized roll moment. Frost *et al.* (1996) created a simulated roll-control model of a full-body vehicle system fitted with a semi-active suspension. This model considers a very complex nonlinear control problem to reduce roll angles over severe inputs. Matsumoto and Tomizuka (1992) studied an independent control of lateral and yaw motions; however, their paper did not discuss rolling, vehicle stability, or safety related issues. Tomizuka and Hedrick (1995) discussed various aspects of chassis control system in terms of vehicle handling and safety, but they did not take rollover into account. Gordon (1995) presented a new model in which the entire vehicle was divided into five simplified subsystems: one was the body of vehicle and four were the quarters of the vehicle. A full-vehicle model was used to control body pitch, roll attitude angles, and body bounce accelerations. Simulations were carried out, and results were obtained based on low-speed undulating and measured road surfaces. It was shown that in the case of an integrated active suspension system, there is significant improvements in the body bounce acceleration and in roll angle and pitch angle responses. While the suspension system performance was shown to be improved, vehicle stability was not verified by experiments. Manus *et al.* (2002) adopted the relative suspension deflection to control the damping force. In addition, Lai and Liao (2002) adopted sliding mode control to control a magnetorheological suspension. Lam and Liao (2003) used a similar method, but with a Skyhook system as a reference, to control the vibration. As stated before, Al-Holou *et al.* (1996) also adopted fuzzy logic to control the vibration of semi-active suspension systems, but not much work has been done to compare the results obtained by fuzzy logic with those obtained by other conventional methods.

The issue of semi-active controller stability and robustness is also an interesting aspect of these controllers, a topic discussed in literature. Although it is generally accepted that semi-active control methods are stable and robust, to avoid any confusion or questions on this matter in this thesis, the issue is briefly reviewed here.

- Proof of Stability of the system: The dynamic systems studied in this thesis are a simple spring, mass, and damper systems, which use a controllable semi-active damper as an actuator. Since the damper cannot generate energy, it is intuitively obvious that the closed

loop dynamic is passive. In all, the dynamic closed-loop mechanical system with dampers only dissipates energy. Therefore, it is clear that the mechanical system presented here is stable regardless of the damping tuning approach (Song and Ahmadian, 2005).

- The discussion on the "robustness" is general and broad; it could be a discussion on the stability robustness or the performance robustness. In any case, the following discussion summarizes the important aspects of robustness for this application:

  o Performance robustness: One of the main features of the semi-active control systems is that they are fail-safe. This means that if the control system fails for any reason (including power failure and sensor failure), the system acts as a passive system. This in turns shows the performance robustness of the system (Preumont, 2002).

  o Robustness due to the model uncertainties: The only identified parameter that may be uncertain in a vehicle model is the mass (m), which might be altered due to the load on the vehicle. However, regarding the mass of the vehicle, the change and uncertainties are small or negligible. In addition, the system is completely robust to the bounded changes of the mass.

  o Importance of the robustness in practical applications: First, the experimental results presented in this thesis show the practical implementation of the control system. Second, different versions of the semi-active controllers (Skyhook and R-S) have been adopted and used in commercial and passengers vehicles and have shown a satisfactory performance. As the controllers proposed in this thesis are of the same nature – the plants and the possible uncertainties are the same – the discussion of the robustness in practice is not an issue for the proposed controllers.

Many publications have appeared in the field of this research, (including (Rakheja and Sankar 1985), (Hrovat, 1997), Ahmadian (Ahmadian, 1999), Cole (Cole 2001), and Shen (Shen *et al.*, 2006)), that have not referenced nor discussed the issue of the robustness and stability of the semi-active controlled systems, it being generally accepted by researchers that "semi-active controllers are stable and robust controllers"

In this chapter, a new semi-active control strategy called "N-R-S" (New R-S) is proposed and the performance of it is compared with those of two conventional semi-active damping control strategies: the Rakheja-Sankar (R-S) and the Skyhook. The proposed semi-active control strategy could be easily

adapted to the existing semi-active control units, offering a higher performance in vibration isolation. In addition, a fuzzy logic controller is proposed, and the controller performance is compared with that of the conventional Skyhook, Rakheja-Sankar, and Limited relative Displacement (LDR) controllers. In addition, the effect of damping on the vehicle rollover is studied and a rollover-prevention assistance controller is designed and tested through simulations using the professional software "CarSim."

The focus in this chapter is to discuss the advantages of the semi-active controllers in general, and the proposed semi-active controllers in particular, in terms of simple one- and two- degree-of-freedom quarter-car model. Many researchers have studied the vibration isolation properties of the suspension system model, including Alanoly (Alanoly and Sankar, 1986); Crosby and Karnopp (1973); and more recently, Ahmadian (1999) and Shen *et al.* (2006).

Although the original plan was to test these proposed control methods on an actual light armored vehicle, but some unforeseen rulings by "The International Traffic in Arms Regulations" (ITAR) it made it impossible to access the vehicle and conduct the real-time experiments. This limitation is also the reason why the information on the heavy vehicle selected for this research is not presented in detail and why just some generic information is used in this thesis.

6.1 An Improved Hybrid Control Based on the Conventional Semi-Active Control Methods

As Shen *et al*. (2006) notes, R-S is an effective and easy way to implement a semi-active on-off control strategy. In Chapter 4, it has been shown that asymmetric dampers improve the vibration isolation properties of a passive system. With improvements in the damper manufacturing technology and the introduction of MR and external solenoid controllable dampers into the market, researchers are focusing on developing effective control strategies to exploit these properties in vibration isolation applications. However, as shown in the experimental results in Figure 79, of the two different commercially available controllable dampers and results presented in the literature, most controllable semi-active dampers are symmetric in operation.

 By combining the effect of the damper asymmetry and the R-S control strategy, the following new control strategy (N-R-S) is established and proposed[9]

---

[9] The notations used in this section are the same as those used in previous chapters unless otherwise stated

$$\zeta_s = \begin{cases} \zeta_{max} & (x-y) \le 0, (\dot{x}-\dot{y}) > 0 \\ \Gamma\zeta_{max} & (x-y) > 0, (\dot{x}-\dot{y}) \le 0 \\ \zeta_{min} = \beta\zeta_{max} & (x-y) > 0, (\dot{x}-\dot{y}) > 0 \\ \zeta_{min} = \Gamma\beta\zeta_{max} & (x-y) \le 0, (\dot{x}-\dot{y}) \le 0 \end{cases}$$

$$0 \le \beta \le 1, \ 0 \le \Gamma \le 1, \ \beta < \Gamma$$

(6-1)

There are four different damping states in this control strategy: damping very high ($\zeta_s = \zeta_{max}$), damping high ($\zeta_s = \Gamma\zeta_{max}$), damping low ($\zeta_s = \beta\zeta_{max}$), and damping very low ($\zeta_s = \Gamma\beta\zeta_{max}$).
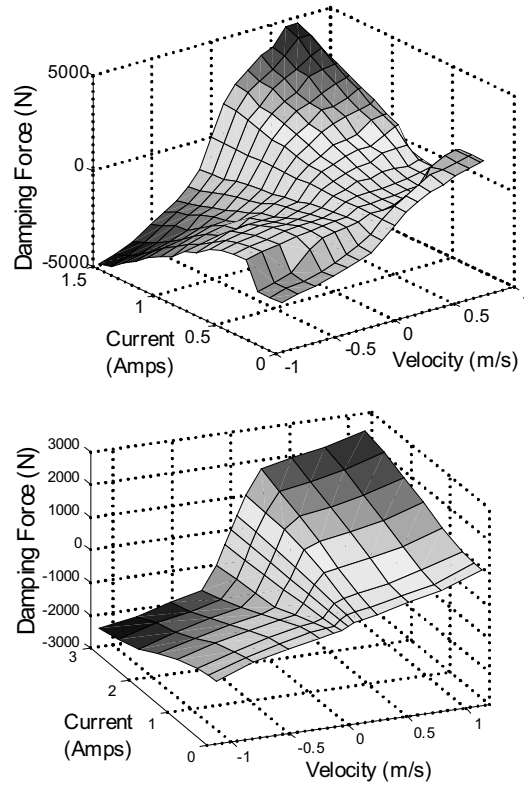
Figure 79: Test results of two commercialized dampers. Top: External solenoid valve damper used in Volvo S-60 models. Bottom: MR damper used in Cadillac SRX models

The proposed control strategy implies that when the relative velocity and the relative displacement are in the same direction, the damping should be low and very low in rebound and compression, respectively. When the relative velocity and the relative displacement are in the opposite directions, the damping should be high and very high in compression and rebound, respectively. Figure 80 shows the effectiveness of this new control strategy based on the numerical simulation results.

With this general control technique and appropriate values for the parameters β and Γ, we can generate different control algorithms. For instance, choosing $\beta = \Gamma = 1$ results in a symmetric passive system, and choosing $\beta = 0$, $\Gamma = 1$ results in the original R-S control strategy.

In general, the ideal value of β is zero, but achieving this is not realistic. The minimum value for β is an inherent property of dampers and cannot be controlled. However, the value for the parameter Γ can be optimized based on the vibration isolation needs (Eslaminasab *et al*., 2007a).
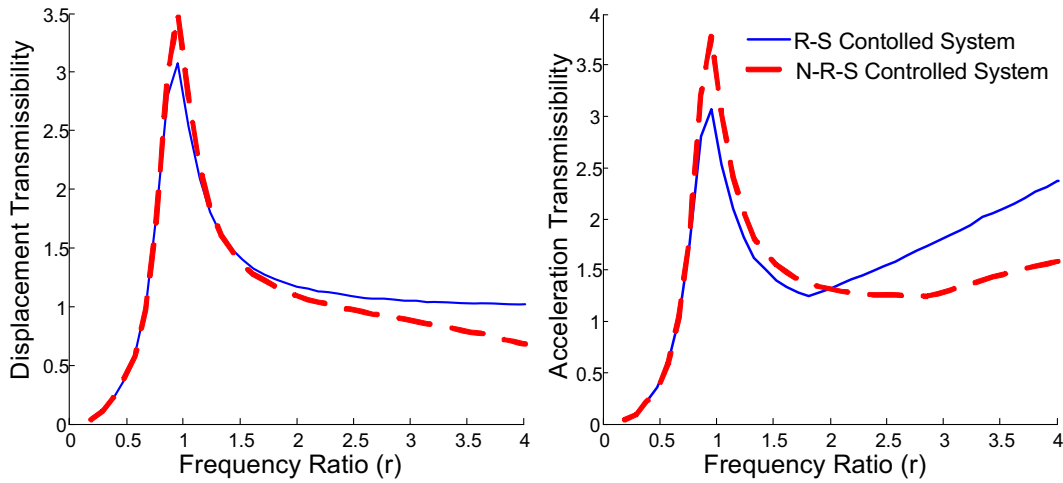
Figure 80: Comparison of the R-S control strategy and N-R-S control strategy (for the case where $\beta = 0$, $\Gamma = 0.7$)

As shown in Figure 50, the N-R-S is capable of reducing the acceleration transmissibility effectively in the high frequency region ($r > 1$). In addition, as detailed in Chapter 4, because in the high frequency region the mass centre of gravity vibrates around a dynamic fix point closer to the ground (for cases where $\Gamma < 1.0$), the vehicle road handling is improved at the same time.

6.1.1 Analytical Analysis of the N-R-S Control Method by Method of Averaging

To explore the behavior of the proposed semi-active on-off control method through mathematical analysis, the method of averaging as described in Chapter 3 is deployed. In what follows, the semi-active system controlled using the N-R-S technique is analyzed.

As stated already, in order to analyze the effect of the nonlinearity with the averaging method, it is necessary to transform the equation of motion to a time-scaled form. The transformed equation of motion is[10]

$$r^2 x'' + x_r = -\varepsilon(2\zeta_s r x' - Y r^2 \, Sin(\tau))$$

$$\zeta_s = \begin{cases} \zeta_{max} & (x-y)\leq 0, (\dot{x}-\dot{y})>0 \\ \Gamma\zeta_{max} & (x-y)>0, (\dot{x}-\dot{y})\leq 0 \\ \zeta_{min} = \beta\zeta_{max} & (x-y)>0, (\dot{x}-\dot{y})>0 \\ \zeta_{min} = \Gamma\beta\zeta_{max} & (x-y)\leq 0, (\dot{x}-\dot{y})\leq 0 \end{cases}$$
$$0\leq\beta\leq 1, \, 0\leq\Gamma\leq 1, \, \beta<\Gamma$$

(6-2)

Although this nonlinear system might have other periodic solutions such as second and third sub/super harmonics, we consider the solution of equation (6-2) for the main resonance case to be in the form of

$$x_r = a_r(\tau)\cos(\phi(\tau))$$
$$\phi(\tau) = \tau + \varphi(\tau)$$

(6-3)

Following the mathematical steps (as in Chapter 3),

$$\frac{d(a_r)}{d(\tau)} = -\frac{1}{r^2}\Big(\big(r^2 a_r \cos(\phi) - a_r \cos(\phi)$$
$$+2\zeta_s \varepsilon r a_r \sin(\phi) + y r^2 \varepsilon \sin(\tau)\big)\sin(\phi)\Big)$$

(6-4)

$$\frac{d(\varphi)}{d(\tau)} = -\frac{1}{r^2 a_r}\Big(\cos(\phi)\big(r^2 a_r \cos(\phi) - a_r \cos(\phi)$$
$$+2\zeta_s \varepsilon r a_r \sin(\phi) + y r^2 \varepsilon \sin(\tau)\big)\Big)$$

(6-5)

To implement the method of averaging, the N-R-S control rules are redefined in terms of the polar coordinates (a,φ) which are used in the analysis. Recall that the system's output is considered to be in the form $x_r = a_r \cos(\phi(\tau))$. Therefore, the transferred N-R-S control rules are

---

[10] The notations used in this section are the same as notations used in Chapter 3 unless otherwise stated.

$$\zeta_s = \begin{cases} \zeta_{max} & 0 \le \phi < \dfrac{\pi}{2} \\ \Gamma\beta\zeta_{max} & \dfrac{\pi}{2} \le \phi < \pi \\ \Gamma\zeta_{max} & \pi \le \phi < \dfrac{3\pi}{2} \\ \beta\zeta_{max} & \dfrac{3\pi}{2} \le v < 2\pi \end{cases}$$

(6-6)

As an approximation, the right side of equations (6-4) and (6-5) can be replaced by their average values ($\bar{a}'$, $\bar{\varphi}'$) in one period. The averaged equations will be:

$$\bar{a}'_r = \frac{-a_1\zeta_s\beta - a_1\zeta_s\Gamma\beta - a_1\zeta_s - a_1\zeta_s\Gamma - 2Yr\cos(\varphi)}{4r}$$

(6-7)

and

$$\bar{\varphi}' = \frac{a_1 r\zeta_s\beta - a_1 r\zeta + a_1 r\zeta_s\Gamma\beta - a_1 r\zeta_s\Gamma}{2r^2\pi a_r}$$

$$+ \frac{-r^2\pi a_r + \pi a_r + \pi Y r^2\sin(\varphi)}{2r^2\pi a_r}$$

(6-8)

Solving these equations for the steady state where $\bar{a}'_r(\tau) = 0$, $\bar{\varphi}'(\tau) = 0$, we find the averaged equation for the amplitude and phase of the relative displacement. To find the parameters of interest, (η, λ), to compare the analytical and simulation results, it is necessary to find the averaged value for the absolute acceleration, $\ddot{x}(t)$, through the following relations:

$$x = \bar{a}_r \cos(rt + \bar{\varphi}) + Y\sin(vt)$$
$$x = a\cos(rt + \theta)$$
$$a = \sqrt{(\bar{a}_r)^2 + (Y)^2 + 2\bar{a}_r Y\cos(\bar{\varphi})}$$

(6-9)

The resultant parameters of interests are

$$\lambda = 2\pi r^2 \left| \frac{1}{\sqrt{A+B+C+D+E+F+G+H}} \right|$$

where :

$A = -8\zeta_s^2 r^2 \beta + 4\zeta_s^2 r^2 \beta^2 + 8\zeta_s^2 r^2 \Gamma$

$B = 4\zeta_s^2 r^2 \Gamma^2 + 4\pi^2 - 8\zeta_s^2 r^2 \Gamma^2 \beta$

$C = 4\zeta_s^2 r^2 \Gamma^2 \beta^2 - 16\zeta_s^2 r^2 \Gamma \beta + 8\zeta_s^2 r^2 \Gamma \beta^2 + 4\zeta_s^2 r^2$

$D = \zeta_s^2 \pi^2 r^2 \Gamma^2 \beta^2 + 8\zeta_s \pi r \Gamma + 4\zeta_s^2 \pi^2 r^2 \Gamma \beta$

$E = 2\zeta_s^2 \pi^2 r^2 \Gamma^2 \beta - 8\zeta_s \pi r \Gamma \beta - 8\zeta_s \pi r \beta - 8\zeta_s \pi r^3 \Gamma$

$F = 8\zeta_s \pi r^3 \Gamma \beta + 8\zeta_s \pi r^3 \beta + \zeta_s^2 \pi^2 r^2 \Gamma^2 + \zeta_s^2 \pi^2 r^2 \beta^2$

$G = 2\zeta_s^2 \pi^2 r^2 \Gamma \beta^2 + 2\zeta_s^2 \pi^2 r^2 \beta + 2\zeta_s^2 \pi^2 r^2 \Gamma + \zeta_s^2 \pi^2 r^2$

$H = 8\zeta_s \pi r - 8\zeta_s \pi r^3 - 8\pi^2 r^2 + 4r^4 \pi^2$

(6-10)

As a result, the acceleration transmissibility is

$$\eta = r^2 \left| \sqrt{(\lambda^2 + 1 \pm 2\lambda \cos(\varphi))} \right|$$

(6-11)

To ensure the averaging method results match the numerical simulations results, let us consider $\beta = \Gamma = 1$. In this particular case, the results derived from the averaging method should match the theoretical results obtained from equations (1-15) and (1-12). Figure 81 indicates how closely the results match.
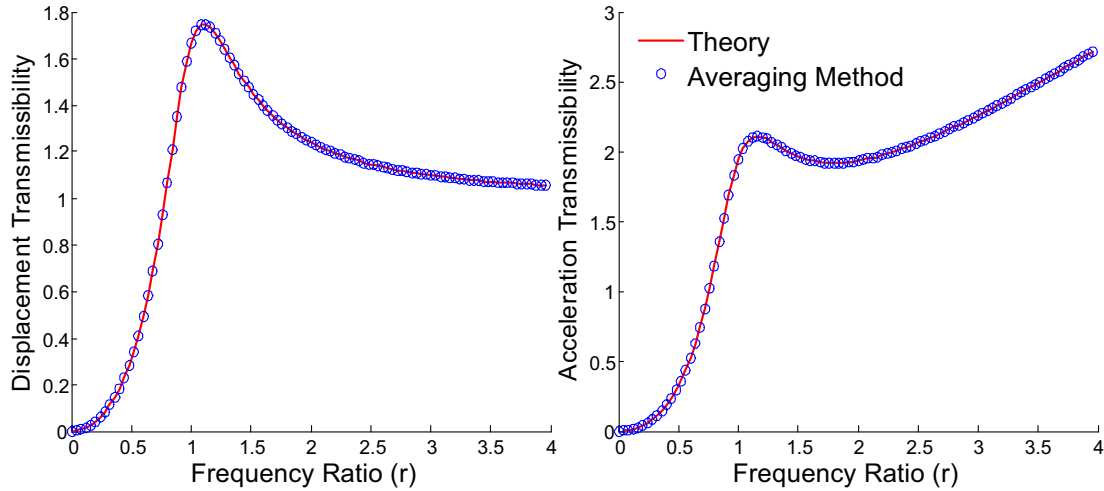
Figure 81: Comparison of the averaging method and the theoretical results for a passive system

6.1.2 Analytical and Numerical Results of the proposed N-R-S Semi-Active Controller

In this section, the performance of the proposed control algorithm is assessed through the numerical simulations and the analytical results obtained by the averaging method. Matlab®/Simulink tools are used to carry out the numerical simulations. The model parameters for the simulations are listed in Table 12. The results are obtained in time domain. To guarantee that the system is in the steady state condition, each simulation was performed for at least 30 seconds. The maximum amplitudes of relative displacement and absolute acceleration were recorded (as discussed in Chapter 3) for every excitation frequency. The results were reported and discussed in the frequency domain. The performance of the N-R-S and R-S control strategies is also compared by adopting the RMS values. Figure 82 shows the simulation algorithm.

Table 12: Simulation data

System parameter	Value
Sprung mass - m_b (kg)	2,000
k_1 (N/m)	55,000
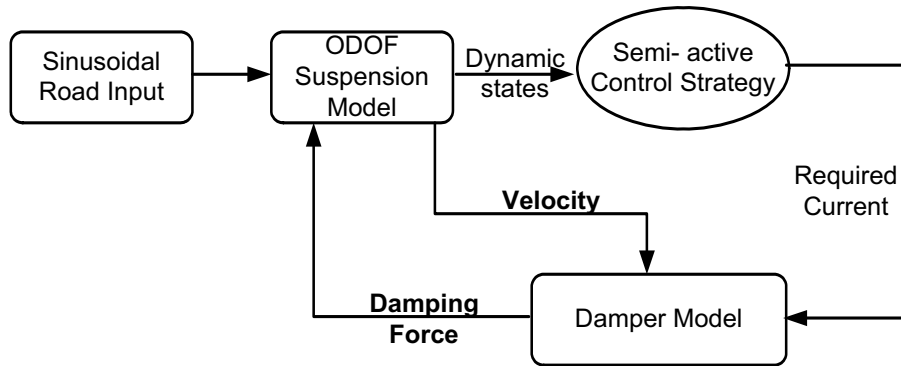
Figure 82: Numerical simulation flow chart

Figure 83 shows a comparison between the averaging method and the numerical simulation method where the on-off control technique is in effect. It is evident that near the natural frequency, the two

methods give similar results but that they start to deviate in the higher frequency ranges for the acceleration transmissibility.

In all the analytical and numerical simulations, the ideal case is considered, where the dampers produce no damping force in the low state ($\beta = 0$). Unless otherwise stated, it is assumed that $\Gamma = 0.7$ for the N-R-S control strategy.
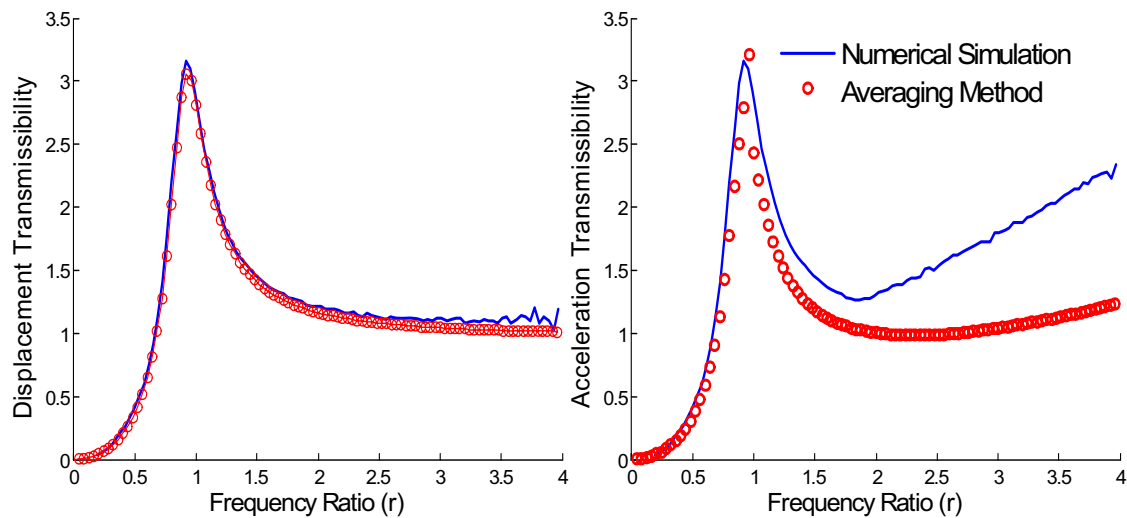
Figure 83: Comparison of the averaging method and numerical simulation for the case where controller is in action

Figure 84 compares the frequency-responses of the 1DOF system for the passive, R-S controlled, and N-R-S controlled systems based on the results obtained by the analytical method of averaging. In the R-S and N-R-S control systems, the damping ratio switches between the high state ($\zeta = 0.8$) and the low state ($\zeta = 0$). The passive system has the constant damping ratio of $\zeta = 0.8$. As illustrated in this figure, the R-S and N-R-S control strategies are capable of reducing the acceleration transmissibility dramatically in the higher frequency region ($r > 1$). In addition, there is a noticeable improvement of the N-R-S strategy over the R-S, reducing the acceleration transmissibility in the high frequency region. At the same time, due to the trade-off between the acceleration transmissibility and the displacement transmissibility, the displacement transmissibility of the R-S and N-R-S controlled systems deteriorated (this effect is discussed in more detail in the next section).
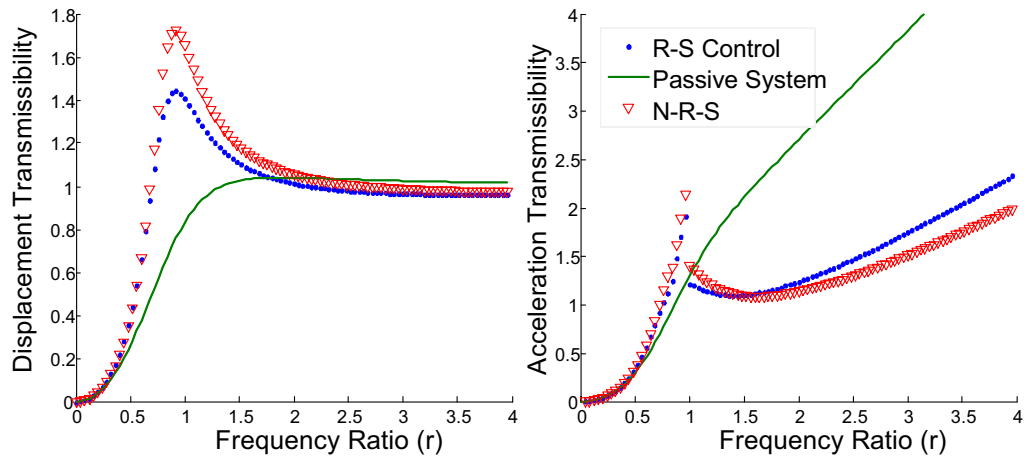
Figure 84: Comparison of passive, R-S control, and New R-S control strategies

Figure 85 shows the results of the sensitivity analysis of the N-R-S control strategy to the asymmetry factor (Γ) while the damping ration is set at 0.8 ($\zeta = 0.8$). As illustrated, the lower values of Γ result in lower acceleration transmissibility at the high frequency region. On the other hand, the displacement transmissibility increases when Γ increases (note that $\Gamma = 1$ implies R-S control technique). As shown, there is a trade-off between the acceleration transmissibility and displacement transmissibility such that Γ can be optimized, based on the specific application requirements.
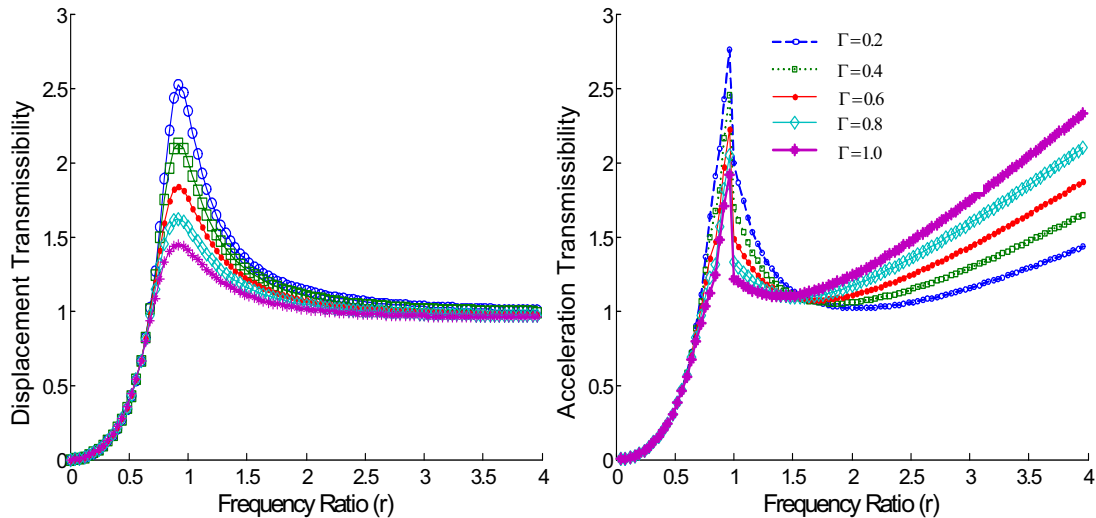
Figure 85: Effect of Γ on system's output

6.1.2.1 RMS Comparison of Control Methods' Performance

As described in section 3.4, the RMS is a useful measure to evaluate the performance of the suspension system and the control strategies. As a result, in order to compare the performances of N-R-S and R-S control strategies, the RMS method is adopted and used in this section. Figure 86 shows the RMS of the absolute acceleration transmissibility versus the RMS of the relative displacement transmissibility for various damping ratios, while Γ is changed from 0.2 to 1.0 (note that $\Gamma = 1$ implies the original R-S control strategy). As shown in this figure, in the N-R-S controller case, when the system is highly under-damped ($0 < \zeta < 0.1$), the trend of the RMS changes differs from the case in which the system's damping is high. In this case (a low damped system), the higher values of Γ result in a lower acceleration and displacement transmissibility. However, this is not usually the case for vibration absorbers and suspension systems. The damping should normally be as high as possible in the on-off control techniques. On the other hand, in the higher damping ratio region, while Γ changes between 0.2 and 1.0, the acceleration transmissibility increases accordingly and, as a result, in the cases where $\Gamma = 1$, we experience the worst ride comfort. At the same time, the results indicate a different trend in the displacement transmissibility: as Γ increases, the displacement transmissibility decreases.

As stated before, there is a conflict between the two parameters of interest (λ, η). However, if we consider $RMS(\eta) = f(\zeta, \Gamma)$ and $RMS(\lambda) = g(\zeta, \Gamma)$, then for the system with a higher damping ratio, we find

$$\left| \frac{\partial(RMS(\eta))}{\partial \Gamma} \right| \geq \left| \frac{\partial(RMS(\lambda))}{\partial \Gamma} \right| \tag{6-12}$$

This is difficult to prove using the numerical simulation method because it is very time-consuming to prove this relation for every frequency and every system; using the results obtained from the method of averaging, it is possible to show the results as much faster and more accurate.
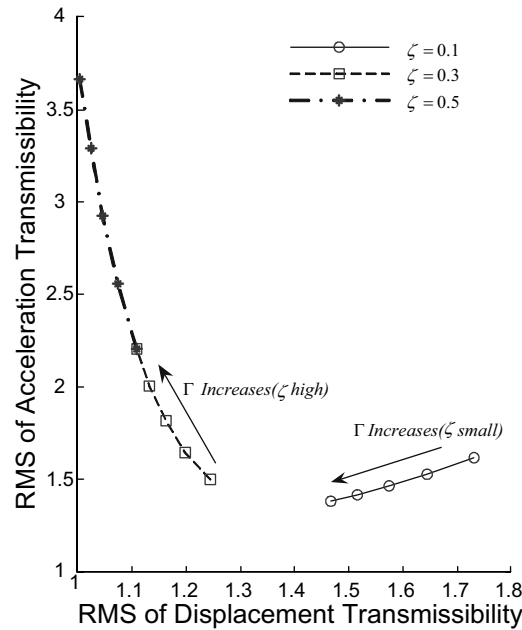
Figure 86: RMS of Acceleration versus Displacement Transmissibility for N-R-S controlled system

For instance, where $\zeta = 0.5$ (see Figure 86), $\dfrac{\partial RMS(\eta)}{\partial \Gamma} = 1.819$ and $\dfrac{\partial RMS(\lambda)}{\partial \Gamma} = 0.129$. As a result, it is possible to find an optimal value for Γ based on the application and the system characteristics.

Figure 87 compares the performance of the passive R-S controlled system with that of the N-R-S controlled system in the frequency range of $0 < r < 10$ while $\Gamma = 0.7$. Based on the data, we can conclude that the R-S and N-R-S lead to the reduction of the RMS of the acceleration transmissibility over the entire range, as well as a slight increment in the RMS of the displacement transmissibility.

Additionally, compared with the R-S control, the results indicate that the N-R-S is capable of reducing the RMS of the acceleration transmissibility more efficiently, while exhibiting a small increase in the RMS of displacement transmissibility. For example,

Table 13 shows and compares the performance of each system, where $\zeta = 0.8$.

Table 13 Comparison of the different systems performance using RMS ($\zeta = 0.8$)

Controller	RMS of Acceleration Transmissibility	RMS of Displacement Transmissibility
Passive (no control)	11.050	0.936
R-S controlled	5.872	0.923
N-R-S controlled	4.996	0.950
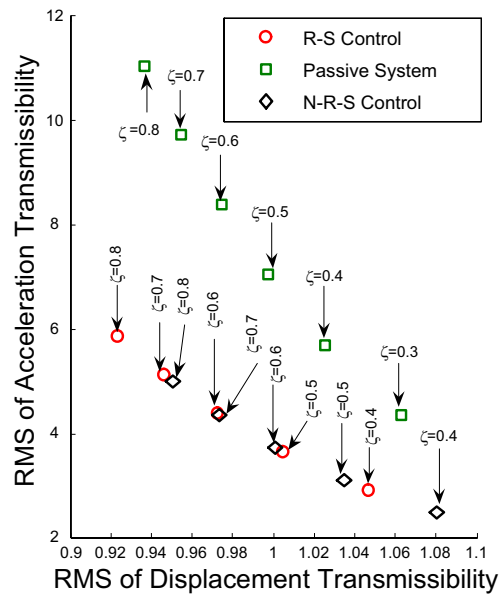
Figure 87: Comparison of Passive, R-S Controlled, and N-R-S Controlled based on the RMS values

6.1.3 Experimental Results

To determine the effectiveness of the N-R-S controller, a 1DOF test bed, as shown in Figure 88, is developed. It is mounted on an LMS-722 magnetic shaker. The 1DOF system has a 6.78-kg sprung mass and a total stiffness of 11.30 kN/m. The natural frequency of the system is 6.3 Hz. To provide the damping force, a sponge-based MR damper (LRD-1097-01) is used. The damping ratio of this damper can be adjusted by controlling the current applied to the damper. Figure 89 shows the force versus velocity curves of this damper for different applied currents.
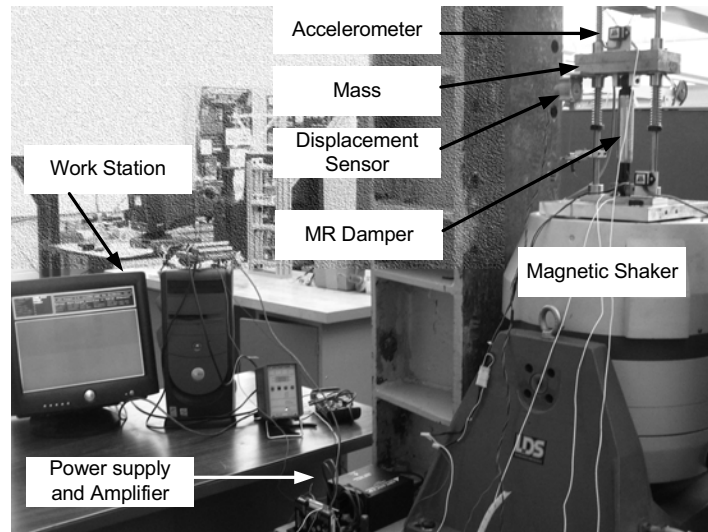
Figure 88: 1DOF system test bed
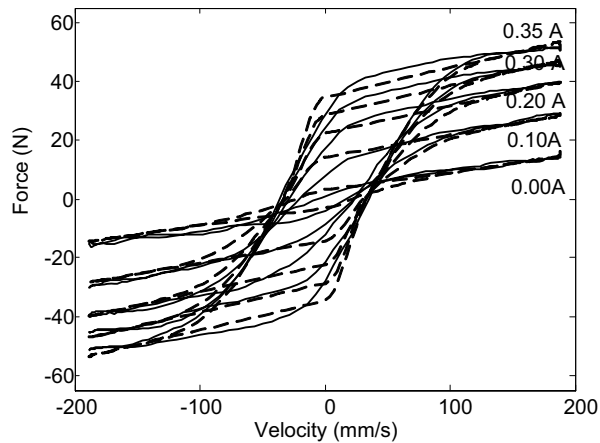
Figure 89: MR damper force-velocity curves for different applied currents

   This kind of damper has the advantages of needing no seals and no bearings — resulting in a low cost
and a compact structure. In the test facility, two types of sensors are used to measure the responses of
the system: a displacement sensor (SP-12-1 from Celesco) to measure the relative displacement, and two
accelerometers (Mechworks MA-A210) to measure the base and mass acceleration, both installed on the
test bed. To control the MR damper's current, a power supply (Advanced Motion Control PS4X3w24)
and an amplifier (Advanced Motion Control 12A8M) are used. To guarantee real-time control of the

127

system, MATLAB/XPC-TARGET was used. The data acquisition system (DAQ) for this experiment is a SENSORAY-626. The system is then tested under a frequency sweep of 5 Hz (min shaker range) to 15 Hz, with a variable damping ratio (variable maximum input current to the damper). Figure 90 shows the control implementation algorithm for the tests.

For the test results shown in Figure 91 to Figure 94, β is set to be zero. The value for Γ is chosen to be 1, 0.8, or 0.6 to compare its effect on the system's response. Four values for the power supply output current, and as a result the corresponding damping ratio (ζ), are considered: $\zeta = Low$ (maximum MR damper current set to 0.1 Amp), $\zeta = Medium$ (maximum MR damper current set to 0.3 Amp), $\zeta = High$ (maximum MR damper current set to 0.35 Amp), and $\zeta = Very High$ (maximum MR damper current set to 0.4 Amp).
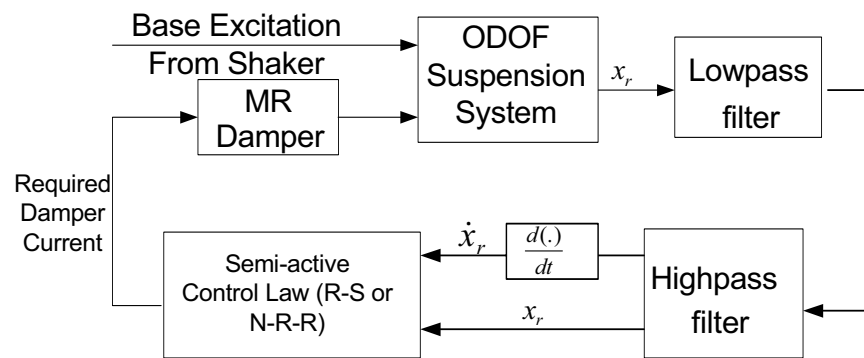
Figure 90: 1DOF system control implementation algorithm

Figure 91 to Figure 94 portray the acceleration transmissibility of the system derived from the test results. It is evident that in all cases, the controlled system performs better than the passive system. Interestingly, as stated in section 6.1.2, using analytical and numerical methods, the new controller demonstrates a better performance than the R-S controller, especially in the higher frequency region. Also, as discussed before and shown in Figure 86, for the higher damping ratio, decreasing Γ eventually increases the system's performance (it reduces the acceleration transmissibility).

In addition, the comparison of these figures proves that the new controller has a superior performance when the damping ratio is higher.
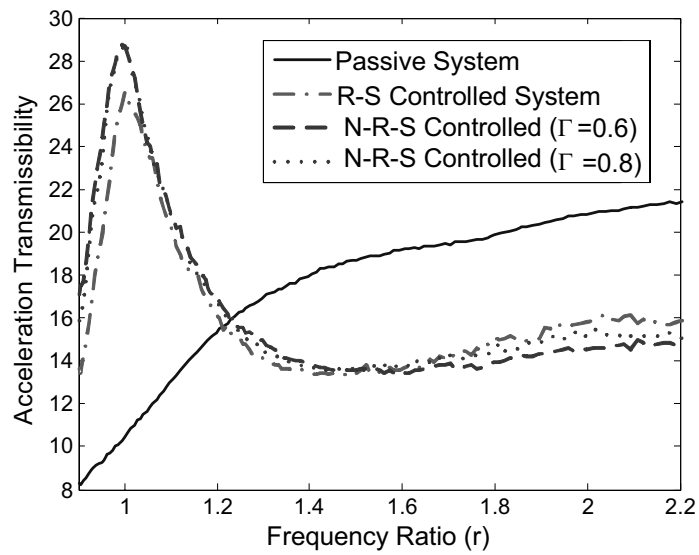
Figure 91: Comparison of the system's performance when damping ratio is set to medium
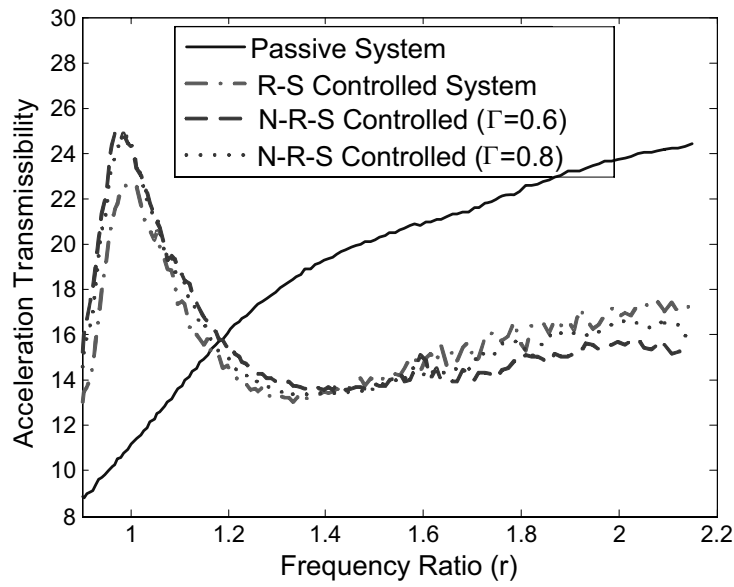
Figure 92: Comparison of the system's performances when damping ratio is set to high
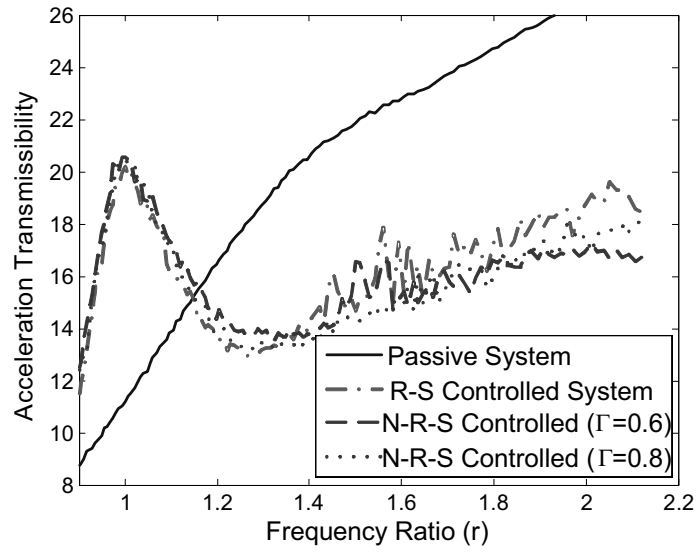
Figure 93: Comparison of the system's performances when damping ratio is set to very high
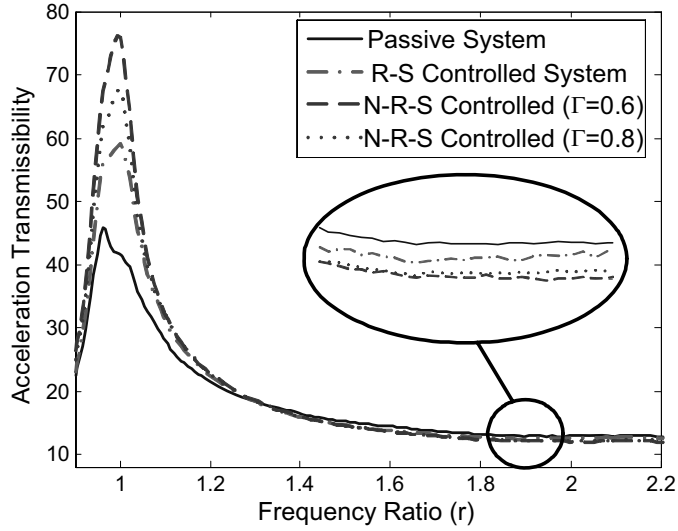
Figure 94: Comparison of the system's performances when damping ratio is set to low

6.2 A Hybrid Neuro-fuzzy Control Method to Improve Heavy Vehicles' Ride-Comfort and Road-Handling

In this section, a unique neuro-fuzzy controller is developed based on the developed internal solenoid valve semi-active damper. For the purpose of control implementation, the damper has been modeled as a neural network, as already discussed in section 2.3. Because of the nature of the control modes for this damper system, two different networks are designed and trained, independently. The first network uses the velocity and current as inputs, and outputs the damping force. The second network has the same characteristics but receives the velocity and damping force as inputs, and outputs the required current.

Fuzzy control uses the principles of fuzzy logic-based decision making to arrive at a control action for a given set of input states. Fuzzy logic is a method of easily representing analog processes on a digital computer; these processes are concerned with continuous phenomena that are not easily broken down into discrete segments, and the concepts involved are sometimes difficult to model. As an example, consider an anti-lock braking system directed by a microcontroller chip. The microcontroller has to make decisions based on brake temperature, speed, and other variables in the system. The variable "temperature" in this system can be subdivided into a range of "states": "cold", "cool", "moderate", "warm", "hot", and "very hot". The transition from one state to the next is hard to define. An arbitrary static threshold might be set to divide "warm" from "hot". For instance, at exactly 90 degrees, warm ends and hot begins. However, this would result in a discontinuous change when the input value passed over that threshold. The transition would not be smooth, as would be required in braking situations. The way around this is to make the states fuzzy – that is, allow them to change gradually from one state to the next. In order to do this, a dynamic relationship must be established between different factors. This dynamic relationship is defined by the membership functions.

To design the fuzzy logic rules for the proposed control system, fuzzy membership functions for the input and output variables must be defined. For each variable, three trapezoidal membership functions are considered. For example, for the damping coefficient in the proposed control strategy, the three membership functions are small, medium, and large. These membership functions are shown in Figure 95, Figure 96, and Figure 97. Adopting this membership functions granulation method, fuzzy logic rules can be defined. These fuzzy rules are extracted by combining 'Skyhook' and 'groundhook' control methods. These rules are categorized in three different sets as shown in Tables 14-16.

131
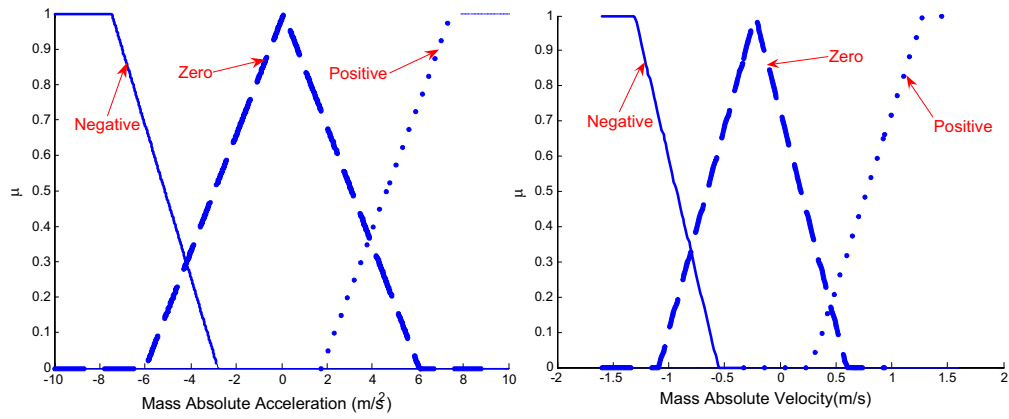
Figure 95: Membership functions for absolute acceleration and velocity of sprung mass
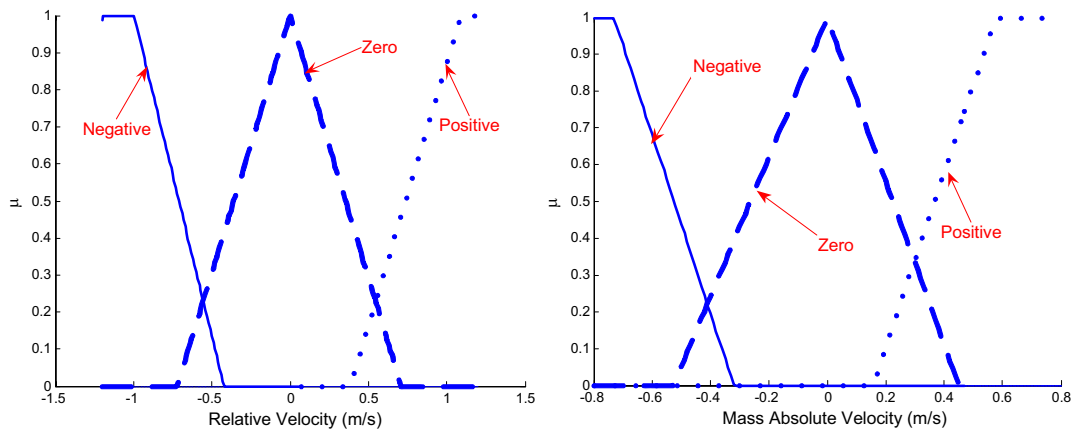
Figure 96: Membership functions for absolute and relative velocities
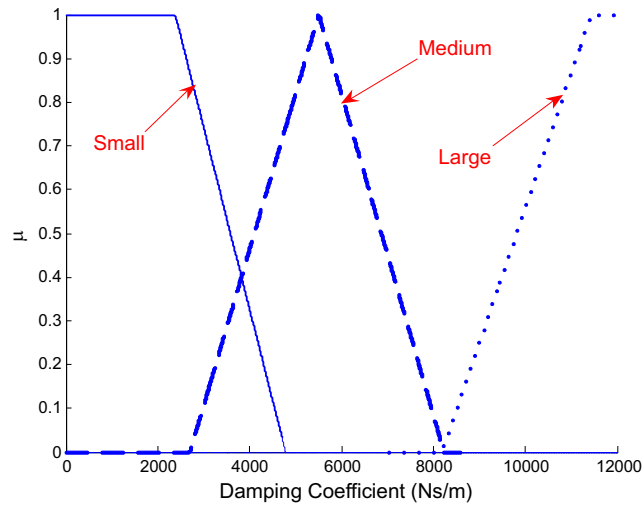
Figure 97: Membership function for damping coefficient

Table 14: The first set of rules for tuning absolute velocity of sprung mass

Item	Rule
1	If V_{abs} is negative and V_{rel} is negative, then ζ is large
2	If V_{abs} is negative and V_{rel} is neutral, then ζ is medium
3	If V_{abs} is negative and V_{rel} is positive, then ζ is small
4	If V_{abs} is neutral and V_{rel} is negative, then ζ is medium
5	If V_{abs} is neutral and V_{rel} is neutral, then ζ is medium
6	If V_{abs} is neutral and V_{rel} is positive, then ζ is medium
7	If V_{abs} is positive and V_{rel} is negative, then ζ is small
8	If V_{abs} is positive and V_{rel} is neutral, then ζ is medium
9	If V_{abs} is Positive and V_{rel} is positive, then ζ is large

The subscript "abs" in this table is used instead of "absolute" and subscript "rel" is used instead of "relative"

Table 15: The second set of rules for tuning absolute velocity of unsprung mass

Item	Rule
1	If V_{abs-w} is negative and V_{rel} is negative, then ζ is small
2	If V_{abs-w} is negative and V_{rel} is neutral, then ζ is medium
3	If V_{abs-w} is negative and V_{rel} is positive, then ζ is large
4	If V_{abs-w} is neutral and V_{rel} is negative, then ζ is medium
5	If V_{abs-w} is neutral and V_{rel} is neutral, then ζ is medium
6	If V_{abs-w} is neutral and V_{rel} is positive, then ζ is medium
7	If V_{abs-w} is positive and V_{rel} is negative, then ζ is large
8	If V_{abs-w} is positive and V_{rel} is neutral, then ζ is medium
9	If V_{abs-w} is positive and V_{rel} is positive, then ζ is small

The subscript "abs-w" in this table is used instead of "absolute of wheel" and subscript "rel" is used instead of "relative"

To implement this fuzzy logic control strategy in semi-active damping control, the Mamdani method (Karray and De Silva, 2004) for fuzzy inference is used to obtain the damping ratio ζ. The centroid method for defuzzification is used to compute the final crisp value of ζ.

Table 16: The third set of rules for tuning absolute acceleration

Item	Rule
1	If a_{abs} is negative and V_{rel} is negative, then ζ is large
2	If a_{abs} is negative and V_{rel} is neutral, then ζ is medium
3	If a_{abs} is negative and V_{rel} is positive, then ζ is small
4	If a_{abs} is neutral and V_{rel} is negative, then ζ is medium
5	If a_{abs} is neutral and V_{rel} is neutral, then ζ is medium
6	If a_{abs} is neutral and V_{rel} is positive, then ζ is medium
7	If a_{abs} is positive and V_{rel} is negative, then ζ is small
8	If a_{abs} is positive and V_{rel} is neutral, then ζ is medium
9	If a_{abs} is Positive and V_{rel} is positive, then ζ is large

The subscript "abs" in this table is used instead of "absolute" and subscript "rel" is used instead of "relative"

6.2.1 Simulation

In this section, we examine the performance of the proposed control through numerical simulations. A diagram model of the simulation is shown in Figure 98. The outputs extracted from the quarter-car model are absolute acceleration of the sprung mass and relative displacement and velocity between sprung and unsprung masses. These three parameters are used as inputs to the controller. The controller renders an optimum damping coefficient. Ideally, it is desired to produce the optimum damping force through changes in the current given to the damper. However, this cannot be accomplished because we are using a real damper rather than an ideal one. Therefore, the real damping force given to the quarter car model deviates from the ideal required damping force. In order to get the real damping force, a new proposed system, the inverse mapping, is used to estimate the current needed to be fed into the real damper. Finally, the actual damping force is fed back to the quarter car model. Matlab/Simulink tools are used to carry out this simulation. The damper parameters used in this simulation are listed in Table 17. The results are obtained and discussed in time domain and frequency domain. The performances of the control methods are also compared with those of the RMS method.
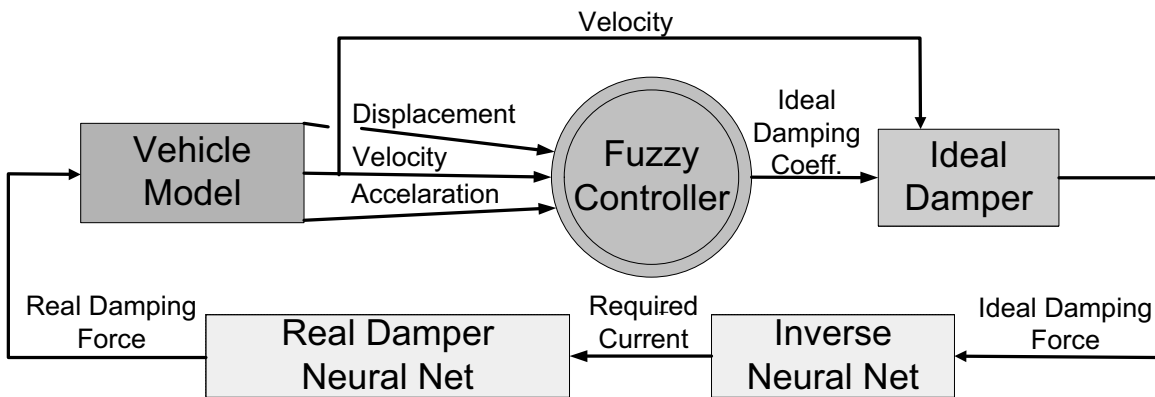
Figure 98: Simulation implementation flow chart

To perform the numerical analysis, a harmonic input $y = Y\,sin(\omega t)$ is applied to the system as an excitation. The amplitude of excitation is set to 0.1 m and the frequency range is 0-10 Hz. The ideal damping coefficient values are set to be in the range of 0-20000 (Ns/m).

Table 17: Simulation data

System parameter	Value
Sprung mass - m_b (Kg)	2000
Unsprung mass- m_w (Kg)	100
k_1 (N/m)	90000
k_2 (N/m)	900000

6.2.2 Time Domain Results

The proposed neural network-based fuzzy control method is compared with that of well-tuned Skyhook, R-S, and LDR control methods. The comparison results in the time domain (in terms of relative velocity and absolute acceleration) are shown in Figure 99, Figure 100, and Figure 101 for a simulation time of 20s. The ideal damping values are chosen to be $C_{\min,\max} = 0,12000 \,(Ns/m)$.
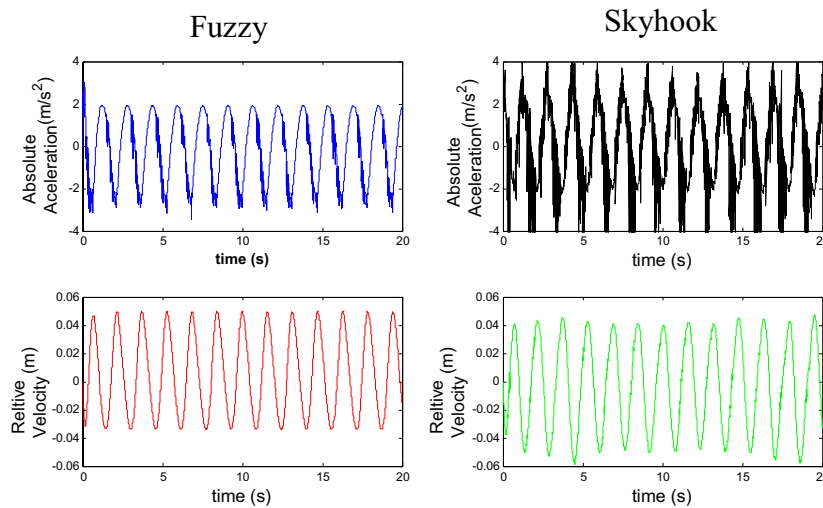
Figure 99: Comparison of time domain simulation results for Skyhook and fuzzy controllers

Table 18 summarizes the time domain results and compares the performance of the different controllers.

The results presented in Figures 99-101 and Table 18 show the effectiveness of the proposed fuzzy controller in steady state and transient responses (although in this paper our focus is on the steady state responses).
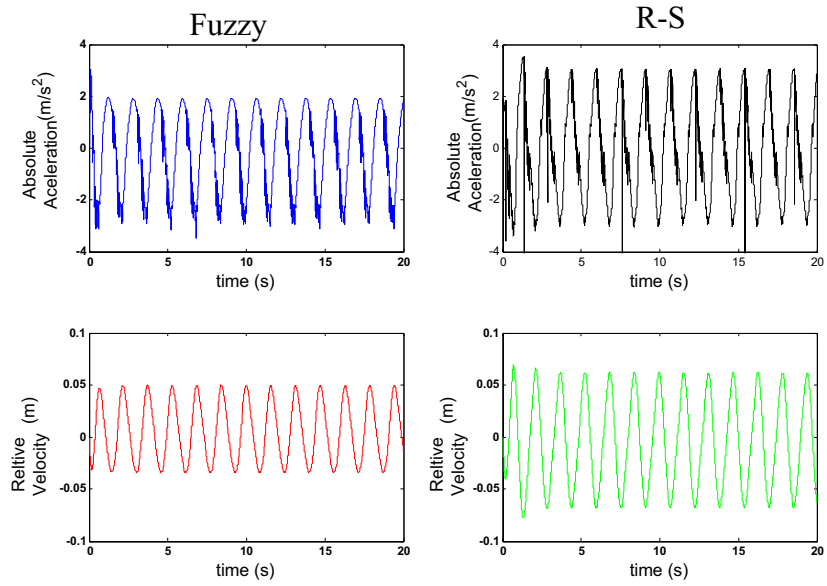
Figure 100: Comparison of time domain simulation results for R-S and fuzzy controllers
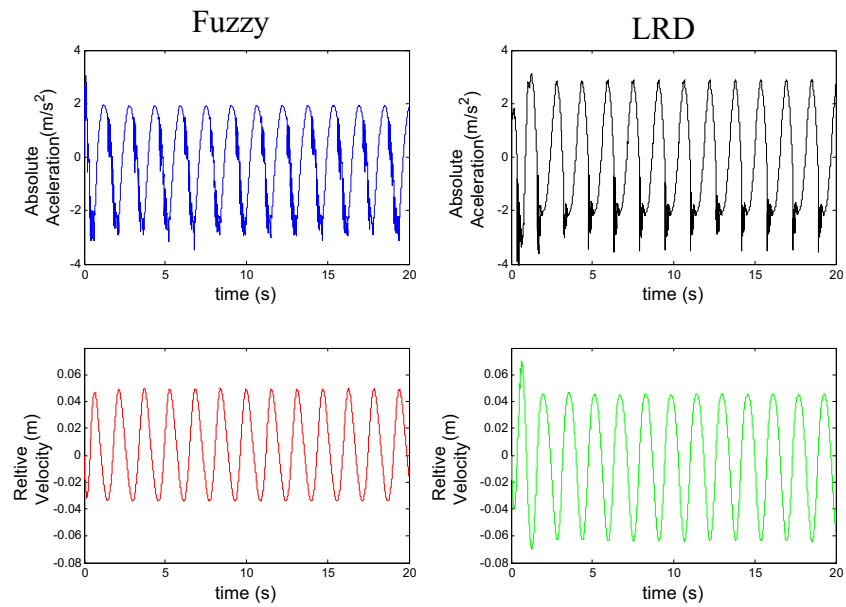
Figure 101: Comparison of time domain simulation results for LRD and fuzzy controllers

Table 18: Comparison of different controllers in time domain

Controller	Reduction in Absolute Acceleration (%)	Reduction in Relative Displacement (%)
Fuzzy	25	43
Skyhook	20	31
R-S	5	0
LRD	0	11

6.2.3 Frequency Domain Results

The frequency-responses of the system for absolute acceleration and relative displacement are illustrated in Figure 102 and Figure 103. To find the steady state response values, the simulations are run for 20 s. The ideal damping values are chosen to be $C_{\min,\max} = 0,12000\,(Ns/m)$.

To analyze the result, two frequency ranges are considered: Low frequency (below 4 Hz) and high frequency (above 4 Hz). When the frequency is low, for ride comfort, no single controller has significant advantages over others. On the other hand, in this comparison the LRD control produces very high acceleration. Overall, the proposed fuzzy controller has the smallest acceleration magnitude. Rakheja-Sankar also produces similar results. As for the relative displacement, while LRD shows better results, fuzzy still has the best performance. Skyhook control is closely tracking the fuzzy in this case.

For a frequency of 4 HZ or more, the difference in the performance of the controllers is significant. For a gradual frequency increases above 6 Hz, the proposed fuzzy controller renders less acceleration while maintaining low relative displacement. In this case, LRD shows better performance in road handling than the R-S and Skyhook controllers. It is worth mentioning that for this case, the R-S control outputs higher acceleration and, hence, has the worst performance. Overall, the fuzzy controller has a better performance in optimizing absolute acceleration for the entire frequency range, and the relative displacement in a major segment of it.
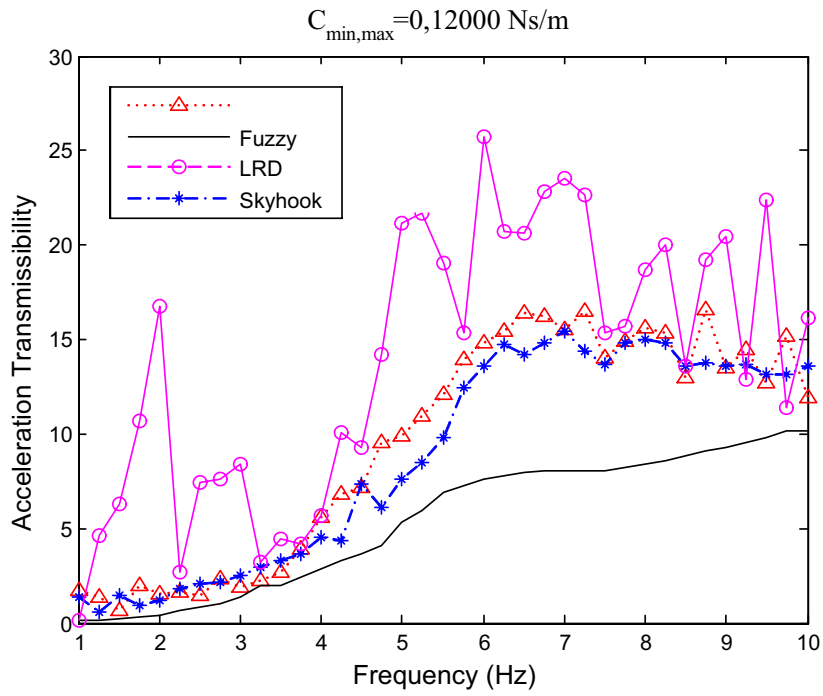
Figure 102: Acceleration transmissibility (η) for different control methods

Figure 103: Displacement transmissibility (λ) for different control methods

6.2.4 RMS Control Performance Comparison

The Root Mean Square (RMS) technique is a useful measure to evaluate the control performance in the applications considered in this paper. The efficiencies of the controllers are compared using the RMS method. Figure 104 shows the RMS of absolute acceleration versus RMS of relative displacement. As shown, the fuzzy controller reduces the transmitted displacement and acceleration at the same time. On the other hand, Skyhook control reduces the transmitted displacement with respect to the Rakheja-Sankar and LRD but, at the same time, is unable to reduce the amount of transmitted acceleration as effectively as the other two. Generally, the results show an approximately 30% improvement in performance when using the fuzzy controller.
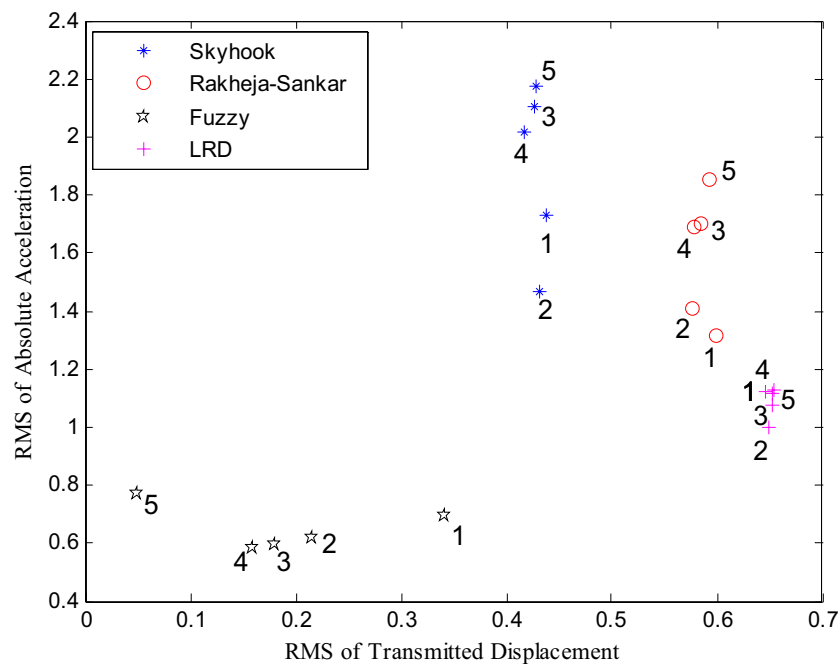
Figure 104 : RMS of absolute acceleration versus displacement transmissibility for different control methods and different maximum ideal damping values. The corresponding damping coefficient for each node in the figure refers to the maximum ideal damping 1. C_{max}=4,000, 2. C_{max}=6,000, 3. C_{max}=8,000, 4. C_{max}=16,000, 5. C_{max}=20,000.

6.3 Anti-Rollover Assistant Controller

As stated earlier, rollover is an obvious indication of vehicle instability. The ability to control the suspension systems with semi-active controllable dampers has been an ongoing area of research for decades. The effects and performance of semi-active controlled systems on ride comfort and road handling of vehicles, as shown in the earlier chapters of this thesis, have been promising. The focus of investigation in this section is to investigate the effect of damping control on the vehicle rollover propensity. There have been numerous attempts to demonstrate the effect of the damping ratio on the rollover stability of the vehicle. For example, Ahmadian (Ahmadian and Simon, 2004) tested this effect using a Skyhook control on a Ford Expedition; the results showed a reduced propensity for rollover of the vehicle.

In the vehicle suspension design, it is generally agreed (Gillespie, 1992) that the situation when the roll angle roughly corresponds to the tire lift off (tire looses its contact with the ground) is the unstable condition; in this section, that is considered the rollover threshold.

Considering the simple vehicle roll model (Figure 3) and equation (1-8), as shown in this equation, if the angular velocity, $\dot{\varphi}(t)$, is zero (or small), the damping has no (or minimal) effect on the systems dynamic. As a first result, it is concluded that the damping control will be effective in rollover stability in sudden maneuvers of the vehicle – for instance a sudden change of direction or an obstacle-prevention maneuver. As a result, damping control has a limited effect on the vehicle's rollover stability. This is the reason why, as suggested in this section, damping control is considered as an anti-rollover assist system.

To investigate the effect of damping control in a sudden vehicle maneuver, consider the simple vehicle roll model (Figure 3) and equation (1-8) (assuming $\ddot{\theta}, \theta << 1$ for simplicity) under a step input ($a_y = a_{y0}$, $t > t_0$). The closed form solution of this equation contains both transient and steady state responses will be

$$\varphi(t) = (\frac{h_b}{I\omega_n^2})f_0\left(1 - e^{-\zeta\omega_n t}\left(\cos(\omega_d t) + \frac{\zeta}{\sqrt{1-\zeta^2}}\sin(\omega_d t)\right)\right)$$

$$\omega_n^2 = \sqrt{\frac{k - m_b g h_b}{I}}, \zeta = \frac{c}{2I\omega_n}, \omega_d = \omega_n\sqrt{1-\zeta^2}, f_0 = m_b a_{y0}$$

(6-13)

Assuming the damping ratio ζ is small ($\zeta << 1$), then equation (6-13) can be rearranged as:

$$\varphi(t) = (\frac{h_b}{I\omega_n^2})f_0\left(1 - e^{-\zeta\omega_n t}\left(\cos(\omega_n t) + \zeta\sin(\omega_n t)\right)\right)$$

(6-14)

As a result, $\ddot{\varphi}(t)$ will be

$$\ddot{\varphi}(t) = (\frac{h_b}{I\omega_n^2})f_0\left(e^{-\zeta\omega_n t}\omega_n^2\left(-\zeta^2\cos(\omega_n t) + \zeta^3\sin(\omega_n t) - \cos(\omega_n t) + \zeta\sin(\omega_n t)\right)\right)$$

(6-15)

Considering that ζ^2 and ζ^3 is are small, then equation (6-15) becomes

$$\ddot{\varphi}(t) = (\frac{h_b}{I\omega_n^2})f_0\left(e^{-\zeta\omega_n t}\omega_n^2\left(-\cos(\omega_n t) + \zeta\sin(\omega_n t)\right)\right)$$

(6-16)

The wheel lift-off happens when $\ddot{\varphi}(t)$ is large enough. Therefore, the effect of the damping ratio, ζ, on the maximum value of the roll-angular acceleration, $\ddot{\varphi}(t)$, is a good metric to illustrate the effect of damping changes on rollover propensity. Figure 105 shows the sensitivity of the peak value of roll-angular acceleration to the change of damping ratio ζ. Another interesting result of this investigation is the role of the centre of mass height (h_b) on the effect of damping ratio. As shown in Figure 105, when h_b (the height of the centre of mass) is relatively large ($h_b = 0.4m$), by changing the damping ratio from 0 to1 we are able to change the maximum value of $\ddot{\varphi}(t)$ from 0.1 to 0.03 (70% reduction). At the same time, when h_b is relatively small ($h_b = 0.1m$), by changing the damping ratio from 0 to1 we are able to change the maximum value of $\ddot{\varphi}(t)$ from 0.25 to 0.03 (220% reduction). This can be interpreted as: "the height of the centre of mass will adversely affect the effectiveness of damping control on the rollover propensity." The CarSim software has also been used to confirm the outcome of the investigation. Double lane-change maneuver[11] has been selected as a sudden vehicle maneuver, and the vehicle roll-angle has been reordered in a low speed maneuver (80 km/h), while the damping ratio has been manually changed between zero and one ($0 < \zeta < 1$). Also, as suggested by the results presented in Figure 106, using the CarSim package, the higher damping ratio decreases the vehicle rollover propensity in sudden vehicle maneuvers.

---

[11] Refer to ISO-3888- 1999 for details of this manoeuvre
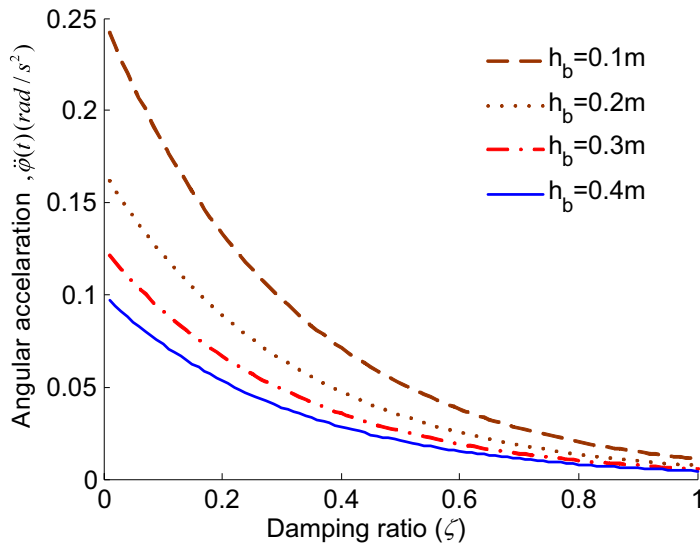
Figure 105: Effect of damping ratio (ζ) changes on roll-angular acceleration
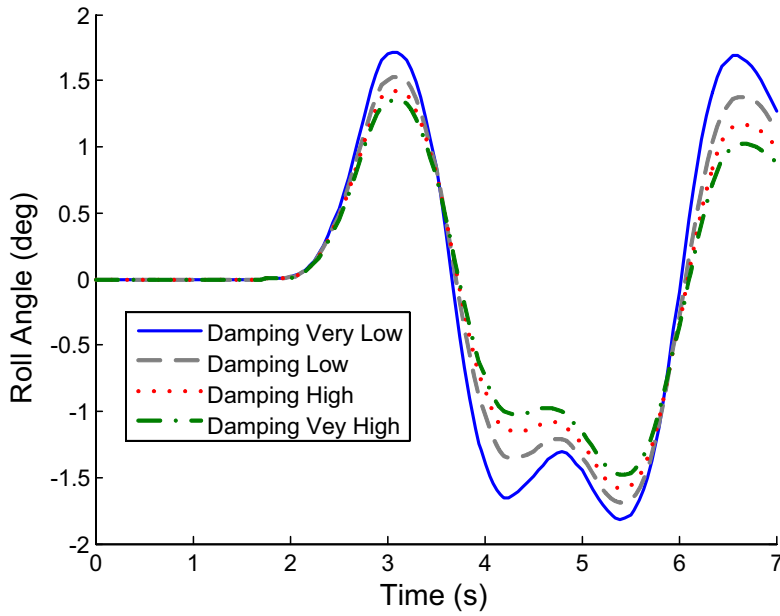
Figure 106: Effect of damping ratio (ζ) changes on roll angle. A sample of the simulation results using CarSim software in a double-lane-change maneuver with a speed of 80 km/h

As stated already and as proved by the foregoing investigation, in a semi-active suspension-controlled system equipped with a ride comfort and road handling controller, as proposed in the previous sections (sections 6.1 and 6.2), there should be a threshold to switch the controller from the ride-comfort and road-handling state to the anti-rollover state, as shown in Figure 107.
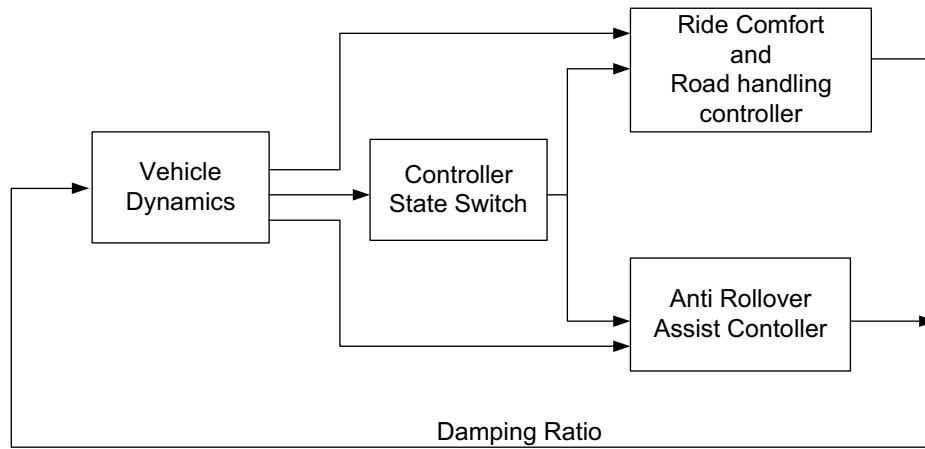
Figure 107: Structure of the integrated controllers

The structure of the state switch is simple: It works based on the existence of lateral acceleration and rolling rate. These simple rules are

$$if \left| a_y \right| > a_{y0} \ or \ \dot{\varphi}_0 < \left| \dot{\varphi} \right| \ then \ activate \ the \ anti-rollover$$

(6-17)

The values of the thresholds, "a_{y0} and $\dot{\varphi}_0$", will be determined through experimental evaluations or numerical studies based on vehicle characteristics. For this thesis, these values were selected based on the numerical simulations by CarSim for a light armored vehicle[12] as listed in Table 19 .

---

[12] Due to confidentiality of the data, it is not possible to disclose the vehicle physical dimensions in this thesis. But to clarify the matter, an existing vehicle in CarSim Library (High Mobility Multipurpose Wheeled Vehicle

Table 19: Threshold values for the controller state switching

Threshold	Value
a_{y0} (g's)	0.05
$\dot{\varphi}_0$ (deg/s)	2.0

To verify the performance of the anti-rollover assistance controller, it was implemented in CarSim software. A series of maneuvers at multiple vehicle speeds were simulated. Sample results from these simulations are shown in Figure 108-Figure 110. The results are the outcome of a double lane change maneuver. Figure 108 shows and compares the vehicle's roll angles. As depicted in this figure, the vehicle roll angle is significantly reduced when the anti-rollover control is in action.
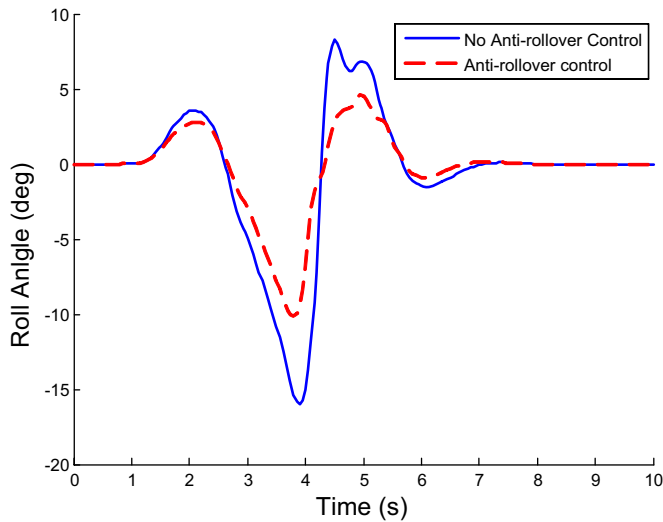
Figure 108: A sample of the simulation results using CarSim software in a double-lane-change maneuver with a speed of 100 km/h

(HMMWV) in CarSim library has been selected, and the physical parameters of that have been modified to match those of the selected vehicle.
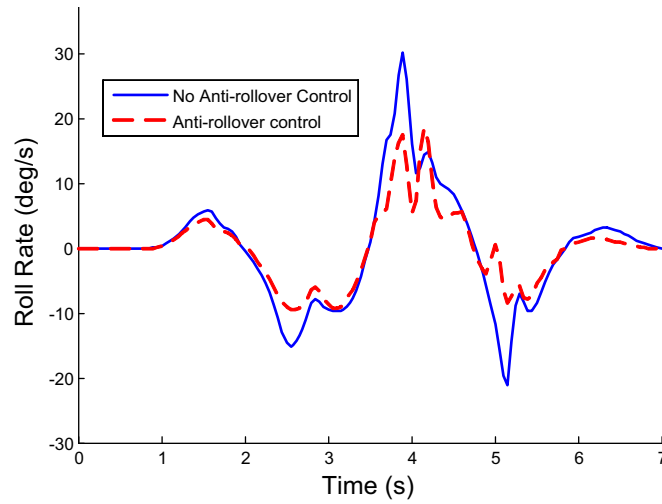
Figure 109: A sample of the simulation results using CarSim software in a double-lane-change maneuver with a speed of 100 km/h
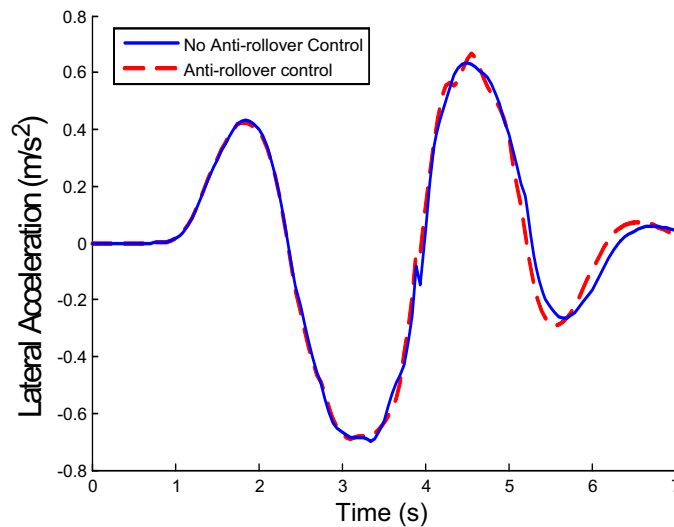
Figure 110: A sample of the simulation results using CarSim software in a double-lane-change maneuver with a speed of 100 km/h

As illustrated in Figure 109, the roll rate of the controlled vehicle is following the same pattern, but the pick values are reduced effectively. On the other hand, the lateral acceleration on the controlled and uncontrolled vehicle, as shown Figure 110, is not changed. This is as expected because the lateral acceleration is mainly a function of the outside environment and vehicle maneuver, not the vehicle suspension characteristics.

6.4 Conclusion

In the first section of this chapter, a new semi-active control strategy based on the R-S control strategy is proposed. The numerical simulation and analytical method of averaging are deployed to exhibit the effectiveness of the new control technique. The RMS values of the relative displacement transmissibility and the acceleration transmissibility are used to compare the performances of the new technique over the passive and the conventional R-S control method. In addition, the test results proved the effectiveness of the newly developed semi-active control strategy. Furthermore, the test results, the data obtained using the analytical method of averaging, and the numerical simulation results simultaneously proved the better performance of this new semi-active controller and the effectiveness of this system in offering a better ride comfort to the vehicles. For the proof of concept, the analysis in this chapter is under the assumption that the road-induced vibration is sinusoidal.

In the second section of this chapter, a fuzzy logic controller based on Skyhook and Groundhook control methods was developed to improve both ride comfort and road handling of heavy vehicles using a home-made semi-active damper. A quarter-car model with a semi-active suspension system was adopted. Three conventional controllers, Skyhook, LDR, and Rakheja-Sankar, are implemented for the model. It was shown through numerical analysis in the frequency domain that fuzzy logic control can address both ride comfort and handling better than other conventional methods. Although fuzzy control may not produce the best solution for both handling and ride comfort, it provides an optimum solution for concurrent control of ride and handling.

The final part of this chapter investigates and proposes a controller to reduce the propensity of vehicles to rollover. In this section, the CarSim simulation package was extensively used and the results have shown the efficiency of this simple control strategy to prevent the rollover. An important point is that this controller only improves the stability region of vehicles; it does not guarantee the absolute stability of the system.

Chapter 7
Summary of the Results and Future Work

This thesis started by considering three key elements as the main objectives of this research project. The first objective was to design and study the performance of a semi-active damper suitable for the heavy and off-road vehicles such as light-armored vehicles. This task involves the fabrication and experimental study of a prototype system. The second goal was to develop control strategies that would minimize the unwanted effects of road condition and driving maneuver on the vehicle and the passengers. The third goal was to address the common technical issues that have been a major source of concern and uncertainty in the development of semi-active controlled systems, such as the response-time and system nonlinearity.

In this thesis, semi-active suspension systems have been studied. A new semi-active damper has been modeled and prototyped, two semi-active control methods have been proposed, and analytical and numerical methods have been deployed to address the semi-active controlled systems nonlinearity and the issue of the semi-active systems response time. The main contributions of this study include the following:

1. A heavy vehicle passive damper is analyzed, tested, and modeled. The model is further verified using the test results. The existing gas spring, a highly nonlinear system, is mathematically modeled, and an adiabatic model is proposed for the modeling process. The test results proved that the proposed model is capable of predicting the gas-spring behavior.

2. The application of neural networks in modeling and mapping the semi-active dampers is proposed; it is successfully implemented in semi-active control algorithms and real-time testing.

3. A new and unique internal solenoid semi-active damper for heavy vehicle applications is designed, modeled, prototyped, and tested. Two commercially available semi-active dampers are selected as the benchmark, and the performance of the newly developed semi-active damper is proven to be acceptable.

4. A different, and probably the most neglected, aspect of the semi-active on-off control strategies, the added nonlinearity effect, is introduced and mathematically established. The two main issues – higher harmonics and performance index calculation – are discussed in detail.

5. A new method to analyze, calculate, and compare the performances of the semi-active controlled systems is proposed. The analytical method of averaging is introduced and used to analyze the conventional semi-active controlled systems.

6. The effect of higher harmonics due to the added nonlinearity of semi-active controlled systems is described in detail. Using numerical simulation analysis and experimental results, the existence of the harmonics phenomenon is confirmed. Also, a new controller based on the observation of actual test data is proposed, to eliminate the effects of added nonlinearities.

7. The effect of asymmetric damping in a 1DOF quarter-car model is analyzed and the effect of asymmetry on the suspension performance indexes is studied. The concept of dynamic fix point of the system due to damper asymmetry is also established. Using the method of averaging, a closed-form solution for the 1DOF asymmetric system is obtained.

8. The effects of the response time of semi-active dampers on the performance of the suspension performance indexes are studied. Numerical simulations and the analytical method of averaging are used to study the effect of the response time on the overall performance of the semi-active, on-off controlled system.

9. An experimental test rig was designed and fabricated to carry out the real-time implementation of proposed semi-active control methods. To ensure the real-time implementation of the control strategy, MATLAB/XPC-Target package has been adopted.

10. The response time of three different semi-active dampers are measured and compared. Test results are used to confirm the difference between the electrical and overall response times of a semi-active damper.

11. A new semi-active control strategy based on the R-S control strategy is proposed. The numerical simulation and analytical method of averaging are deployed to exhibit the effectiveness of the new control technique. The RMS values of the relative displacement transmissibility and the acceleration transmissibility are used to compare the performance of the new technique with that of the passive and the conventional R-S control method. In addition, the test results proved the effectiveness of the newly developed semi-active control strategy.

149

12. A fuzzy logic controller based on Skyhook and Groundhook control methods was developed to improve both ride comfort and road handling of heavy vehicles using an in-house semi-active damper. A quarter-car model with a semi-active suspension system is adopted. Three conventional controllers, skyhook, LDR, and Rakheja-Sankar, are implemented for the model. It was shown through numerical analysis in the frequency domain that fuzzy logic control can improve both ride comfort and road handling more effectively than other conventional methods.

In addition, this research project advances the state of knowledge in the semi-active suspension design system while making new contributions in many related areas such as the manufacture and design of semi-active dampers, mathematical modeling, control, and non-linear dynamics application. In addition, this research study has already resulted in the following academic publications:

▪ *Journal Papers*

1. *Eslaminasab, N*., Biglarbeigian, M., Melek, W., and Golnaraghi, M. F., 2007, "A Neural Network Based Fuzzy Control Approach to Improve Ride Comfort and Road Handling of Heavy Vehicles Using Semi-Active Dampers" International Journal of Heavy Vehicle Systems, Vol.14, No.2.

2. *Eslaminasab, N*., and Golnaraghi, M. F., 2007, "A Semi-Active Control Strategy for Vibration Isolation to Improve Ride Comfort of Vehicles" To Appear in the International Journal of Modeling Identification and Control.

3. *Nima Eslaminasab*, Tom Gillespie*,* Behrad Khamesee, and Farid Golnaraghi, "Modeling and Testing of a Prototype Twin-tube Semi-Active Damper", International Journal of Heavy Vehicle Systems, (Accepted, Ref#: IJHVS2009_16).

▪ *Refereed Papers in Conference Proceedings*

1. *Eslaminasab, N*., and Golnaraghi, M. F., 2007, "An Investigation on the effect of on-off control strategies on the suspension system performance using FRF analysis and averaging method" Proceedings of 21st Canadian Congress of Applied Mechanics, Ryerson University.

150

2. *Eslaminasab, N.*, Arzanpour, S., and Golnaraghi, F., 2007, "Optimal Design of Asymmetric Passive and Semi-active Dampers" Proceedings of IMECE 2007, paper no. IMECE2007-42176, November 11-15, 2007, Seattle, Washington, USA.

3. *Eslaminasab, N.* and Golnaraghi, F., 2007, "The Effect of Time Delay of the Semi-active Dampers on the Performance of on-off Control Schemes" Proceedings of IMECE 2007, paper no. IMECE2007-42724, November 11-15, 2007, Seattle, Washington, USA.

4. *Nima Eslaminasab*, Tom Gillespie, and Farid Golnaraghi, 2007, "Modeling, mathematical simulation and non-linear analysis of magnetorheological valve damper", International Association of Science and Technology for Engineering Development, Modelling and Identification Conference, Montreal Canada, Paper #567-130, pp227-232.

5. Arzanpour, S., *Eslaminasab, N.*, Schubert, B., Narimani, A., Golnaraghi, F., 2006, "A Novel Technique for Frequency and Time Optimization of Automotive Engine Mount Parameters" International Mechanical Engineering Conference and Exposition, IMECE-2006, Paper No. 14911, Chicago, Illinois.

6. *Eslaminasab, N,* and Golnaraghi, F., 2007, "Vibration Control Schemes of Semi-active Hydro-pneumatic Dampers for Military Vehicle Suspension" International Mechanical Engineering Conference and Exposition, IMECE-2006, Paper No. 14786, Chicago, Illinois.

▪ *Conference Presentation with Refereed Published Abstracts*

1. *Nima Eslaminasab* and Farid Golnaraghi, 2007, "The Effect of Intelligent Suspension on Rollover Stability of Vehicles", MMO Discovery 2007, Toronto, Canada.

2. *Nima Eslaminasab* and M.F. Golnaraghi, 2006, "Intelligent Suspension System for Military Vehicles.", UW Graduate research conference, Waterloo, On, Canada.

3. **Nima Eslaminasab**, Tom Gillespie, Behrad Khamesee, and Farid Golnaraghi, 2006, "Semi-Active Intelligent Suspension System for Military Vehicles", MMO Discovery 2006, Toronto, Canada.

- **Sample of Technical Reports (non-refereed)**

    1. **Nima Eslaminasab** and Thomas Gillespie, 2006, "Development of Semi-Active Damper for Heavy Off-Road Military Vehicles" Submitted to General Kinetics Engineering Corporation.

    2. **Nima Eslaminasab** and M.F. Golnaraghi, 2006, "A Neural Network Based Fuzzy Control Approach to Improve Ride Comfort and Road Handling of Heavy Vehicles Using Semi-Active Dampers" Submitted to General Kinetics Engineering Corporation.

    3. **Nima Eslaminasab**, Thomas Gillespie and Anthony Kim, 2006 "Mathematical Modeling and simulation of a hydro pneumatic strut" Submitted to General Kinetics Engineering Corporation.

Based on my completed work on semi-active dampers and semi-active controlled suspension systems, the following research is recommended for further study.

1. Development of an industrial final version of the prototyped internal solenoid-valve semi-active damper and commercialization process of this product is an important aspect of future work.

2. Development of a microcontroller for each of the proposed control methods. Theoretical and experimental studies of three semi-active control methods applied to a quarter-car model have already been done.

3. In this thesis, a sinusoidal response analysis of the suspension system has been conducted. As the real-life excitations to a vehicle are varied random inputs, more research on the nonlinear system response to a general random input is an important area for further study of suspension system design.

4. Real-time testing of the developed semi-active dampers and the control strategies on an actual light-armored vehicle and testing of the vehicle on the standard test tracks are also

152

recommended. Comparing the real-time test results with the results obtained through numerical simulation using CarSim would be beneficial as well.

Appendix A
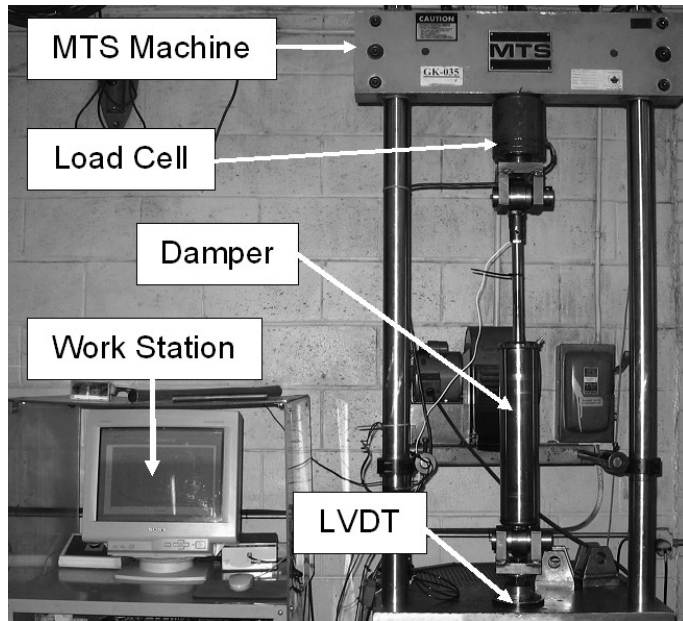## Test Set-Up

The tests on the existing GKEC damper to characterize and validate the damper mathematical models were conducted at the GKEC test facilities in Brampton, Ontario. These facilities include an MTS damper dynamometer with a maximum velocity of 100 in/sec, equipped with a load sensor with a maximum load measuring capacity of 20000 lbf and an internal LVDT (details are unknown). The system operates through a work station which runs an MTS Test Star II controller which has the ability to generate a wide rage of common base excitation inputs including sinusoidal waves and step inputs (the set-up is shown in Figure 111).

To characterize the damper and validate the model, two different tests were performed:

A static test of the damper was performed to measure the effects of compressing the gas chamber on the damper force. In the static test, the damper gas chamber was charged to a pressure of 360 psi and the damper was manually compressed by increments of 10 millimeters, and the damper force versus displacement was recorded. This test was used to validate the gas spring model

The dynamic test program, including in the Test Star II controller, tests the damper at various velocities and under different inputs as programmed by the operator. As a standard method to test the dampers, the controller was programmed to perform a series of sinusoidal compression and extension strokes of the damper with constant amplitude of 30 millimeters. The damper is stroked at seven different frequencies from 0.21 Hz to 4.25 Hz. The time, displacement, velocity, and transferred force were measured and recorded at a frequency of 600 data per cycle (one complete extension and compression stroke).

Figure 111: Test set up at GKEC test laboratory

Bibliography

Ahmadian, M., 1999, "On the Isolation Properties of Semi active Dampers" Journal of Vibration and Control, Vol. 5, No. 2, pp. 217 - 232.

Ahmadian, M., Marjoram, R. H., 2000, "Effects of Passive and Semi active Suspensions on Body and Wheel Hop Control", Journal of Commercial Vehicles, Vol. 98, pp.595-604.

Ahmadian, M., Simon, E., 2004, "Can Semiactive Dampers with Skyhook Control Improve Roll Stability of Passenger Vehicles", SAE Transaction, 01-2099.

Alanoly J., Sankar S., 1986, "A New Concept in Semi-active Vibration Isolation", ASME Design Engineering Technical Conference, t86-DET-28.

Al-Holou, N., Joo, D. S., Shaout, A., 1996, "The Development of Fuzzy Logic Based Controller for Semi-active Suspension Systems", Proceeding of the 37th Midwest Symposium on Circuits and Systems, IEEE, pp. 1373-1376.

Anon, B., 1997, "Mechanical vibration and shock- evaluation of human exposure to whole-body vibration." International Organization for Standardization, ISO 2631.

Arzanpour, S., Eslaminasab, N., Schubert, B., Narimani, A., Golnaraghi, F., 2006, "A Novel Technique for Frequency and Time Optimization of Automotive Engine Mount Parameters" International Mechanical Engineering Conference and Exposition, IMECE 2006, Paper No. 14911, Chicago, Illinois.

Audenino, A.L., and Belingardi, G., 1995, "Modelling the Dynamic Behaviour of a Motorcycle Damper", Proceedings of the Institution of Mechanical Engineers, Part D: Journal of Automobile Engineering, vol. 209 no. 4.

Bendat, J. S., Piersol, A. G., 1980, "Engineering Applications of Correlations and Spectral Analysis" Wiley, New York.

Bernard, J., Shannan, J. and Vanderploeg, M., 1991, "Vehicle Rollover on Smooth Surface" SAE technical paper series, 891991.

Box, G. E. P., 1979, "Robustness in the Strategy of Scientific Model Building In R. L. Launer, and G. N. Wilkinson, (eds.) Robustness in Statistics", New York: Academic Press.

Brach, R. M. and Haddow, A., 1993, "On the Dynamic Response of Hydraulic Engine Mounts," SAE paper, #931321.

Brennan, S., & A. Alleyne, 2000, "The Illinois Roadway Simulator: A Mechatronic Test bed for Vehicle Dynamics and Control," IEEE/ASME Transactions on Mechatronics, 5:4 349-359.

British standard guide to measurement and evaluation of human exposure to whole body mechanical vibration and repeated shock. British Standards Institution, BS6841, 1987.

Carlson, J. D., Chrzan, M.J., 1992, "Magnetorheological Fluid Dampers," US Patent 5,277,281, June 18,.

Carter, A. K., 1998, "Transient Motion Control of Passive and Semi-active Damping for Vehicle Suspensions", M.A.Sc thesis, Virginia Tech.

Cengel, Y. A., 1997, "Introduction to Thermodynamics and Heat Transfer" McGraw-hill series in mechanical engineering, ISBN: 0-07-114109-X.

Cole, D. J., 2001, "Fundamental Issues in Suspension Design for Heavy Road Vehicles" , Vehicle System Dynamics, Vol. 35, No. 4&5, pp. 319-360.

Crosby, M.J., Karnopp, D.C., 1973, "The Active Damper", Shock and Vibration Bulletin, 43.

Davis, L. C., 1999, "Model of Magnetorheological Elastomers," Journal of Applied Physics 85(6), 3348-3351.

Dixon, J. C., 1999, "The Shock Absorber Handbook." Society of Automotive Engineering, Inc., ISBN 0-7680-0050-5

Elmer, K.F. , and Gentle, C.R., 2001, "A Parsimonious Model for the Proportional Control Valve", Proceedings of the Institution of Mechanical Engineers, Part C: Journal of Mechanical Engineering Science, vol. 215 no. 11.

Eslaminasab, N., and Golnaraghi, M. F., 2007, "An Investigation on the effect of on-off control strategies on the suspension system performance using FRF analysis and averaging method" Proceedings of 21st Canadian Congress of Applied Mechanicals, Ryerson University.

Eslaminasab, N., Arzanpour, S., and Golnaraghi, F., 2007a, "Optimal Design of Asymmetric Passive and Semi-active Dampers" Proceedings of IMECE 2007, paper no. IMECE2007-42176, November 11-15, 2007, Seattle, Washington, USA.

Eslaminasab, N., Biglarbeigian, M., Melek, W., and Golnaraghi, M. F., 2007b, "A Neural Network Based Fuzzy Control Approach to Improve Ride Comfort and Road Handling of Heavy Vehicles Using Semi-Active Dampers" International Journal of Heavy Vehicle Systems, Vol.14, No.2.

Eslaminasab, N., Gillespie, T., Khamesee, B., and Golnaraghi, F., 2008, " Modeling and Testing of an in-House-Prototype Twin-Tube Semi-active Damper", to Appear in the International Journal of Vehicle Design.

Eslaminasab, N., Kim, A., Gillespie, T., 2004, "Mathematical Modeling and Simulation of a Hydro-pneumatic Strut" University of Waterloo Department of Mechanical Engineering, Technical Report.

Esmailzadeh, E., Bateni, H.,1992a, "Active Vehicle Suspensions with Adaptive Preview Control", Proceeding of the International Symposium on Robotics and Manufacturing, Santa Fe, New Mexico, USA .

Esmailzadeh, E., Bateni, H.,1992b, "Optimal Active Suspensions with Full State Feedback Control", SAE transactions, Journal of Commercial Vehicles, 101:784-79.

Esmailzadeh, E., Taghirad, H. D., 1996, "Active Vehicle Suspensions with Optimal State- Feedback Control", SAE Transactions, Journal of Commercial Vehicles, International Journal of Mechanical Science.

Frost, G. P., Howell, M. N., & Gordon, T. J., 1996, "Dynamic Vehicle Roll Control Using Reinforcement learning", Proceedings of the 1996 UKACC International Conference on CONTROL 96, Exeter, UK, pp 1107-1112.

Gillespie, T.D., 1992, "Fundamental of Vehicle Dynamics" Society of Automotive Engineering, Inc., ISBN 1-56091-199-9.

Gordon, T. J., 1995, "An integrated Strategy for the control of a Full Vehicle Active Suspension System", Proceedings of the 14th IAVSD Symposium on Dynamics of Vehicles on Roads and Tracks, Ann Arbor, Michigan, USA, pp 229-242, ISBN 90-265-2474-3.

Grifin, M. J., 1998, "A comparison of standardized methods for predicting the hazards of whole-body vibration and repeated shocks." Journal of Sound and Vibration, 215(4), pp. 883-914.

Hedrick, J. K., Rajamani, R., and Yi, K, 1994, "Observer Design for Electronic Suspension Aapplications," Vehicle System Dynamics, 23:413-440.

Hrovat, D., 1997 "Survey of Advanced Suspension Development and Related Optimal Control Applications", Automatica, vol.33, no.10, pp1781-1817.

Inman, D.J., 2001, "Engineering Vibration", Upper Saddle River, NJ: Prentice-Hall, Inc.

Jazar, G. N. and Golnaraghi, F., 2002," Engine Mounts for Automotive Application, A Survey," Shock and Vibration Digest 34, 363-379.

Jolly M. R., Bender J. W., and Carlson J. D., 1999, "Properties and Application of Commercial Magnetorheological Fluids," Journal of Intelligent Material Systems and Structures, 10: 5-13.

Jolly, M. R. and Carlson, J. D., and Munoz, B. C., 1996, "A Model of the Behavior of Magnetorheological Materials," Journal of Smart Materials and Structure 5, 607-614.

Jolly, M.R., Bender, J.W., Carlson, J.D., 1998, "Properties and Applications of Commercial Magnetorheological Fluids," SPIE 5th Annual International Symposium on Smart Structures and Materials, San Diego, CA.

Jolly, M.R., Carlson, J. D., Prindle, D. R., 2000, "Adjustable Valve and Vibration Damper Utilizing Same," US Patent 6,131,709, October 17.

Karray, F.O., De Silva C., 2004, "Soft Computing and Intelligent Systems Design" Pearson education, Harlow.

Kim, A., Gillespie, T., Eslaminasab, N., 2004, "Evaluation of Existing Active-valve Technologies for Use in Semi-active Shock Absorbers" University of Waterloo Department of Mechanical Engineering, Internal Technical Report.

Kim, K., D. Joen, 1999, "Vibration Suppression in an MR Fluid Damper Suspension System", Journal of Intelligent Material Systems and Structures, 10:779-786, 1999.

Kitching, K.J., Cole, D.J., and Cebon, C., 2000, "Performance of a Semi-active Damper for Heavy Vehicles", Journal of Dynamic Systems, Measurement and Control, Transactions of the ASME, vol. 122 no. 3.

Koo, J., Goncalves, F., D., and Ahmadian, M., 2006, "A Comprehensive Analysis of the Response Time of MR Dampers" Journal of Smart Material and Structures, 15 351–358.

Kyongsu, Y., Jangyeol, Y., Dongshin, K., 2007, "Model-based Estimation of Vehicle Roll State for Detection of Impending Vehicle Rollover" American Control Conference, ACC '07 , vol., no., pp.1624-1629, 9-13.

Lai, C. Y., Liao, W. H., 2002, "Vibration Control of a Suspension System via a Magnetorheological Fluid Damper", Journal of Vibration and Control, 8:527-547.

Lam, A.H. F. and Liao W. H., 2003, "Semi-active Control of Automotive Suspension Systems with Magnetorheological Dampers", International Journal of Vehicle Design, 33 (1-3):50-75.

Matsumoto, N. and Tomizuka, M., 1992, "Vehicle Lateral Velocity and yaw Rate Control with Two Independent Control Inputs," ASME JDSMC, Vol. 114, pp. 606-613, December.

Mc Manus, S. J., ST. Clair, K. A., Boileau, P.E., Boutin, J. and Rakheja, S., 2002, "Evaluation of Vibration and Shock Attenuation Performance of a Suspension Seat with a Semi-active Magnetorheological Fluid", Journal of Sound and Vibration, 235(1):313-327.

McCloy , D., Martin, H., 1980, "Control of Fluid Power: Analysis and Design" Ellis Horwood Limited, ISBN: 0-85312-135-4.

Milliken, William F., 1988, "Active Suspension," Society of Automotive Engineers, Paper 880799.

Mollica, R. and Youcef-Toumi, K., 1997, "A Nonlinear Dynamic Model of a Monotube Shock Absorber", Proceedings of the Americal Control Conference, vol. 1.

Nakhaie Jazar, G., Narimani, A., Golnaraghi, M.F. and Swanson D.A., 2003, "Practical Frequency and Time Optimal Design of Passive Linear Vibration Isolation Mounts" Vehicle system dynamics, Vol. 39, No. 6, pp. 437-466.

Narimani, A., 2004, "Development of Linear and Nonlinear Isolation Techniques for Passive and Semi-Active Applications," Ph.D. Dissertation, University of Waterloo, Canada.

Park, K., Kim, J. , and Kim, D., 2005, "A Study on the Dynamic Characteristics of the Continuously Variable Shock Absorber for Semi-Active Damping Control System", SAE Technical Paper No. 2005-01-1711, Warrendale, PA: Society of Automotive Engineers.

Peel, D. J., Stanway, R., and Bullough, W. A., 1996, "Dynamic Modelling of an ER Vibration Damper for Vehicle Suspension Applications," Journal of Smart Materials and Structures 5, 591-606.

Preumont A. (2002) "Vibration Control of Active Structures" Kluwer Academic Publishers Dordrecht, eBook ISBN: 0-306-48422-6.

Rakheja, S., Sankar, S., 1985, "Vibration and Shock Isolation Performance of a Semi-active 'On-off' Damper," Journal of Vibration, Acoustics, Stress, and Reliability in Design, 107(4):398-403.

Reybrouck, K., 1994, "A Nonlinear Parametric Model of an Automotive Shock Absorber", SAE Technical Paper No. 940869, Warrendale, PA: Society of Automotive Engineers.

Sampson, D. J. M. & Cebon, D., 2003, "Active Roll Control of Single Unit Heavy Road Vehicles," Vehicle System Dynamics, Vol 40, No. 4. pp 229-270.

Segel, L, 1993, "An Overview of Developments in Road-vehicle Dynamics: Past, Present and Future," Proc. of International Conference on Vehicle Ride and Handling, Birmingham, November 1993, IMECHE, paper# C466/052, pp. 1-12.

Shannon, J. E., Venderploeg, M. J., 1989, "A vehicle Handling Model with Active Suspensions", Journal of Mechanics, Transmissions, and Automation in Design, 111(3):375-381.

Shen, Y., 2005, "Vehicle Suspension Vibration Control with Magnetorheological Dampers," Ph.D. Dissertation, University of waterloo, Canada.

Shen, Y., Golnaraghi, M. F. and Heppler, G. R., 2006, "Semi-active Vibration Schemes for Suspension Systems Using Magnetorheological Dampers" Journal of Vibration and Control, 12(1), pp. 3-24.

Smith, S.W., 2003, "Digital Signal Processing, A Practical Guide for Engineers and Scientists" Newnes, ISBN 0-75067444-X.

Snowden, J. C., 1979, "Vibration Isolation: Use and Characterization," Journal of Acoustic Society of America 66, 1245-1274.

Son, S., Isik, C., 1996, "Application of Fuzzy Logic to an Automotive Active Suspension System", Proceedings of the Fifth IEEE International Conference on Fuzzy Systems, Volume 1, 8-11, pp.:548-553.

Song, X, Ahmadian, M, 2005, "An Adaptive Semi-active Control Algorithm for Magnetorheological Suspension Systems" Journal of Vibration and Acoustics, Vol.127, pp493-502.

Spencer, B. F., Dyke, D. T., Sain, M. K., and Carlson, J. D., 1997, "Phenomenological Studies of a Magnetorheological Damper," Journal of Engineering Mechanics, 123(3):230-238.

161

Tomizuka, M., and Hedrick, J. K., 1995, "Advanced Control Methods for Automotive Applications," Vehicle System Dynamics, Vol 24, pp. 449-468.

Uys, P.E., Els, P.S., and Thoresson, M.J., 2006, "Criteria for Handling Measurement" Journal of Terramechanics, pp. 43-67, 43.

Vaughan, N.D. and Gamble, J.B., 1990, "The Modeling and Simulation of A Proportional Solenoid Valve", Proceedings of the Winter Annual Meeting of the American Society of Mechanical Engineers, Nov 25-30.

Wei-Chau X., 2006, "Dynamic stability of structures", Cambridge press, ISBN-10: 0521852668.

Winslow, W. M., 1947, "Method and Means for Translating Electrical Impulses into Mechanical Forces," U.S. Patent No. 2417850.

Yu, F., Crolla, D. A, 1998, "Optimal Self-tuning Controller for an Active Suspension", Vehicle System Dynamics, 29 (1):51-65.

Yue, C., Busten, T. and Hedrick, J. K., 1989, "Alternative Control for Automotive Active Suspensions", ASME journal of Dynamic Systems, Measurements, and Control, 111:286-290.